NTNU
Norwegian University of
Science and Technology

Fatigue of Threaded Rods Subjected to Axial Load

Nina Løkken

Department of Structural Engineering

Faculty of Engineering Science and Technology

NTNU- Norwegian University of Science and Technology

MASTER THESIS 2016

SUBJECT AREA: Timber structures	DATE: 20.06.2016	NO. OF PAGES: 95

TITLE:

Fatigue of Threaded Rods Subjected to Axial Load

Utmatting i Gjengestenger ved Aksial Belasting

BY:

Nina Løkken

SUMMARY:

This thesis involves the investigation of threaded rods inserted into glulam elements subjected to axial forces imposed by traffic load in bridges. Fatigue of timber elements and connectors are generally investigated in a literature study. In addition, experimental tests were conducted investigating the behavior of this connection in both static and cyclic load application. This research was conducted to obtain a better understanding of the fatigue behaviour in threaded rods, and to compare with other solutions for connections in similar situations. A literature review was conducted on recent reports and relevant theory concerning fatigue. The information were processed and used to evaluate obtained experimental test results. Two different grain-to-rod angles were tested in static and cyclic load application (90˚ and 45˚ rod-to-grain angle).

Five specimens were tested for establishing static reference load in withdrawal. One failed in splitting, and were not included to establish static reference load. 45˚ specimens did show larger capacity in withdrawal than expected, which might be contributed to stronger wood lamellas in the specimen (higher density). Cyclic tests were conducted on thirteen specimens, two of which were terminated after few cycles. Results from five specimens with α=90˚ and six with α=45˚ were processed. The number of completed tests was limited by different expected and unexpected problems.

The number of tests were not sufficient to make any firm conclusions. However, there might be observations pointing to fatigue in withdrawal of these connections not becoming a problem. This is because the steel capacity of fatigue might prove to be the limiting value.

RESPONSIBLE TEACHER: Kjell A. Malo

SUPERVISOR(S): Kjell A. Malo, Haris Stamatopoulos

CARRIED OUT AT: Department of Structural Engineering

Institutt for konstruksjonsteknikk

FAKULTET FOR INGENIØRVITENSKAP OG TEKNOLOGI
NTNU – Norges teknisk-naturvitenskapelige universitet

MASTEROPPGAVE 2016

for

Nina Løkken

Fatigue in Threaded Rods Subjected to Axial Load

Utmatting i Gjengestenger ved Aksial Belasting

Background

Threaded rods are increasingly used as a fastener in wooden structures. This solution will often be considered to be more cost effective and practical. The example here is the network arch bridge, in which the connectors are arranged in a net along the arch. The hangers are connected to the timber arch by the threaded rods subjected to cyclic axial loading. These connections are yet to be tested in fatigue, and the field of research concerning fatigue in wood in general is not well documented. EC5 part 2 is containing some tentative recommendation concerning fatigue design. This report contains fatigue testing on this connector with the purpose of investigating if it needs to be included in the upgrade of Eurocode5 part 2.

Goal

1. Experimental testing on connections of threaded rods embedded in timber elements. Static reference tests and cyclic testing with different load level and grain-to-rod angle.
2. Evaluation of results in both static and cyclic testing.
3. Present and process relevant literature on fatigue concerning timber structures and connections.

Suggested activities

1. The candidate will find relevant literature on different research on fatigue in timber structures and connectors.
2. The candidate will process obtained data from experimental testing and evaluate the results, while making the necessary observations and changes.
3. The candidate will use the knowledge from literature with results from tests to provide a base and recommendation on how to proceed with further testing.

Besvarelsen organiseres i henhold til gjeldende retningslinjer.

Veileder(e): Kjell A. Malo og Haris Stamatopoulos

Besvarelsen skal leveres til Institutt for konstruksjonsteknikk innen 24. juni 2016.

II

Abstract

This thesis involves the investigation of threaded rods inserted into glulam elements subjected to axial forces imposed by traffic load in bridges. Fatigue of timber elements and connectors are generally investigated in a literature study. In addition, experimental tests were conducted investigating the behavior of this connection in both static and cyclic load application. This research was conducted to obtain a better understanding of the fatigue behaviour in threaded rods, and to compare with other solutions for connections in similar situations.

A literature review was conducted on recent reports and relevant theory concerning fatigue. The information were processed and used to evaluate obtained experimental test results. Two different grain-to-rod angles were tested in static and cyclic load application (90° and 45° rod-to-grain angle).

Five specimens were tested for establishing static reference load in withdrawal. One failed in splitting, and were not included to establish static reference load. 45° specimens did show larger capacity in withdrawal than expected, which might be contributed to stronger wood lamellas in the specimen (higher density). Cyclic tests were conducted on thirteen specimens, two of which were terminated after few cycles. Results from five specimens with α=90° and six with α=45° were processed. The number of completed tests was limited by different expected and unexpected problems.

The test setup evolved during the process. Fatigue failure in withdrawal of rods was desired, to investigate the timber behavior. However, as tests were conducted, it became evident that the desired failure mode proved difficult to obtain. The fatigue capacity in the steel of threaded rods mostly did not exceed the capacity of the glulam. The introduction of more than one embedment depth was required. All static tests were conducted with l_{eff} = 440mm without steel failure, and withdrawal capacity is the limiting property. In fatigue testing, the test was restarted if obtaining steel failure. The largest problems surfaced at maximum load level 60% of reference load. To obtain failure in withdrawal of the rod, the tests had to be restarted many times. The amount of restarts were limited by the length of rod available for gripping in the machine.

The number of tests were not sufficient to make any firm conclusions. However, there might be observations pointing to fatigue in withdrawal of these connections not becoming a problem. This is because the steel capacity of fatigue might prove to be the limiting value.

Sammendrag

Denne oppgaven tar for seg undersøkelse av gjengestenger skrudd inn i limtreelementer når de utsettes for aksialkrefter under statisk og syklisk lastpåføring. Utmatting i tre-elementer og festemidler i tre er undersøkt gjennom en litteraturstudie av emnet. Det ble gjennomført eksperimentelle tester for å undersøke oppførselen til forbindelsen ved forskjellig lastpåføring.

En litteraturgjennomgang på rapporter fra nyere tid og relevant teori om emnet ble gjennomført. Informasjonen har blitt bearbeidet, og har blitt brukt for å evaluere resultatene fra gjennomførte tester. To forskjellige vinkler mellom gjengestang og fiberretning ble testet med både syklisk og statisk lastpåføring ($\alpha=90°$ og $\alpha=45°$). Denne forskningen er gjennomført for å oppnå en bedre forståelse av oppførselen til gjengestanger innskrudd i tre, når den er utsatt for situasjoner der utmatting kan utvikle seg. Skruen sammenlignes med andre løsninger for forbindelse som kan brukes i lignende situasjoner.

I alt ble fem prøvestykker ble testet for å etablere statisk referanse last i uttrekk av gjengestang. En av disse prøvestykkene oppnådde splitting langs fibrene, og ble derfor ikke inkludert for å etablere statisk referanselast. Prøvestykkene med 45° fiberretning viste en større kapasitet i uttrekk av gjengestang enn forventet, noe som kan være på grunn av innhold av sterkere tre lameller i prøvestykket (høyere tetthet). Tretten prøvestykker ble testet med sykliske last, hvorav to ble avsluttet etter få sykluser og er ikke inkludert. Resultater fra fem prøvestykker med $\alpha=90°$ og seks med $\alpha=45°$ ble behandlet i resultatene. Antall fullførte tester ble begrenset av problemer som oppsto i testgjennomføringen, både forventede og uforventede.

Oppsettet av testen utviklet seg i løpet av testprosessen. Ideen var å oppnå et godt grunnlag for undersøkelse av utmatting i gjengestenger innskrudd i limtreelementer i form av uttrekk av stangen. Men i løpet testingen ble det klart at denne bruddmekanismen var vanskelig å oppnå. Kapasiteten i utmatting for stal i gjengestengene viste seg å ikke overstige kapasiteten i uttrekk fra limtre. Testing med mindre innskrudd dybde ble brukt for resten av testingen. Alle statiske forsøk ble utført med $d_t = 440mm$ uten å oppnå brudd i stålet. De største problemene oppsto når det maksimale lastnivå ble senket til 60% av referanse last. For å oppnå den ønskede bruddmekanismen måtte testen startes på nytt opptil flere ganger. Antall ganger testen kunne startes på nytt var begrenset av lengden av stangen som var tilgjengelig for maskinen å gripe.

Antall utførte tester er ikke tilstrekkelig for trekke noen endelige konklusjoner. Men resultatene kan tyde på at utmatting med denne bruddmekanismen ikke vil være noe problem i denne type forbindelse. Resultatene tyder på at utmatting i stål kan vise seg å være den begrensende faktoren i forbindelsen.

Preface

This thesis was conducted at the Faculty of Engineering Science and Technology in the department of Structural Engineering. It was made in connection with the final evaluation at Norwegian University of Technology and Science in conclusion of a Master's degree.

I would like to thank my supervisors Kjell Arne Malo and Haris Stamatopoulos for help and advise during the process of experimental testing. Both have also provided advise on how this thesis would be written and discussing different possibilities. Their combined experience on this connection and timber structures in general have been valuable and highly appreciated. This thesis would not have been possible if not for their guidance.

Also, I am greatful for the help recieved from laboratory technichians. I would especially like to thank Ragnar Moen. He prepared the machines for testing, installed and made parts needed in the setups in addition to conducting tests and monitoring the relevant parameters. Terje Petersen did a wonderful job making the specimens with great accuracy according to the provided illustrations. Steinar Seehuus and Christian Frugone both provided technical assistance on issues connected to computer logging and displacement trancducers.

Table of contents

List of figures

List of tables

Symbol list

a, b	The relevant characteristic strength
b	Width specimen
d	Diameter of the threads at the top of the rod(M20)
d_{min}	Minimum diameter threaded rod, wooden screw
d_s	Shear diameter of the threads at the top of the rod(M20)
d_t	Outer diameter of the threaded rod
F_a	Load amplitude from fatigue action
$f_{ax,k}$	Characteristic withdrawal parameter perpendicular to grain
$F_{ax,\alpha,Rk}$	Characteristic withdrawal capacity of screw
F_{est}	Estimated maximum static failure load
f_k	The relevant characteristic strength
F_m	Mean load level from fatigue action
F_{max}	Maximum load level from fatigue action
f_{max}	The normalized maximum stress
F_{min}	Minimum load level from fatigue action
F_{ref}	Static reference strength of component
f_u	Ultimate limit, steel
F_{ult}	Ultimate load
$f_{w.est}$	Estimated withdrawal strength
f_y	Yield limit, steel
h	Height specimen
L	Length specimen
l_1	Distance between the grip of the support for transducers on the threaded rod relative to the surface of glulam element
l_{eff}	Embedment depth
N	Number of cycles
n_{ADT}	The expected annual average daily traffic of the structure
n_{ef}	Effective number of screws
N_{obs}	The number of constant amplitude stress cycles
P_l	Withdrawal capacity from [1] linearly scaled for embedment
$P_{l.d}$	Withdrawal capacity from [1] linearly scaled for embedment and rod diameter

$P_{u.mean}$	Mean withdrawal capacity from [1]
R	Stress ratio
$S45$	Specimen with $\alpha = 45°$
$S90$	Specimen with $\alpha = 90°$
t_L	The numerically smallest design stress from the fatigue loading
W	Weight
α	Angle between the grain direction and the embedment of the rod
$\gamma_{M,fat}$	Material partial factor for fatigue loading
Δf	Normalized load range
Δ_{max}	Displacement at max force
$\Delta\sigma$	Stress range
ρ	Density
ρ_a	The density with connection to $f_{ax,k.}$
ρ_k	The characteristic density
ρ_m	Mean density
σ_a	Stress amplitude
$\sigma_{d,max}$	Numerically largest design stress from the fatigue loading
$\sigma_{d,min}$	Numerically smallest design stress from the fatigue loading
σ_m	Mean stress level
σ_{max}	Maximum stress from fatigue action
σ_{min}	Minimum stress from fatigue action

Abbreviations

DOL	Duration of load
EC3	Eurocode 3
EC5	Eurocode 5
EP	Epoxy adhesive
GFRP	Glass fibre reinforced plastic
HBV	Holz-Beton-Verbundsystem (Wood-Concrete-Composite system)
HCF	High cycle fatigue
LCF	Low cycle fatigue
LSB	Long screw bolt
LVL	Laminated veneer lumber
NA	National Annex
NTNU	Norwegian University of Science and Technology
PRF	Phenol-resorcinol formaldehyde adhesive
PUR	Polyurethane adhesive
RH	Relative humidity
TCC	Timber-concrete composite

1 Introduction

Timber structures have been increasingly more popular and they have gained a larger share of the market. However, the knowledge on timber in different load situations is limited compared to other construction materials. Involving a more careful planning process, the solution using timber elements can be expensive and loose in competition with other materials. Experience from new structures creates valuable knowledge and consequently better and safer structures. Connections in timber can be especially challenging, as they determine the overall structural stiffness. The challenges are low stiffness of connectors together with their incapability to transfer moments efficiently. [2](Stamatopoulos, 2016).

1.1 Wood as a structural material

Wooden materials in a society with a sustainable forestry, like Norway, is beneficial. The increased environmental focus of the last decades have made timber more attractive as a structural material. The production from making the raw material into desired construction elements results in little waste [3]("Limtreboka"). Rest products can be used to produce low-level energy in heating. In addition to great strength and stiffness, wood is often desired for aesthetical reasons.

1.1.1 Special properties

Timber used as a structural material differ in many ways from other materials like steel and reinforced concrete. Wood is a natural composite with cellular structure and it is characterized by anisotropy, which results in great variability depending on the direction [4]("Limtreboka"). The tension strength is normally 30 – 50 times smaller perpendicular to the grain than in the fibre direction [5]. The fracture in tension is brittle, while in compression it is much more ductile. Wood is characterized by many types of natural discontinuities. This is an important aspect to take into consideration, as it will influence the material properties. The material has cracks and knots that will affect the performance, which is not possible to eliminate fully when manufacturing timber elements.

Moisture content is another important variable for the determination of material properties. The mechanical properties can be drastically different depending on the level of moisture in the timber. Both strength and stiffness have a tendency to decrease if the moisture content is increased, and the material will become more ductile. However, this only applies to the level of moisture at which the cell walls are saturated. Standing trees in the forest sway in the wind, and the branches from living trees have large strength in bending. In dead trees however, the branches snap, and experiences a highly brittle fracture. Moisture content is considered in Eurocode 5: NS-EN 1995-1-1, 2.3.1.3 [6]. This section divides structures into classes depending on the climate and moisture the material is expected to endure in its lifetime.

1.1.2 Glued laminated timber

The properties of glulam (glued laminated timber) makes it very attractive for use in big structures. One of these is the ratio between strength and weight for glulam. This ratio is

larger than for other common structural materials like steel [3]("Limtreboka"), which enables the possibility of building with longer spans. In addition, the material is made up of thin and flexible lamellas, which can also be easily manufactured into curved shapes. Because the production of the construction materials are flexible, the specially produced parts are often cheaper in comparison to other materials. Glulam arches in bridge designs can therefore be a good and economically beneficial solution.
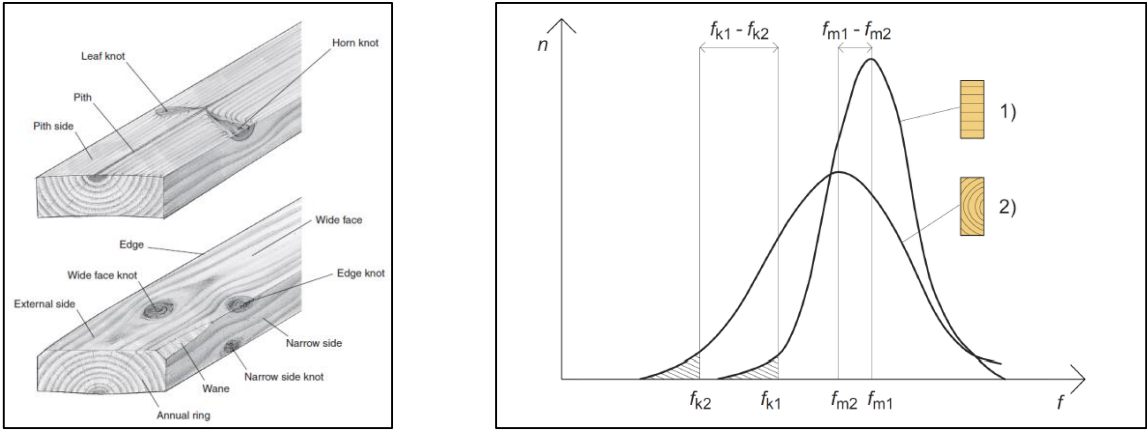
Figure 1: Natural growth defects (left), glulam strength scatter vs structural timber (right), "Limtreboka" [3]

Glulam is made up from several lamellas of wooden boards, placed along the grain in direction of the beam length. The different lamellas are extended to get the desired length of components with finger joints bonded with adhesive. The lamellas are then glued together on top of each other to get the desired height of the beam. With this configuration, the growth defects that naturally resides in wood will have less effect on the performance. As a result, the glulam has strength properties higher than solid timber of similar dimensions. In addition, there is less scatter in the strength properties. This is because the defects in timber have less impact on the structural element (Figure 1).

Today, glulam elements are used as load bearing components in many different structures. Everything from regular residential buildings to windmills and large-span bridges have been successfully constructed with glulam elements. The insulation capacity of wood is good, and the use in residential buildings is especially beneficial to counteract the build-up of thermal bridges. Timber and wood-based materials like glulam also have great fire resistance. In the event of a fire, the material will carbonize on the surface and protect further destruction of the material. This might be a lifesaving attribute, as it will contribute to stability and predictability during a fire.

If the wooden surface is properly protected against moisture and climate effects, wood can be a reliable and resistant material. These structures can, if correctly installed and protected, have very long longevity. There are old buildings in Norway still standing after more than eight hundred years. One example is the Urnes Stave Church, which was built around 1130-1140 AD and is currently the oldest stave church in Norway [7].

1.2 Network arch bridges

Bridges are typically long-span structures, which are subjected to both static and cyclic loads. They are usually designed for a longevity of hundred years, and need to be capable of withstanding short time and long-time effects from different load situations. Cyclic load from traffic may cause fatigue, and this might pose a limitation to the design of bridges.

The network arch bridge consists of tied arches with inclined hangers, which crosses each other at least twice [8] (Tveit, 2014). Figure 2 shows the placement of the hangers suspending the deck of the bridge with two-times crossing of the hangers. In principle, this design will have cables that are either relaxing or stretching depending on where the load is placed along the bridge. Therefore, it is important that the bridge have sufficient and stable dead load to maintain tension in the cables at all times.
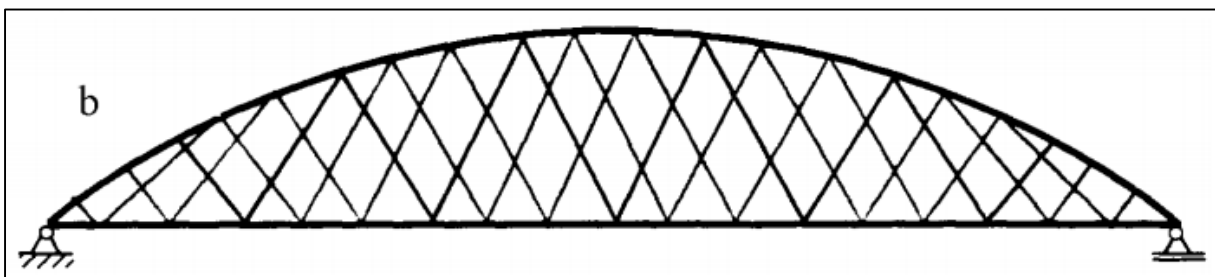
Figure 2: Network arch bridge, Tveit [8]

Many timber bridges in Norway have been constructed with the deck suspended to an arch truss using vertical hangers. The tendency of increasing use of renewable material have resulted in a greater interest of timber elements in bridges. This, along with the aesthetical value, has led to using network arch systems with timber arches. The system with inclined hangers is distributing the concentrated loads along the bridge arch, and moments will be small in comparison to the use of vertical hangers.

Figure 3: Tynset Bru, PLAN Arkitekter AS [9]

Tynset Bru is an example of a bridge constructed with glulam arches with vertical hangers suspending the deck of the bridge. Displayed in Figure 3, the arch trusses of glulam are carrying the large moments occurring along the bridge. The bridge consists of three sets of arches, two smaller and one large with a span of 70 meters. The bridge was at the time of construction in 2001, constructed with the largest span involving timber arches. Two miles south of Tynset Bru, another bridge with timber trusses is currently under construction. Steibrua, which is located in Alvdal, Norway, is a network arch bridge. It will have a single span of 88.2 meters with arches of glulam trusses [10]. The project is estimated to be complete by autumn of 2016.

Figure 4: Steibrua, Statens Vegvesen [10]

Dowel joints with slotted-in steel plates have been used in many timber arch bridges the last decades, like in Tynset Bru (Figure 3). This solution involves guessed plates combined with steel dowels loaded perpendicular to their axis. The dowels introduce forces in tension perpendicular to the grains. In addition, the installation of the steel plate requires cutting into the beam and any intervention in the timber might cause the fibres to split. Reinforcement in the form of self-tapping screws or plates might be needed to increase the mechanical properties of the connection (Stamatopoulos, 2016) [2].

It is proposed that the solution of screwed-in threaded rods might introduce a better alternative to dowel joints. They are cheaper and require less labour on site. Currently, many different dimensions of threaded rods exist on the market. They are easily accessed and can be bought with almost any desired length. Threaded rods have shown good potential as axially loaded connectors in timber elements (Stamatopoulos and Malo, 2015) [1]. With great withdrawal capacity and stiffness, they may, to some extent be used with similar effect as reinforcement bars in concrete. If inserted at an angle, the rods will counteract the propagation of crack in the directions of the fibres (Stamatopoulos, 2016) [2]. The threaded rod has the ability to distribute forces along the length of the rod, and this makes it less sensitive to local defects in the material. This is an important feature, which can make threaded rods competitive with other solutions.

When mentioning axially loaded connectors, it is also important to include the glued-in-rods. This connection is used in similar situations as the screwed-in rod the solution. However, the glued-in rod introduces one more component. The adhesive involves more uncertainty, and requires careful installation. It has to be carefully inserted in the pre-drilled hole with the adhesive without any unwanted particles that will compromise the contact between rod and adhesive. In addition, it is difficult to ensure that the thickness of the adhesive is constant along the length of the rod. This limits the strength in which the bonded-in rods can be inserted with good contact and thickness of the adhesive. Screwed-in-rods are less brittle, more fire resistant and have less problems connected to installation.

1.3 Method

Knowledge on different connectors used in timber is usually sparse and not well documented. Threaded rods have been tested in static load combinations with positive results (Stamatopoulos, 2016) [1]. However, little knowledge currently exists on the behaviour of the rod when subjected to cyclic load. As these connectors might have the potential to be used in bridges, this is relevant information to obtain. The upgrade of the Eurocode 5 part 2 [11] will soon be conducted. Research concerning fatigue behaviour in threaded rods connections might obtain valuable information, which can be used to determine design rules for structures subjected to cyclic loads.

A literature review on recent reports and relevant theory on fatigue in wood and timber connections are conducted. An experimental investigation of axially loaded threaded rods embedded in glulam will be presented. The obtained information are used when evaluating the experimental tests results. Two different grain-to-rod angles are tested in cyclic and static load situations. This research were conducted to compare with other competing connections, which can be used in similar situations.

2 Fatigue in timber

Wooden elements used in large structures are often subjected to cyclic loading. Structures like large factory building floors, subjected to heavy vehicle loads wind load on timber roofs, and traffic across bridges are just some examples on situations where fatigue in timber should not be neglected.

The effect of sustained load has historically always been recognized as a potential problem. Sagging beams after long duration of load or collapse under heavy snow load are common acknowledged possibilities. Creep is defined as damage caused by a load of less than maximum short-term capacity sustained for a long-term period.

The focus on timber failure when subjected to cyclic load has been sparse throughout time. Many generations of ship builders have known that the different types of wood do not always have similar properties in cyclic loading. Over 270 years ago, the French naval architect Georges Louis La Clerc, Compt de Buffon made a statement concerning fatigue in wood (Smith et al., 2003) [4]. He recommended that the stress level for oak beams should not exceed 0.5, and estimated with this rule that the beams would be able to withstand infinite number of load cycles. However, the famous WW1 aircraft engineer Dr. Fokker is reported to imply that wood was immune to the effect of fatigue (Smith et al., 2003) [4]. Many engineers after him did follow his example neglecting this effect. The continued growth of interest in timber structures has sparked an interest in the field during the past few decades. However, as mentioned this field is still largely undiscovered.

2.1 Basic theory

Fatigue failure is defined as the continuous growth of a small fracture or discontinuity of a material when subjected to cyclic or sustained stresses of lesser value than the static short-term strength. Fatigue effects are divided into three phases characterized by the behaviour: crack initiation, growth of crack and the final failure. The failure is a result of reduced area and the localised stresses at the weakest point. This is due to propagating fracture, and after a certain number of cycles the concentration of stresses will exceed the ultimate limit.

It is common to separate into low cycle fatigue (LCF) and high cycle fatigue (HCF). It is estimated that LCF failure occurs before 10^4 cycles, while HCF happens after a higher number of cyclic load repetitions (Ansell, 1995) [12]. Typical LCF load situation is the event of an earthquake, with large stress levels and a relatively low number of cycles. In other situations, the structure can be subjected to a lower cyclic stress level and still experience fatigue failure. This is defined as HCF, and the number of load repetitions is higher before failure. Traffic load on a bridge or wind load in a windmill are typical examples where HCF can develop.

Metal alloys are often sensitive to tensile stresses, especially at critical areas with interventions like notches or welding. Any imperfection can greatly affect the fatigue capacity of metals. However, wood is much less susceptible to tension stresses, as the fatigue failure will occur as microstructural damage throughout the volume of the wood (Ansell, 1995) [12].

This is why fracture mechanics are not an appropriate tool to describe the tensile fracture propagation across the grain of a timber element.

The imposed stresses that are acting during cyclic load are often complex in reality [12]. The real load cycles will contain a large spectre of load amplitudes, and the ideal of constant frequency and load range is rare. To understand the principle of fatigue however, it is easier to look at constant values because the real load conditions are difficult to replicate. The cycles with largest stress range will cause most damage and greatly influence the fatigue capacity. This is why while assessing the fatigue life according to the Eurocode 5 [11], only load from heavy traffic is taken into account.

2.2 Fatigue load parameters

In this case a constant sinusoidal cyclic load is applied to the test specimens. The wave has continuous amplitude and a constant mean value throughout the load cycle. This is called a harmonized wave. It is also possible to assess fatigue in an element subjected to triangular- or square-shaped waves in the cycle [13] (M. Gong et al. 2008). The sinusoidal wave is the best fit to simulate the traffic load on a bridge. The load is moving smoothly along with the vehicle passing the bridge. The force does not have a sudden drop or is sustained for a longer time at the peak. When comparing waveforms, the square waveform is most damaging while the triangular is the least damaging. The peak stress is sustained for a longer time in the sinusoidal wave, which is why the triangular waveform will inflict less damage.
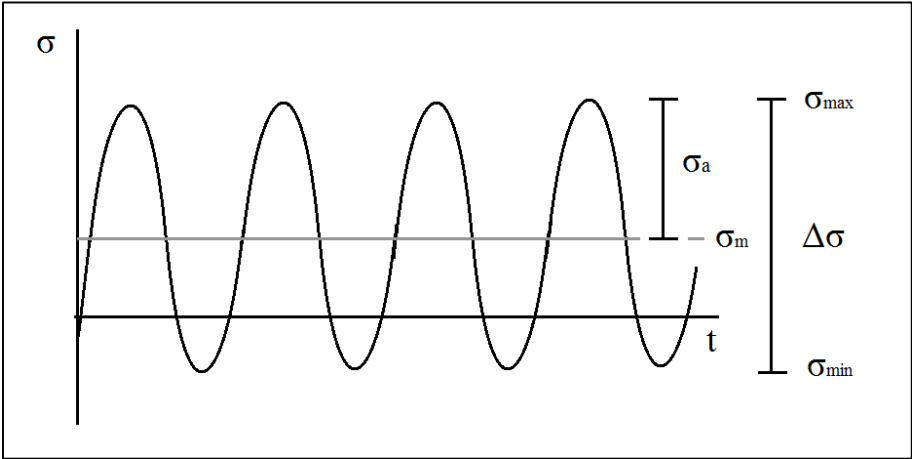
Figure 5: Illustration of cyclic harmonized loading

$$\sigma_{max} = \sigma_m + \sigma_a \tag{1}$$

$$\sigma_{min} = \sigma_m - \sigma_a \tag{2}$$

$$\sigma_m = \frac{\sigma_{max} + \sigma_{min}}{2} \tag{3}$$

7

$$\sigma_a = \frac{\sigma_{max} - \sigma_{min}}{2} \tag{4}$$

$$\Delta\sigma = \sigma_{max} - \sigma_{min} \tag{5}$$

σ_{max}	Maximum stress level of the cycle
σ_{min}	Minimum stress level of the cycle
σ_m	Mean stress level
σ_a	Stress amplitude
$\Delta\sigma$	Stress range

The stress ratio R is the ratio of the minimum load and the maximum load during a cycle. The stress parameter will greatly influence the behaviour in fatigue. To evaluate the connection fully, different stress ratios should be used. However, the connection in this report will only be subjected to axial load in tension. R=0.1 is tension-tension loading with minimum load during one cycle with value at 10% of the maximum load. This load ratio is considered the representative value of load situations in timber bridges with hangers. The difference in stress ratio values are illustrated in Figure 6.

$$R = \frac{\sigma_{min}}{\sigma_{max}} = \frac{F_{min}}{F_{max}} = \frac{\sigma_m - \sigma_a}{\sigma_m + \sigma_a} \tag{6}$$

$R = -1$	Fully reversed. The maximum and minimum peaks during one cycle are of equal stresses in tension and compression.
$0 < R < 1$	Tension-tension. All imposed stresses are positive (tension).
$-1 < R < 0$	Compression-tension. During the cycle, the stress changes between compression and tension.
$R > 1$	Compression-compression. All imposed stresses are negative (compression).
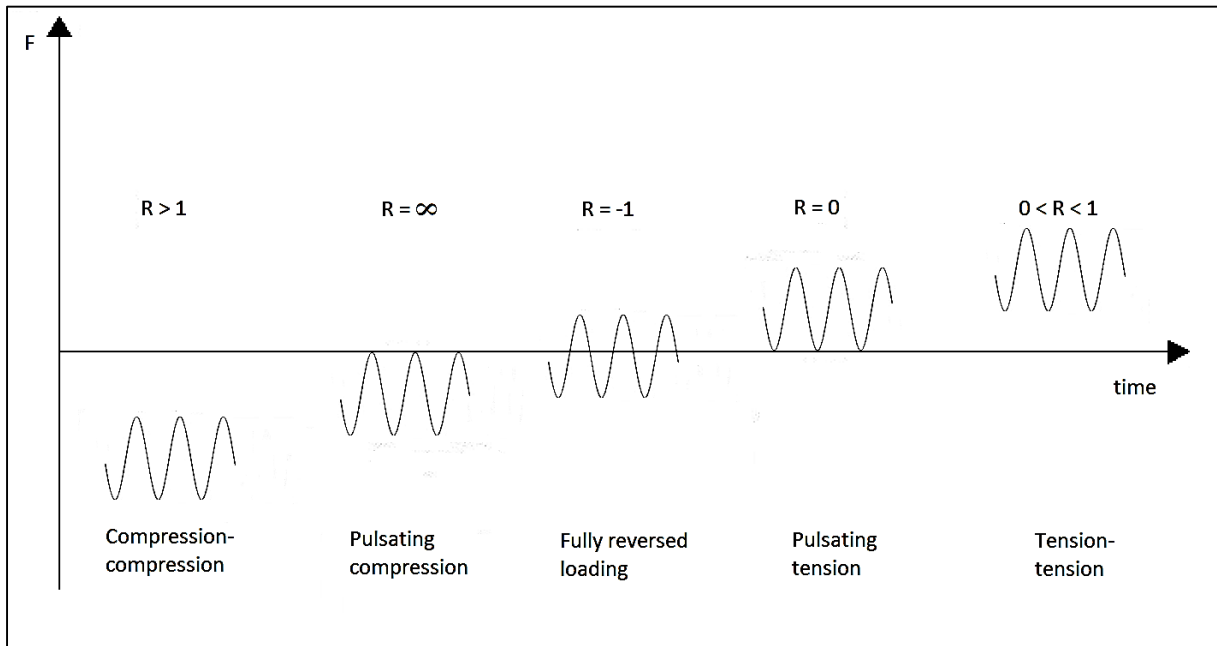
Figure 6: Stress ratio

Normalized stress range *(Δf)* is the rate of the range between maximum and minimum peak in the cycle divided on the reference stress. *f_{max}* is the normalized maximum stress. This is the rate between the maximum peak stress (or load) applied during one cycle and the static reference load. With normalized values, it is possible to evaluate similar elements of different size provided they are subjected to similar conditions. All terms for the fatigue parameters can be used with both stress and load. Both will be used here depending on what term is most practical at the time.

$$\Delta f = \frac{F_{max} - F_{min}}{F_{ref}} = \frac{\sigma_{max} - \sigma_{min}}{\sigma_{ref}} \tag{7}$$

$$f_{max} = \frac{F_{max}}{F_{ref}} = \frac{\sigma_{max}}{\sigma_{ref}} = \frac{\Delta f}{1 - R} \tag{8}$$

2.3 S-N curves

The S-N-curve is the traditional method of displaying fatigue life of a timber element. Plotted along the x-axis is the value of logarithm of number of cycles reached before fatigue failure. Different properties can be plotted along the y-axis, depending on what relationship or data that is inspected. During present testing, the load level (f_{max}) will be plotted to be able to compare results with test specimen of different static capacity.
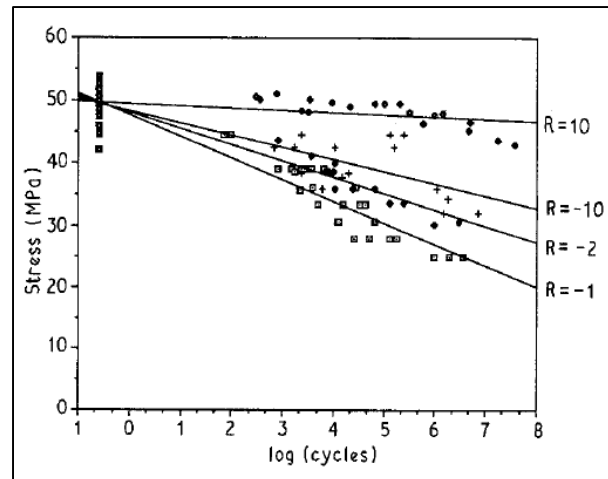
Figure 7: Example S-N-curve from [14] (Ansell et al. 1991)

The points that makes up the scatter represent one specimen. Static test results are plotted to the left in the x-axis at the value of -0.6. This value represent the application of one quarter of a cycle: from middle value to first peak. The trend lines are derived from the scatter obtained from testing conducted with different load levels. This line might indicate a proposed limit or trend of the fatigue life for this particular connection or wood. It is difficult to compare different wood species, because of the large deviations in properties and moisture content.

Figure 7 displays the different S-N-curves for testing on Khaya ivorensis done by (Ansell et al. in 19919 [14]. Different stress ratios represent each of the trend lines in the curve. The lines are linearly decaying with starting point at the static capacity. The most critical load situation for the stress ratios In Figure 7 is the fully reversed load cycle. This trend line decays at a higher rate than the others do, and fatigue failure will occur after a lower number of cycle repetitions. This situation will not be evaluated in the present experimental testing. As earlier mentioned, the hangers in the network arch bridge will always be subjected to tension if properly designed. This way the forces are distributed correctly along the arch.

2.4 Constant life diagram

Linear Goodman equation (9) and the curved Gerber line (10) can be used to estimate constant life curves [4]. Constant life curves allow the fatigue life of materials to be described as a function of stress ratio R, and can be plotted with experimental values. The mean stress is plotted along the x-axis versus alternating stress in the y-axis. Each curve represent one specified lifetime before failure while the linear rays represent the different stress ratios.

10

$$\sigma_a = \sigma_e \left(1 - \frac{\sigma_m}{\sigma_u} \right) \tag{9}$$

$$\sigma_a = \sigma_e \left(1 - \left(\frac{\sigma_m}{\sigma_u} \right)^2 \right) \tag{10}$$

σ_e Stress at R= -1.0 (fully reversed)

σ_u Ultimate strength
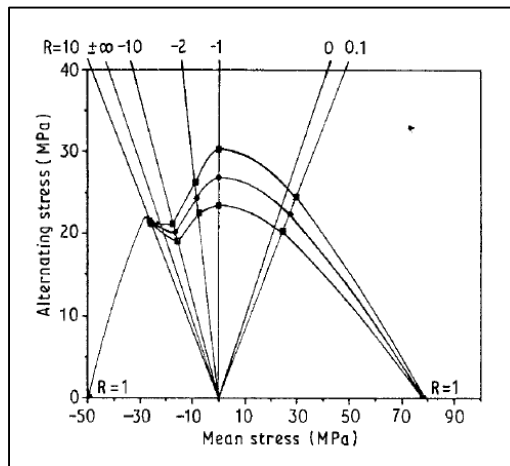
Figure 8: Example constant life diagram from [14] (Ansell 1991)

No constant life diagrams will be made based on experimental testing because on the single stress ratio used. However, it is a useful tool when considering different stress ratios and is mentioned in reports in the literature. It is important to understand which properties will influence the fatigue life, and the connection between them.

2.5 Displacement development

The development of the range of displacement for each cycle during fatigue life is interesting when researching cyclic behaviour of an element. This will give information on the behaviour of stiffness and damage accumulation during fatigue life. Wood will progressively experience micro-cellular damage during fatigue, which is why relative displacement will grow with number of cycles applied (Ansell, 2003) [15]. The changes in material property need to be studied for better understanding of the behavior. It is important to be able to predict changes of the properties of a connection to obtain safer structures.

The hysteresis loop is the stress/strain plot during cyclic loading. It contains information of the energy dissipation and the dynamic modulus can be measured. The area within a

hysteresis loop is the energy dissipated per cycle. Dynamic modulus is the ratio stress/strain during cyclic load conditions, and is the slope of the hysteresis loop.

2.6 Sustained load

Traditionally the fatigue damage caused by sustained stress has been the main attention of the engineers (I. Smith et al. 2008) [4]. The duration of load has been perceived to be the dominant variable in predicting the fatigue life of wood. The definition of creep is the deformation of an element subjected to sustained load for a period of time. Wood is a rheological material, and therefore the properties will be dependent on the load history and the length of time under loading. For example, wooden beams that sag if dead load is too high. Rupture caused by creep is also called static fatigue, R=1. Sustained load can highly influence the residual capacity. It is recognized that the duration of load will have an impact on the fatigue life, however this effect is not further evaluated in testing. Traffic load is assumed to be applied for a short time.

3 Literature

3.1 Intro

This chapter is containing information that originates from a collection of literature connected to fatigue in timber. Some literature on withdrawal capacity of threaded rods is also included, to make a basis to compare with the static testing. The literature study is important, as the research on the area of fatigue in timber is not very developed yet. To get a better view on how much information that exists and to get independent result. The goal is to obtain information and results that are comparable with the laboratory testing. There is a lot of different research conducted in the last few years concerning fatigue in timber. To limit the amount of articles, the ones with information on other timber connections subjected to fatigue testing were prioritized. Especially interesting is the research involving bonded-in rods, as they are used in a similar way and might be the largest contestant to threaded rods.

3.2 NS-EN 1995-2:2004/NA:2010 (EC5 - Part 2)

Eurocode 5, hereafter referred to as EC5, is the European standard for design of timber structures. This standard was adopted as a Norwegian Standard in February of 2005. Part 2 regulates bridge design and is the relevant part on information regarding fatigue design. Eurocode 5: Design of timber structures – Part 2: bridges [11] is containing the current general design rules concerning fatigue in timber structures. When designing bridges, it is important to include the effect of cyclic load imposed by traffic load. The current Eurocode is limited to general rules for the full bridge, and does not take into account different connections or structural elements.

EC5 part 2 is covering some guidance to how to design structures in timber subjected to cyclic loading. Fatigue is mentioned with a sentence in EC5 - Part 2, 6.2(1)P:

> "For structures or structural parts and connections that are subjected to frequent stress variations from traffic or wind loading, it shall be verified that no failure or major damage will occur due to fatigue."

A simplified method for deciding if a fatigue control is needed is given in EC5 – part 2, A.1 (3):

$$\kappa = \frac{|\sigma_{d,max} - \sigma_{d,min}|}{\frac{f_k}{\gamma_{M,fat}}} \tag{11}$$

$\sigma_{d,max}$ The numerically largest design stress from the fatigue loading.

$\sigma_{d,min}$ The numerically smallest design stress from the fatigue loading.

f_k The relevant characteristic strength.

$\gamma_{M,fat}$ The material partial factor for fatigue loading.

The factor κ from the equation above is a limit value. If κ is bigger than the given value for the structure in EC5 – Part 2 6.2(3), an extended control of the effects of fatigue is needed. In this case with screwed-in threaded rods, the limit value is 0.15 for "other connections", while the characteristic strength would be the characteristic withdrawal strength. This formula shows a small limit value before the extended fatigue control has to be conducted:

NS-EN 1995-2:2004/NA:2010 table NA: $\gamma_{M,fat} = 1.0$

$$\kappa = \frac{|\sigma_{d,max} - \sigma_{d,min}|}{\dfrac{f_k}{\gamma_{M,fat}}}$$

$$0.15 = \frac{|\sigma_{d,max} - \sigma_{d,min}|}{f_k}$$

Switching with the notation from chapter 2.2:

$$0.15 = \frac{|\sigma_{max} - \sigma_{min}|}{\sigma_{ref}} = \Delta f$$

It the normalized stress range is larger than 0.15 an extended fatigue control is necessary. In Eurocode 5 part 2 paragraph A.3, the extended fatigue verification is described.

$$\sigma_{d,max} \leq f_{fat.d} \tag{12}$$

$$f_{fat,d} = k_{fat} \frac{f_k}{\gamma_{M,fat}} \tag{13}$$

$$k_{fat} = 1 - \frac{1 - R}{a(b - R)} \log(\beta N_{obs} t_L) \tag{14}$$

$$N_{obs} = 365 n_{ADT} \alpha \tag{15}$$

N_{obs}	The number of constant amplitude stress cycles.
t_L	The design lifetime of the structure.
a, b	Coefficient from EC5 part 2 Table A.1
n_{ADT}	The expected annual average daily traffic of the structure. (>1000)
α	The expected fraction of observed heavy vehicles passing the bridge.
β	The factor that takes into account the failure consequences.
$f_{fat,d}$	The design fatigue strength.
k_{fat}	Factor for reduced strength depending on number of cycles.

When using $\beta=1.0$ (No major damages) and knowing that N_{obs} is the number of constant amplitudes from the fraction of heavy vehicles in the traffic load. $N_{obs}\, t_L$ is the full number of cycles estimated that the structure has to endure throughout its lifetime. This can be plotted in the S-N curve to compare with experimental results in later chapters.

$$\beta N_{obs} t_L = N$$

$$k_{fat} = 1 - \frac{1-R}{a(b-R)}\log(N)$$

$$f_{fat,d} = f_k \left(1 - \frac{1-R}{a(b-R)}\log(N)\right)$$

$$\sigma_{d,max} \leq f_{fat.d}$$

Some values for the coefficients a and b can be found in EC5 part 2, Table A.1. None of these values corresponds directly to the connection with threaded rods, and this shows that the general experimental basis is limited. Example of the formula using the values given for structural elements subjected to tension ($R=0.1$):

$$k_{fat} = 1 - \frac{1-0.1}{9.5(1.1-0.1)}\log(N)$$

3.3 Withdrawal Capacity of Threaded Rods Embedded in timber Elements [1]

This is a journal article conducted by Haris Stamatopoulos and Kjell A. Malo. Haris Stamatopoulos is currently at the Department of Structural Engineering at Norwegian University of Science and Technology with the title of postdoctoral fellow. His doctoral thesis was delivered in February of 2016 with the title "Withdrawal Properties of Threaded Rods Embedded in Glued-Laminated Timber Elements" [2]. Kjell A. Malo is a professor at the Department of Structural Engineering at Norwegian University of Science and Technology. He is lecturing at the university in the subject Timber Structures. Both are supervisors for this thesis. This article presents an investigation on withdrawal capacity of screwed-in threaded rods embedded in glulam elements. It was included as a part of the doctoral thesis by Haris Stamatopoulos.

The goal in this paper was to investigate the withdrawal capacity and stiffness of threaded rods embedded in timber. Other reports concerning similar tests have the tendency to neglect the withdrawal stiffness. Several experimental tests were conducted to support a theoretical approach. The theory is developed based on classical Volkersen theory [16] on glued connections applied to axially loaded connectors [17] with the use of a bi-linear constitutive law. The theory is fund to provide a good prediction of the experimental results achieved in this report. By the experimental studies, it is shown that it is close to linear relation between the withdrawal capacity and the embedment depth in the glulam specimen.

The experimental tests were conducted to obtain values, which could be used to validate the theory. These results are relevant with respect to the static tests conducted in this thesis. Similar elements of glulam are used with the similar moisture content and temperature from the same manufacturer. The dimensions of the threaded rods are constant with a diameter of 20 mm, which deviates from the present experimental testing. Embedded in glulam elements, the tests have variating embedment depth, element geometry and rod-to-grain angle. The results can be compared with present experimental static reference tests with linearly scaling in respect to difference in embedment depth and rod diameter. This is a rough estimate, but it is assumed to support the values obtained for withdrawal capacity. Results obtained from experimental research on static reference tests are included in chapter 5.

3.4 Fatigue Strength of Dowel Joint in Timber Structures [18]

Kjell A. Malo, who is previously introduced in 3.3, conducted this report. The background for this paper was the increased use of dowel-type connections, while the fatigue characteristics still are largely unknown. This investigation was connected to the project "Fatigue of Timber Bridges", which constitute a part of the Nordic Timber Project. Fatigue properties of dowel-type connections were investigated and compared with available design rules in EC5.

The screwed-in threaded rods and dowel joints investigated in this paper can be used in similar bridge connections in tension. Dowel joints can be used in a large range of connections in timber. This type of connection have been increasing the economic competitiveness of large-span timber structures. The length of the spans are often limited by

the transportability. Dowel joints enable several beams to be jointed on site, and consequently larger spans can be reached.

Dowel joints with slotted-in steel plates has been used with great success to connect large spans of timber elements in roof structures in sports arenas. These joins have also been used in timber bridges; one example is the bridge in Figure 3. Subjected to cyclic loading, the properties had to be properly tested and assessed. Three static tests, nine embedding strength tests and 42 tests on fatigue have been conducted on the connections.

A table containing the fatigue test results from the experimental tests are included (Table 3 in the report). This table is used as a base for guessing at which load range the fatigue failure will occur in the HCF area with threaded rods. Fatigue failure occurred after 10^4 cycles but before $2 \cdot 10^6$ for stress ratio 0.1 in the load ranges between 0.675 and 0.563.

This paper concludes that dowel joint may experience fatigue failure when subjected to cyclic load. Stress ratio is found to be an important parameter in demining the fatigue strength. The fatigue strength can be considered in accordance with Wöhlers classical work, with a decaying linear function of the logarithm of the number of cycles to failure (S-N- curve). From the experiments, it was observed that the use of maximum stress as fatigue parameter seems more reasonable than the use of stress range. Lastly, a tentative proposal of design verification was made.

Based on Eurocode 5 [11] :

$$\sigma_{d,max} \leq f_{fat.d}$$

$$f_{fat,d} = k_{fat} \frac{f_k}{\gamma_{M,fat}}$$

$$k_{fat} = A \log N + \log B \tag{16}$$

Table 1: Values of strength parameters

R	A	B
0.1	-0.066	0.96
-1.0	-0.098	0.94
Independent of R	-0.07	0.95

3.5 Fatigue Behaviour of Lagscrewbolted Timber Joints [19]

This is paper by Meng Gong, Kohei Komatsu and Makoto Nakatani refers to the research on fatigue behaviour of lagscrewbolted timber joints in axial loading at high load ranges. Meng Gong is a PhD at the Faculty of Forestry and Environmental Management at the University of New Brunswick. He began his research in wood science in 1987. His area of expertise is within and timber engineering, lumber quality and wood mechanics [20]. Kohei Komatsu is a professor at Kyoto University, and a strong advocate of internationally collaborate research. He has authored or co-authored more than 90 publications on timber engineering and developed the fastener tested in this research. Makoto Nakatani joined the Wood Research Institute at Kyoto University in 1999. In 2004, he was working on his doctoral degree in timber engineering.

Lagscrewbolts (LSB) was at the time, a newly introduced type of fastener. The behaviour of lagscrewbolted connections during extreme events like earthquakes or cyclones were investigated. The specimens were made of lagscrewbolts embedded in Douglas-fir glulam parallel to the grain. The effect of different embedment depth are investigated.

As previously mentioned, low-cycle fatigue is characterized by a low number of cycle repetitions before experiencing failure. The testing was conducted with application of high stress levels of $F_{max} = 0.95\ F_{ult}$ and $F_{min} = 0.1\ F_{ult}$. Tests were terminated if the failure did not occur before reaching 500 cycles. The load was inflicted on the specimens with a frequency of 0.1 Hz with a triangular waveform (constant rate of stress).
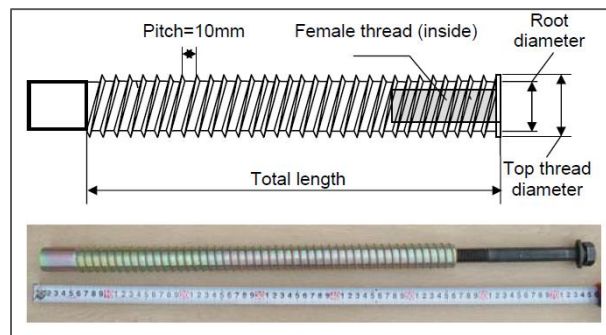
Figure 9: Geometry of LSB [19]

The outer thread diameter was 30mm, embedded in glulam specimens with cross section of 150x150mm of different lengths. Figure 10 shows the results obtained for the three embedment depths, 200mm, 300mm and 400mm. Static tests show that the max capacity were reached at about 2mm regardless of the embedment depth. The capacity drops to the point of 10mm slip, where the capacity is held and somewhat increased and decreased again when reaching 20 mm slip. This effect might be attributed to the pitch of 10 mm, where the LSB is "setting" the pitches in the pattern inside the wood made by the original pitch.
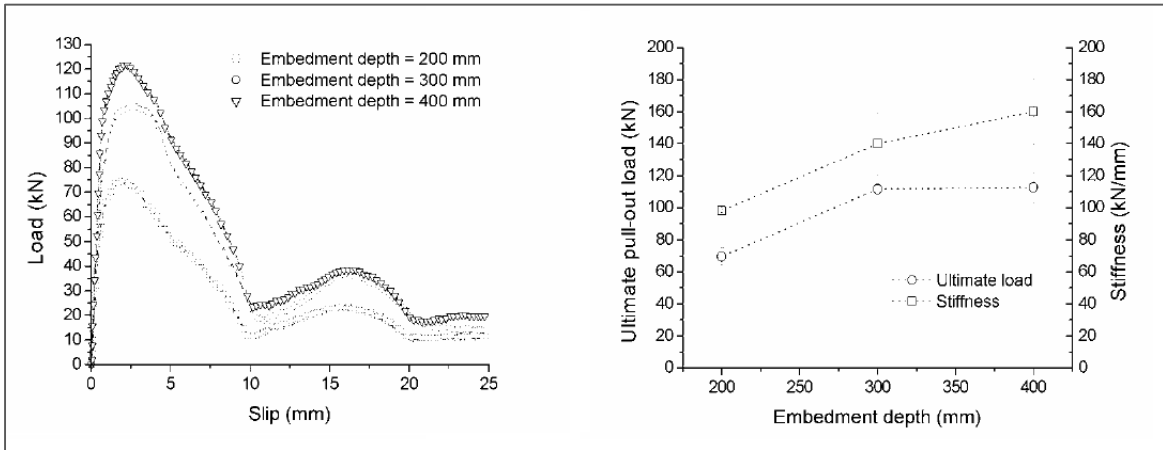
Figure 10: Results from static testing [19]

Information on cyclic residual stiffness and cyclic creep slip are also included in the report. However, this is not that relevant as the testing is conducted at LCF. Visual inspection after both cyclic and short-term loading tests shows big difference in fracture of static and cyclic testing. The cyclic test failure is characterised by more fibres breaking and coarse fracture surface. Static test failure have more whole sections of broken fibres and the fracture surface is smoother.
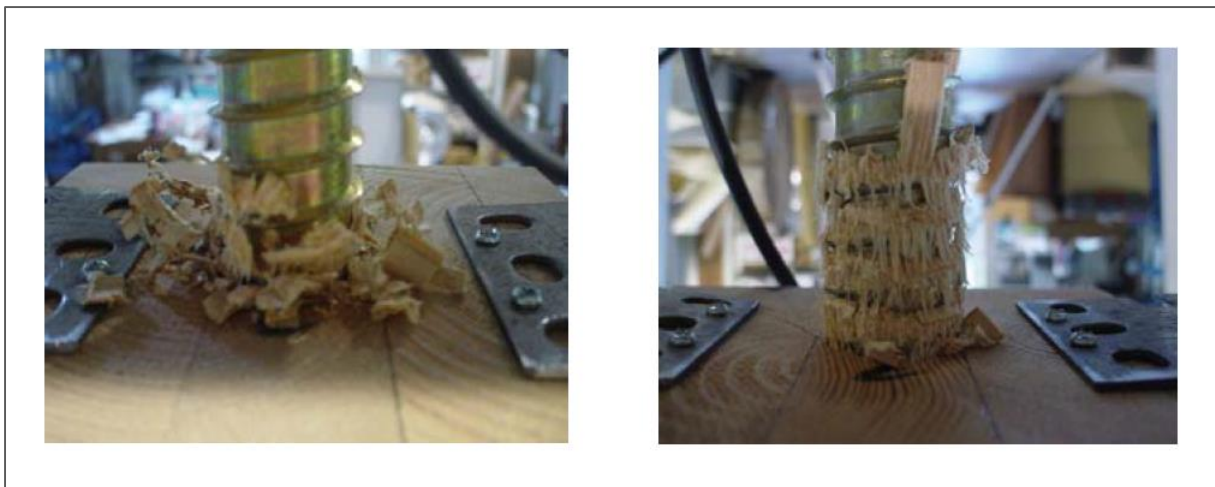
Figure 11: Fracture morphology under static test (left) and cyclic test (right) [19]

3.6 Fatigue properties of wood in tension, compression and shear [14]

The authors of this article are Martin Ansell and Peter Bonfield. This article was first published in 1991, and was republished as a part of the book "Wood composites" by Elsevier Inc. in 2015 with Martin Ansell listed as author.

Martin Ansell is currently an associate professor in the Department of Mechanical Engineering at the University of Bath. He was awarded his degree in Materials Science from the University of Sussex before continuing to take a PhD in Solid State Physics at Chelsea College, University of London. His research includes creep and fatigue of wood and natural fiber composites, the development of bonded-in technology for joints in timber structures and characterization of polymers and composites for industrial applications [21]. He is author and co-author of many of the articles presented in later chapters.

Peter Bonfield is a visiting professor in the Department of Architecture and Civil Engineering at the University of Bath, where he has also been awarded an honorary doctorate in engineering. He has a PhD in wind energy and the design of turbine blades. He joined BRE (British Research Establishment) in 1992 and in 2012 he took up the role of chief executive of the BRE Group [22].

The background for this research was the need for fatigue assessment of wind turbines. Two types of veneer laminates were used in testing: 4 mm thick Khaya ivorensis and duglas fir. It was conducted to investigate the properties of wood laminates in tension, compression and shear. One concern was associated with gripping of the specimen in axial, but this was overcome. The solution of introducing a sacrificial veneer between the aluminum tabs and the end of the sample showed effective. The test sample was protected from compression from the grips, and the plastic deformation happens in the sacrificial veneer.

Tests was conducted on the specimen with different stress ratios to investigate the effect of different stress ratios. Many different stress levels were used to gain information to determine the S-N-curves. The stress ranges are not given by the authors, but is estimated from the plot for R=0.1 to span from 0.3375 to 0.7875 with most at larger stress ranges. For this stress rate S-N-curve is displayed in Figure 12 above to the right.
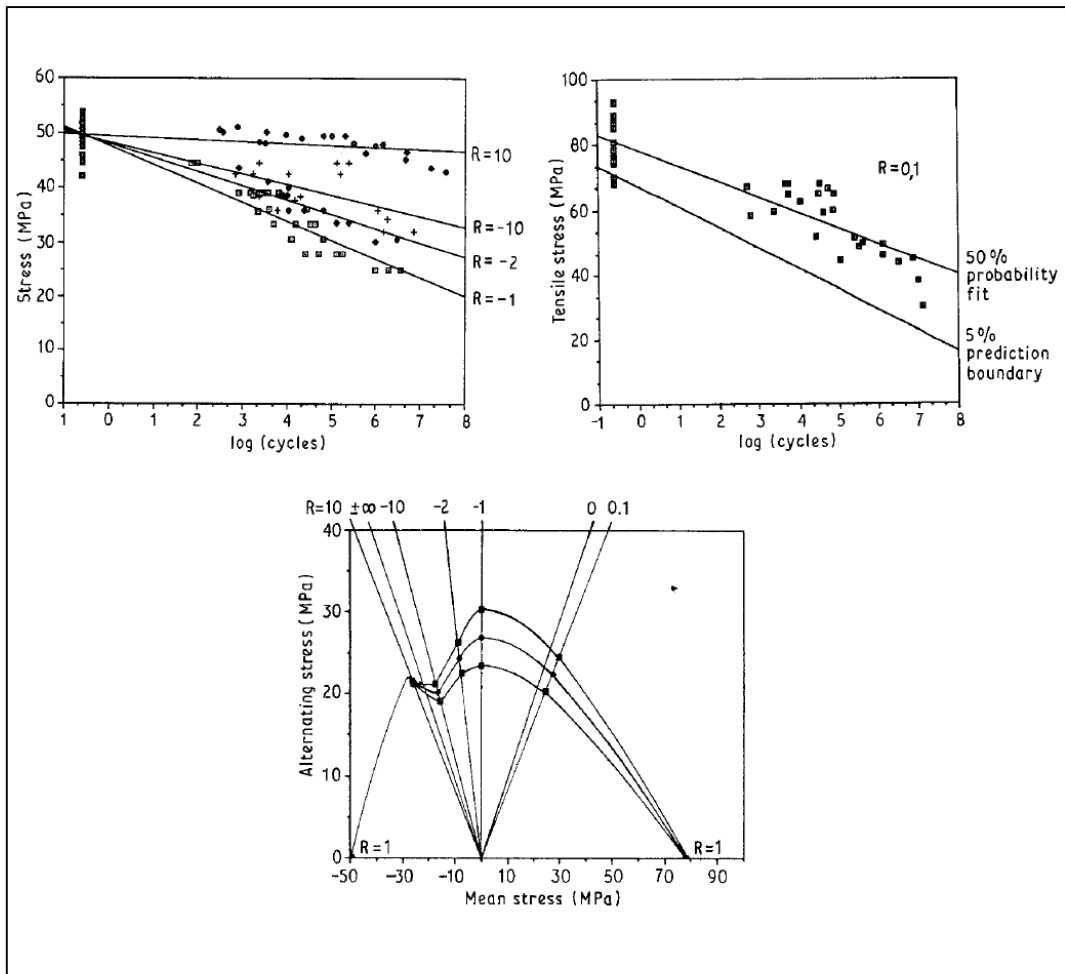
Figure 12: S-N-data for Khaya axially loaded (above), constant life diagrams for axially loaded Khaya (below) from [14]

The static reference tests gave a maximum reference load 49.5 kN in compression and 80.0 kN in tension. Wood has better resistance in tension than in compression. The tension failure is characterized by the brittle tearing of the fibers, while in compression the failure happens by collapsing of cell walls and shows a more ductile behavior. The results support the theory that fully reversed loading (R=-1) is the most critical situation. The steep S-N-line in Figure 12 displays this effect where fatigue life decays at a higher rate than with other stress ratios.

A new observation was discovered in the constant life diagrams at the point where load becomes all compressive. Below in Figure 12, the break from the otherwise smooth curve is visible. The size effect was tested on some samples with four times the cross-sectional area with R=-1, and showed no significant reduction in fatigue life at any particular maximum stress.

21

3.7 Fatigue Properties of Jointed Wood Composites [23]

The article consists of two parts and are written by Ian P. Bond and Martin Ansell which was introduced in chapter 3.6. Only part one is included here: Part 1 Statistical analysis, fatigue master curves and constant life diagrams. Part two is containing research on effect of alternating amplitude and is not particularly relevant here.

Professor Ian P. Bond, works at University of Bristol with B.Sc. in Materials Science from 1991 and later a Ph.D. in Materials Science from 1995. He is a recognized expert on multifunctional composites; including self-healing, adaptive materials, damage tolerance and bio-inspiration/bio-mimetics [24].

The veneer elements used in wind turbine blades are end-jointed with scarf joints. Former testing was conducted on whole members [14], and there was a need to understand the jointed element. Static testing on similar geometries with and without joints were compared. Table 2 summarize the static tests. It appeared that the scarf joints reduces the difference of static capacity in tension and in compression. This might be explained by the joints acting as initiations sites in tension, while in compression they are not notably influential on the capacity.

Table 2: Strength data for scarf and unjointed Khaya laminate

	Unit	Compression		Tension	
		Unjointed	Jointed	Unjointed	Jointed
Mean	[MPa]	-49.47	-54.16	81.8	76.16
S. D.	[MPa]	-2.77	-5.98	9.3	5.59
C. o. V.	[%]	5.6	11.04	11.37	7.35
No. of samples		32	11	17	9

These connections were tested with Khaya, black poplar and European beech in an effort to find a better wood source to use in wind turbines with better economic and environmental properties. The stress was applied with a constant rate of stress (triangular shaped cyclic load), and at three different load ratios (3, 0.33, -0.84, -1, -3). In single-mode loading (tension-tension or compression-compression), values with large scatter were obtained. It resulted in almost coincidental regression lines for the S-N-curves. However, it was found that the results of R = -1 cyclic load of the different wood species were remarkably similar when normalized with the compressive strength. An S-N master curve for a generic scarf-jointed wood laminate with reversed load was derived:

$$\sigma = \sigma_c(0.97 - 0.103 \log N) \tag{17}$$

3.8 Fatigue Damage and Hysteresis in Wood-Epoxy Laminates [25]

This article is authored by C. L Hacker and Martin Ansell. Ansell is previously mentioned, but no information on C. L. Hacker was found. He/she did work for Ove Arup and Partners in the research and development department in 2001. The report was conducted at the Department of Engineering and Applied Science, University of Bath.

The properties of Khaya veneer were investigated at stress ratios 10, 0.1 and -1. Tests were performed similar the tests in "Fatigue properties of wood in tension, compression and shear" [14]. Hysteresis loops were logged at certain intervals during the test, with the goal of following the damage accumulation of fatigue. This was successfully done for all the different stress ratios. Results concerning tension-tension load is the most relevant information, and are therefore included.
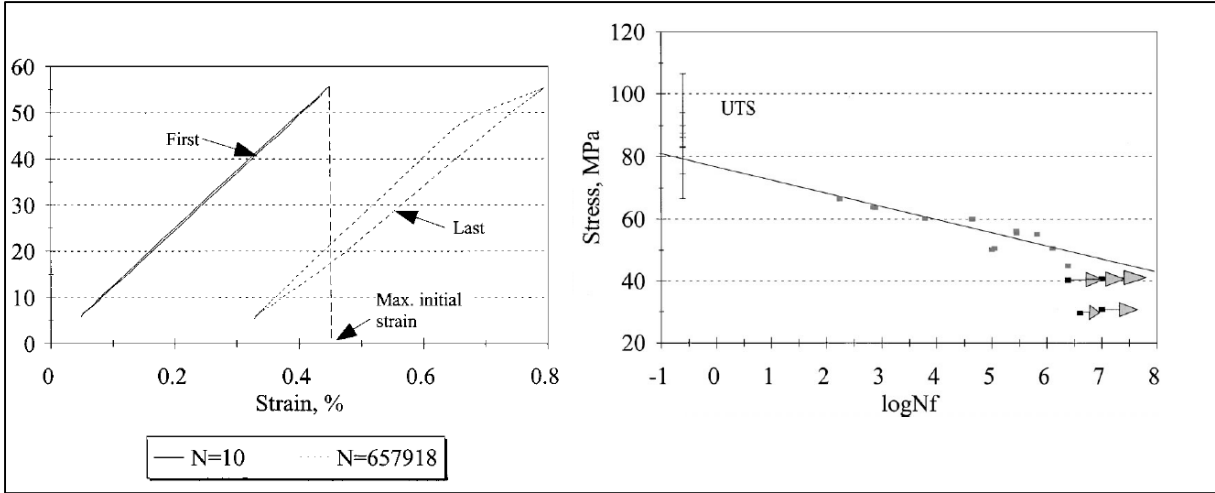
Figure 13: First and last hysteresis loop with R=0.1 and a peak stress of 55 MPa (Left), S-N curve plotted for R=0.1 with different load levels [25]
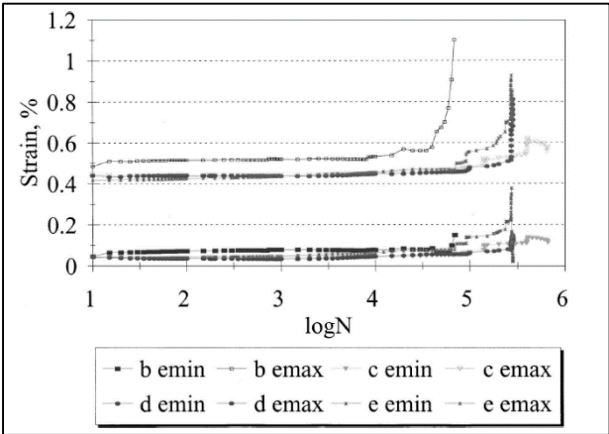
Figure 14: Maximum and minimum strain plotted for four specimens at R=0.1 with a peak stress of 55 MPa [25]

The mean tension strength was measured at 85.4 MPa. With *R*=0.1, changes in loop shape was relatively small for run out tests and the tests with almost instantaneous failure. The run

out tests were observed at tests with peak stress of 40 MPa and less, which corresponds to 0.468 in normalized maximum stress level. Tests with peak stress of 65 MPa, or normalized maximum stress of 0.761, where found to reach a small number of cycles before failure. However, at intermediate stress level the progressive crack growth could be observed. In this case at a normalized maximum stress level of 0.644 (peak stress 55 MPa), which is displayed in Figure 13. Strain behavior was relatively constant for tension-tension until end of fatigue life, then there were sudden damage events. The hysteresis loop at the last cycle shows that there the area has increased. From first to last loop, the area has increased from relatively small to large which means there is a high level of energy dissipation at the end.

3.9 Fatigue of Wood and Wood Panel Products [15]

This is a chapter authored by Martin P. Ansell in the book "Fatigue in Composites" from 2003. The book were edited by Bryan Harris. This contains in most parts a general picture on wooden structure and considers the conditions of fatigue in wood. Many of the articles described in this chapter is previously included. Lastly, the chapter concludes with an assessment of fatigue in timber joints with bonded-in rods. The bonded-in rods are here assessed with the original proceedings in 3.10.

3.10 Fatigue Performance of Bonded-In Rods in Glulam, Using Three Adhesive Types [26]

Four authors are listed on this work. Martin P. Ansell and K. Harvey from the University of Bath. From TRADA (Timber Research and Development Association) at the time, chief research engineer Christopher J. Mettem and research engineer R. J. Bainbridge. This proceeding from the Working Commission W18 – Timber Structures in Delft from 2000 is supported by a later released journal article, "Bonded-in rod connections for timber structures – Development of design methods and test observations" [27] from 2002. Both papers are released by the same authors based on the same experimental tests. This work was conducted as a part of including design rules regarding bonded-in rods in Eurocode 5 – part 1 [6]. A work group was put together and found that the existing knowledge at the time was not sufficient as source for the standardisation needed. The EU GIROD (Glued-in rods) project involved several countries and aimed to draft an acceptable standard for joints with glued-in rods.

The properties of different connections with bonded-in rods using three types of adhesives were tested. Especially the two component polyurethanes was thoroughly investigated. This adhesive has proved to be less brittle than traditional adhesives used in timber connections. At the time, there were no standardized test methods or requirements to the application of the adhesive component. With adhesive bonding, there are several challenges with connections that have to be investigated. Adhesives were placed in three generic classes based on the nature of failure when subjected to axial loading (Table 3).

PRF	EP	PUR
Failure within adhesive, brittle	Wood failure around bond line	Wood-adhesive interface failure
Good adhesion to wood	Good adhesion to wood	Low adhesion to wood
Low adhesion to steel	Good adhesion to steel	Good adhesion to steel
Steel rod is "loose", and only steel rod is pulled out	Rod is pulled out with a "plug" of wood fibres	Adhesive surface to wood contains bubbles, probably due to reaction with moisture

Two specimen geometries were tested, based on two different steel rods: 8mm diameter high tensile steel and 16 mm diameter mild steel. Rods are inserted parallel to the grain. Experimental tests were conducted with axial load application at low frequency of 1 Hz with stress ratio of R=0.1. The objective were to investigate the fatigue damage in various load situations. Two different specimen geometries, three types of adhesive at three load levels were tested. With three tests for each type of specimen, it makes in total 54 tests. Figure 15 shows test show the two geometries with different steel grade, rod diameter, bonded-in length and size of the specimen. The steel rods were inserted by hand with constant pressure and rotation, in a 0.5mm thick bond.
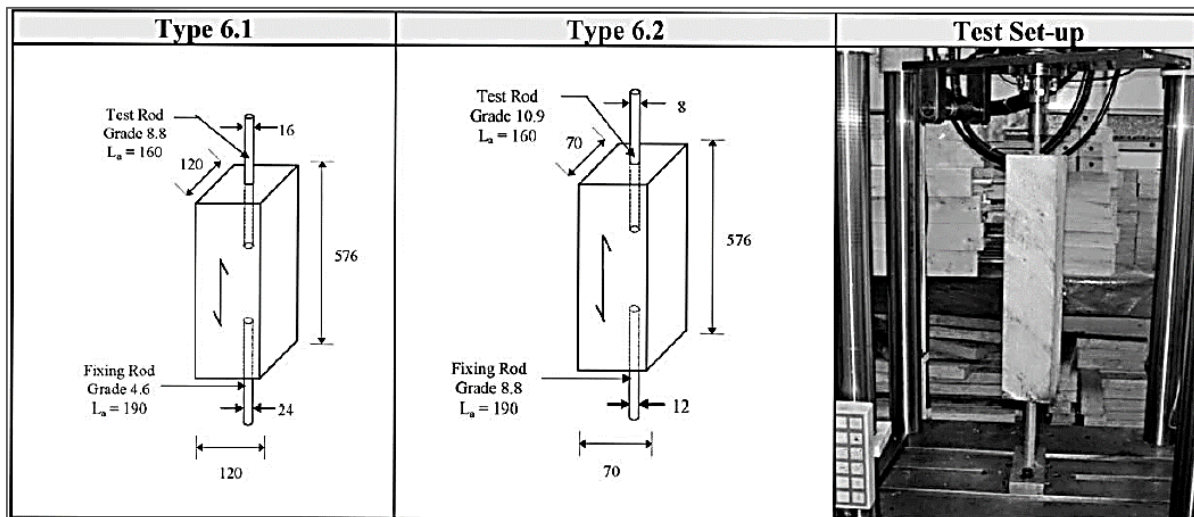
Figure 15: Two specimen geometries, Setup [27]

Test series	6.1a	6.1b	6.1c	6.2a	6.2b	6.2c
Laminate class	C35	C35	C35	C35	C35	C35
Moisture content	12% ±1%	12% ±1%	12% ±1%	12% ±1%	12% ±1%	12% ±1%
Static capacity	55kN	68kN	57kN	28kN	34kN	28kN
Load level 1	0.91	0.81	0.88	0.68	0.68	0.86
Load level 2	0.78	0.69	0.79	0.57	0.59	0.71
Load level 3	0.64	0.59	0.70	0.46	0.50	0.61
Rod diameter	16mm	16mm	16mm	8mm	8mm	8mm
Rod steel grade	8.8	8.8	8.8	10.9	10.9	10.9
Glued-in length	160mm	160mm	160mm	160mm	160mm	160mm
Adhesive type	PRF	PUR	EP	PRF	PUR	EP

Load levels in Table 4 were estimated from S-N plots in (R. Bainbridge et al. 2002) [27], with the formula from 2.2:

$$f_{max} = \frac{F_{max}}{F_{ref}}$$

Four different failure modes were observed: Failure in rod, failure in the adhesive, failure in the interface between wood and adhesive and failure in the wood. There is sufficient variation in failure modes to confirm that fatigue failure can occur in any of the components. The different adhesives are found to be acting fundamentally different with respect to both fatigue failure and ultimate failure. Timber failure was observed in both tests with PUR and EP adhesive and resulted in a plug of timber surrounding the rod with the adhesive bond intact.
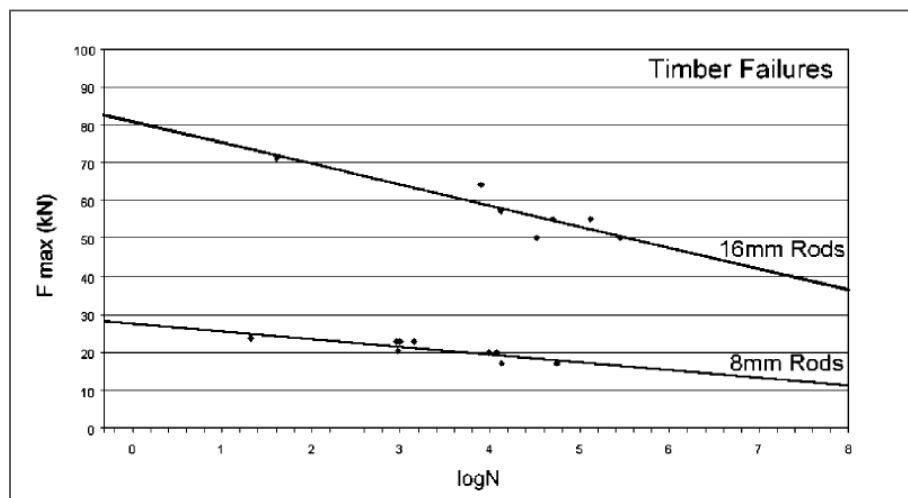
Figure 16: Fatigue failure in specimens with failure in timber [27]
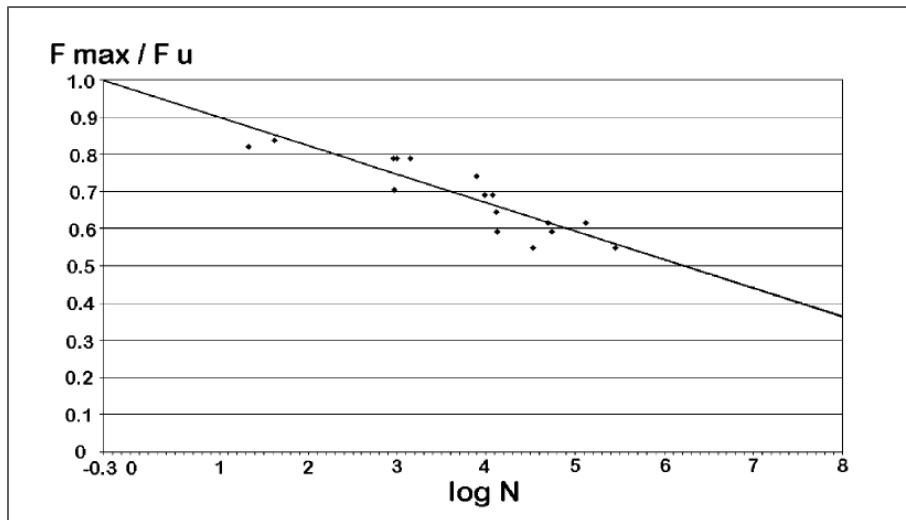
Figure 17: Normalized values for all specimens with fatigue failure in timber [27]

It is in general shown that the fatigue performance of epoxy adhesive is better than the alternatives of PRF and PUR. The plots show that for greater load levels, the specimens with epoxy have longer fatigue life. This was the case of both rod and specimen dimensions.

3.11 Experimental Study of Static and Fatigue Strengths of Pultruded GFRP Rods Bonded Into LVL and Glulam [28]

Authors of this journal article from 2004 are Mehrab Madhoushi and Martin P. Ansell. Mehrab Mahhoushi is currently an associate professor in the Department of Wood and Paper Engineering at the Gorgan University of Agricultural and Natural Resources. He finished his doctoral degree in 2003 at the University of Bath with Martin P. Ansell as supervisor.

This paper investigates the fatigue behaviour in glass fibre-reinforced plastic rods (GFPR rods) subjected to cyclic load with a stress rate of 0.1. The rods are inserted into elements of laminated veneer lumber (LVL) supplied by Kerto, and Swedish glulam cubic samples supplied by TRADA Technology Inc. In particular, the effect of different adhesive thickness and rate of loading on fatigue life were examined. An EP adhesive was chosen in accordance with the results from (R. Bainbridge et al. 2002) [27].

The glued-in rods have many great properties. They show great stiffness in axial loading and since they are bonded in the wood, they have a high fire-resistance. In addition, the aesthetic appearance is beneficial and makes them ideal to repair old rotted beam-ends in rehabilitation work in traditional buildings. This paper deals with the properties of GFRP rods, to investigate the possibilities of using it as an alternative to the traditional steel rods. GFRP rods are lighter and have better resistance against humid environment. GFRP have improved performance as it has good compatibility with both timber and adhesive.

Experimental testing was conducted on timber elements of 63x63x63mm, with the rod embedded full length of the specimen. 8mm rods were inserted with three different adhesive

thicknesses (0.5mm, 2mm and 4mm). stress levels for cyclic loading were selected at 80%, 75%, 50%, 40% and 25%.

Table 5: Results from five static tests on each specimen

Specimen	Adhesive thickness	Mean max. tensile load	Mean max. shear stress, τ_{ra}*	Mean max. shear stress, τ_{at}**
	[mm]	[kN]	[MPa]	[MPa]
LVL	2	12.50	7.90	5.27
Glulam	2	15.80	9.99	6.66
Glulam	4	16.68	10.53	5.27

*Rod-adhesive interface shear stress
**Adhesive-timber interface shear stress

It was discovered that 4mm glued-lines suffered instantaneous failure at load level 80%, 75% and 50%. While 4mm showed better static performance than the samples with 2mm, the bond is not ideal with respect to different load cycles. This result prompted the study of effect of load rate on fatigue life. It was found that the 4mm samples fatigue life was highly dependent on load ratio, while the 0.5mm where not very affected.

Figure 18: Failure modes in stress-rate-effect study (a) 0.5 mm, (b) 2 mm and (c) 4 mm glue-line thickness for LVL

Table 6: Percentile distribution of failure modes in study of the effect of rate of loading

Failure mode	0.5mm (%)	2mm (%)	4mm (%)
RR*	0	50	89
T**	73	50	11
RR & T	27	0	0

*Resin-rod interface failure
**Timber failure

The failure modes in fatigue testing of specimens with 4mm bond were dominated by the failure in the adhesive, without any damage in the wood or the rod. The adhesive was found to be the weak component in respect to fatigue performance with larger bond thickness. In the cases where the bound had thickness of 0.5mm, the tests were dominated by failure in the wood. This is the similar adhesive thickness as in the study of bonded-in steel rods (R. Bainbridge et al. 2002) [27].
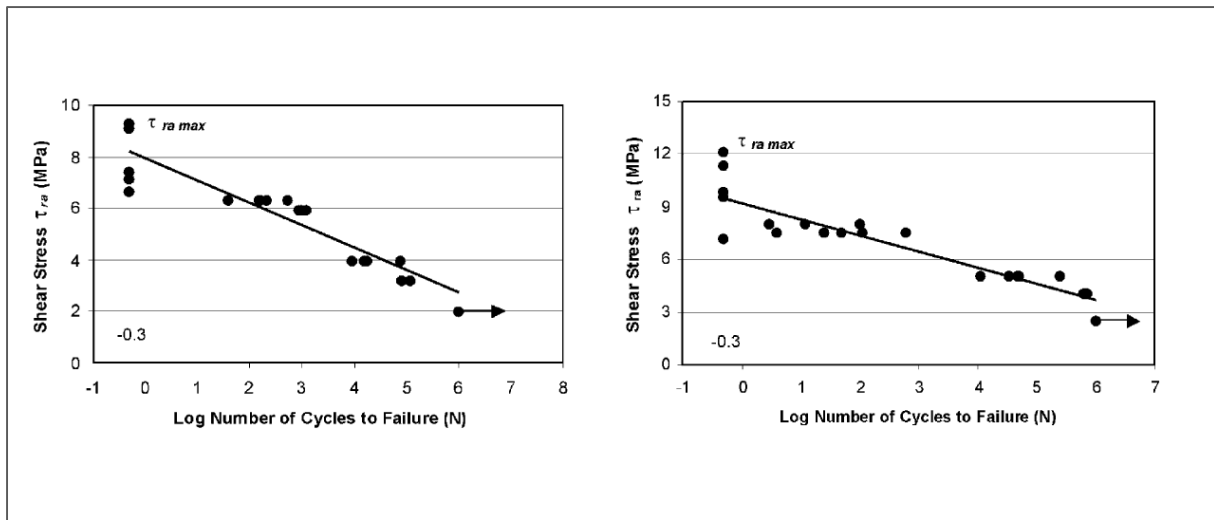
Figure 19: Shear stress in rod-adhesive interface with 2mm adhesive thickness in LVL (left) and glulam (right)

The authors concluded that although increasing the thickness of the adhesive in question can give better static strength, it might decrease the fatigue life depending on the loading. The dominant failure of 0.5 mm tests were in the timber. Failure modes changed with the rate of loading, the 4 mm specimen were more sensitive to the changes than the rest. The results given in the proceeding are limited to the plot of maximum shear stress in respect to N for failure in the rod-adhesive interface. Complete results would have been relevant to compare with present testing.

3.12 Fatigue and Cyclic Loading of Moment-Resisting Structures Connected using Glued-In GFRP Rods [29]

This research is conducted by Mehrab Madhoushi and Martin P. Ansell. This paper investigates the fatigue strengths of moment resisting timber structures (LVL-Laminated veneer lumber) connected with GFRP bonded-in rods. The background was to investigate the capacity on connections with simulated seismic load action. The ability of timber elements to absorb and dissipate energy generated from cyclic load is low and wooden members often show brittle failure in tension, bending and shear. It is therefore important that the joint are ductile and able to distribute the energy along the members, in particular in zones where there is a possibility of earthquake.

Two different joint configurations were investigated:

- L-shaped moment resisting timber structure of LVL with two GFRP bonded-in rods. Subjected to tension-tension at R=0.1.
- U-shaped frame of LVL with two pairs of bonded-in rods, with R=-1.
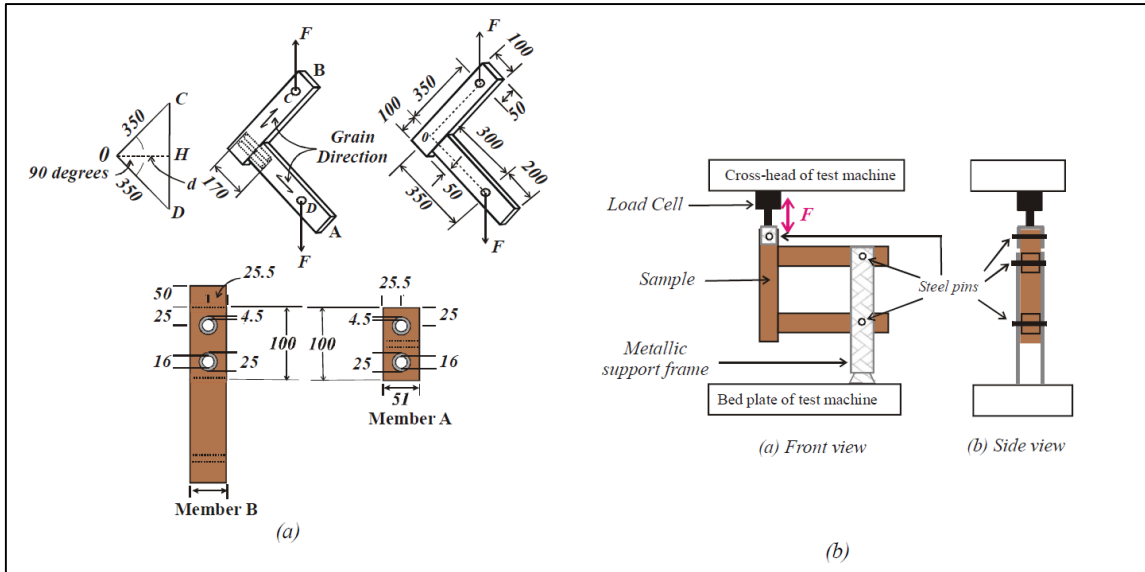
Figure 20: Illustration of sample geometry used in (a) L-shaped and (b) U-shaped connections

Rods with 16mm diameter and length of 170mm was used bonded with epoxy adhesive. It was determined that for the L-shaped connections, the fatigue life was dependant on the size of the stress level. The specimen was subjected to four stress levels: 75%, 50%, 40% and 30%. It can be seen from the bending moment-log N-curve, that 75% and 50% are acceptable load levels to obtain results in LCF. Lower load levels results in HCF failure.
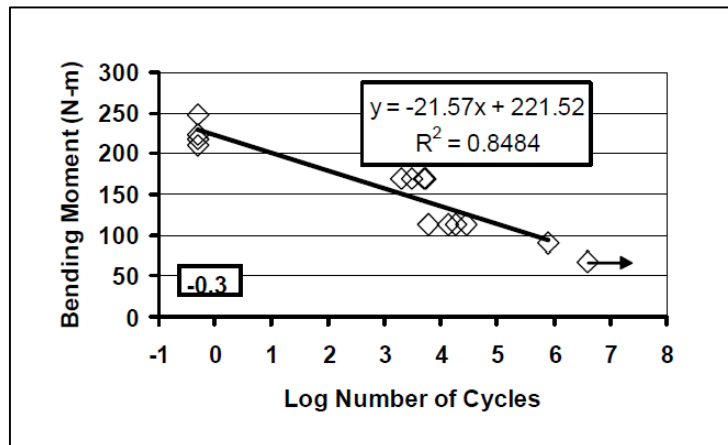
Figure 21: Results from L-shaped connections [29]

The L-shaped connection showed a trend of reduced cyclic modulus over time regardless of the stress level. Dynamic modulus is the ratio of stress to strain under cyclic load conditions, and is the slope of the hysteresis loop. It is a property of viscoelastic materials. Finally, this report concludes that both the connections displayed ability to dissipate the required energy from simulated seismic forces in displacement mode.

3.13 Behaviour of Timber Connections using Glued-In GFRP Rods under Fatigue Loading

This paper is by Mehrab Madhoushi and Martin P. Ansell, and consists of two parts regarding different connections. Both are investigating the fatigue properties of GFRP rods bonded-in in LVL elements with epoxy adhesive. The investigation is conducted to observe the strength and stiffness of connections in moment resisting structural joints when experiencing seismic forces. Part II is an extended research paper of the proceeding from the previous chapter [29].

3.13.1 Part I: In-line beam to beam connections [30]

This paper investigates the behaviour of bonded-in rods in an in-line beam-to-beam connection. The rods are tested with static and cyclic force application with a four point bending test. Cyclic load is subjected to the beam with R=10 (compression-compression) at load levels of 75%, 50% and 30% of the average strength, with frequency of 0.5, 0.75 and 1.25 Hz respectively. This setup is simulating the behaviour of a typical connection in a repaired beam, which is useful in restoration projects.
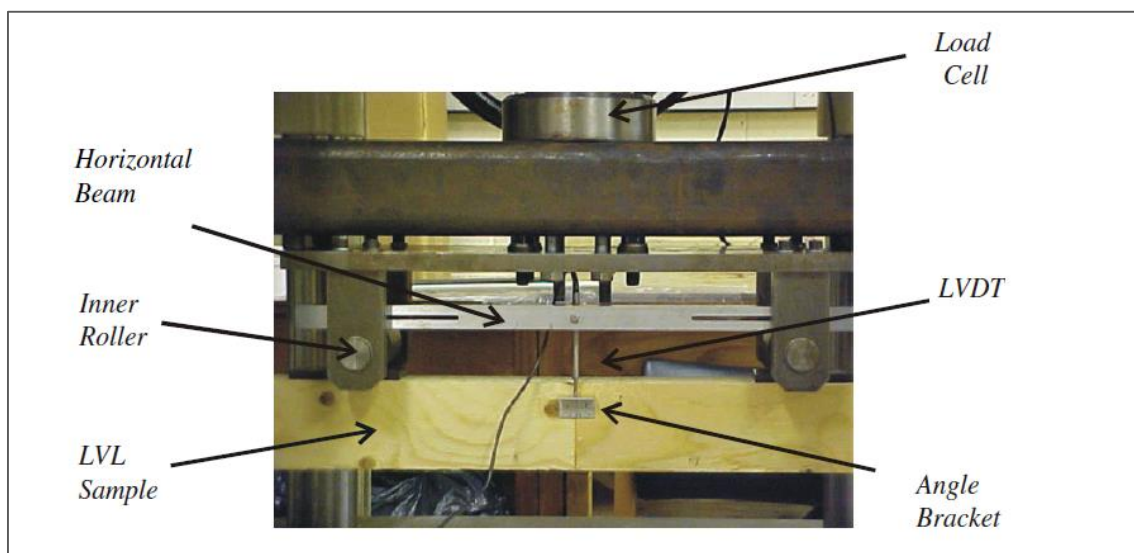
Figure 22: Setup in-line beam-to-beam connection [30]

Different beams tested, five static and nine cyclic:

       A: Unjointed LVL beam
       B: 8 mm diameter rod, 0.5 mm adhesive thickness
       C: 8 mm diameter rod, 1 mm adhesive thickness
       D: 16 mm diameter rod, 4.5 mm adhesive thickness

The different configurations were tested with two glued-in lengths and bonded with epoxy adhesive. The average maximum static failure loads is measured for each point in the four-point bending test. Static bending capacity in specimen A, B, C and D were measured to 33.75kN, 16.69kN, 15.88kN and 19.38kN respectively. The unjointed specimen showed

greater capacity, while the joints did not show significant variations in in respect to each other.

Specimens were marked as run-outs and terminated if failure is not obtained after experiencing more than 10^6 cycles without failure. Specimen A (unjointed sample) showed better fatigue strength than specimens with bonded-in rods. Out of specimens connected with rods, the specimen of type D showed largest capacity in fatigue at higher load levels. However, the regression line for specimen D was steeper. The observed failure modes in both static and fatigue testing were lower rod pull-out and timber splitting from compression in the connection along the upper rod.
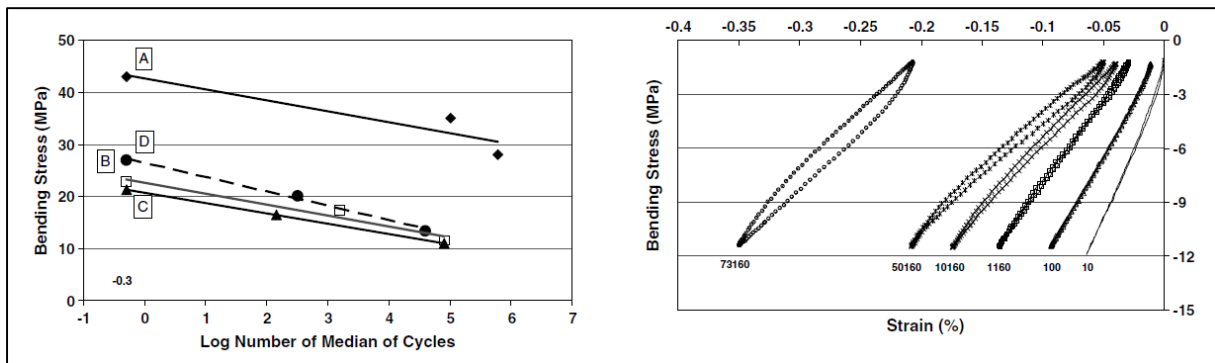
Figure 23: S-N curves for the different specimens (left) and hysteresis loop for specimen B at 50% stress level

The hysteresis loop area in Figure 23 increases with the number of cycles. This shows that more energy is distributed as the internal damage is increased and allow for more deformation and dissipation of energy. In general, the specimen without joint (A) is less able to dissipate energy during cyclic loading. This is not surprising, as the member will be stiffer with the absence of a joint. Specimen D was found to smallest ability in dissipating energy with 75% and 50% load level testing. The report concludes with the statement that glued-in joints with GFRP rods show good ductility and have enough ability to dissipate energy to be applied in structures located in earthquake zones.

3.13.2 Part II: Moment-resisting connections [31]

The fatigue of beam-to-column connections is investigated in this paper. L-shaped and U-shaped structure configurations were tested in both static and cyclic load conditions. This paper is written by the same authors as the paper presented in 3.12 and the specimens are illustrated in Figure 21. The results are the same as before, including more information connected to stiffness properties. Five static tests and ten fatigue tests were conducted on the L-shaped connection. The U-shaped connection was tested once in static and twice in cyclic load.

L-shaped frame

At low design fatigue load levels, the joint will be somewhat rigid. However, subjected to overload, such as from seismic load, the joint will experience an initial damage and be able to dissipate more energy. Figure 24 shows the shape of the hysteresis loop during the fatigue testing. The test at 50% stress level has an increase in area and a visible decline in the slope. While the results from 40% stress level shows little change in the overall shape, it is also somewhat increasing in deformation. The tendency is that at higher stress levels, the ability to dissipate energy is greater.
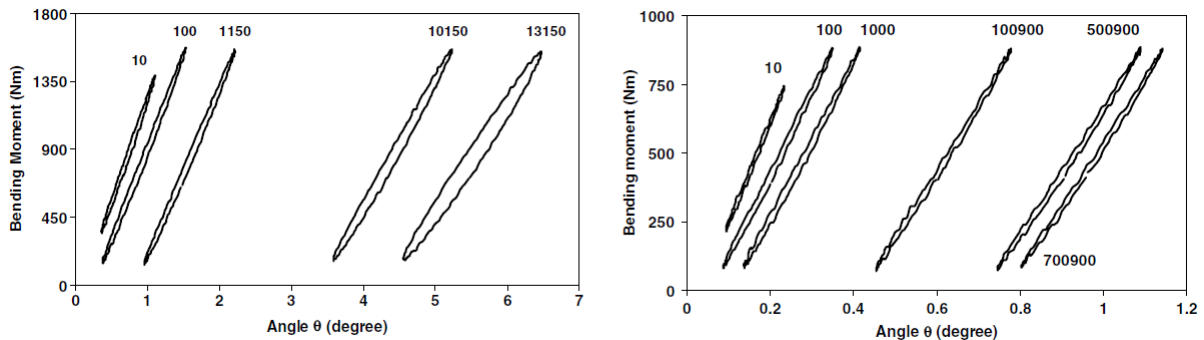
Figure 24: Hysteresis loop for an L-shaped connection at 50% (left) and 40% (right) stress level

The fatigue life of the L-shaped connection is increasing with decreasing stress level, and the tests at 30% were stopped after 10^6 cycles. Failure modes involves rod-pull-out of the inner rods and splitting of timber where the glued-in rods are perpendicularly inserted.

U-shaped frame

This frame was subjected to fully-reversed cyclic load in displacement control mode. It was found to have enough capacity in fatigue as well as the ability to dissipate energy. The stiffness decreases with increased displacement in three stages in both the tensile and the compression side of the hysteresis loop. The frames with GFRP rod connections will fail in the connection area, and can be designed to fail progressively and safely when subjected to seismic action.

3.14 Round Timber Bolted Joints Exposed to Static and Dynamic Loading [32]

This report is made by Doc. Ing. Antonín Lokaj, P.hD., and Ph.D. Kristýna Klajmonová in 2014 at VŠB-Technical University of Ostrava, Czech Republic. Antonín Lokaj is head of the Department of Building Structures at the Faculty of Civil Engineering. The tests in this report are conducted on round timber bolted connections with slotted-in steel plates, which makes them similar to the dowel joints. The problem is that the Eurocodes only cover connections where square timber and the round timber element do not behave similarly.

Round timber-connections are increasingly popular to use in structures like bridges, watchtowers and in playground equipment. The possibility of reinforcement of these

connections are also investigated, as these connections often are the weak link of the structure. In Figure 25, the highest round timber watchtower in central Europe (53 meters) is displayed. In a structure like this, the cyclic loads due to wind load are obviously an important issue for the design.

Figure 25: Watchtower near Lázně Bohdaneč (left), setup round timber bolted joint with slotted-in plate (right)

Tests on the connection in static and cyclic loading were conducted. In total, 47 test specimens were made. Round timber of spruce was used, with 12.4% moisture content and average density of 487 kg/m^3. The bolts had a diameter of 20mm and the slotted-in steel plate was 8 mm thick and 70mm wide. The round timber element had a height of 450mm and a diameter of 120mm. Holes for the bolts were made with 22mm diameter openings. In addition, different types of reinforcement of the connection were also tested in both static and cyclic load situations. Cyclic testing was conducted with frequency between 3 and 4 Hz.

The static capacity in tension were 67.26kN, and the specimens showed rather large variability. Static testing showed that the maximum tension forces was between 80% and 140% of the average static capacity. All unreinforced samples experienced failure in splitting of the wood in tension perpendicular to the grain, without any damage to the bolts. With reinforcement, the most common observed failure mode was in plug shear. The use of reinforcement made fracture less sudden and some fracture development would occur before complete loss of capacity.

Results from unreinforced samples indicated good correspondence with EC5 in static and cyclic performance. The S-N curve was derived with trend lines for all specimen configurations. Bolted joint with reinforcement showed significant increase in both static and cyclic performance. Five different solutions for reinforcement was investigated, and solutions with modified washers was found to be most effective. However, a solution with two screws to arrest the cracks were considered best suitable in this case because of its simplicity and low cost. The authors concluded that the reinforcements would increase the capacity of the joint with respect to static and cyclic load capacity.

3.15 Fatigue Design of Adhesive Connections using Perforated Steel Plates [33]

This research paper were conducted by professor Leander Bathon, Ph. D. student Oliver Bletz-Mühldorfer, M. Eng. Jens Schmidt and B. Eng. Friedemann Diehl at Hochschule ReinMain, University of Applied Sciences Wiesbaden Rüsselsheim Geisenheim, Germany. This paper were made for the World Conference on Timber Engineering 2014.

The behaviour of an innovating steel-to-timber connection when static and cyclic load conditions is investigated. The connection (hbv-system) is shown in Figure 26. This connection consists of a steel plate connected to timber elements using an epoxy adhesive. The perforated steel plate is interlocked within the timber element due to adhesive dowels, which makes it a highly rigid connection. The design is based on achieving failure in the steel, and therefore a sufficient capacity in the adhesive dowels is required.
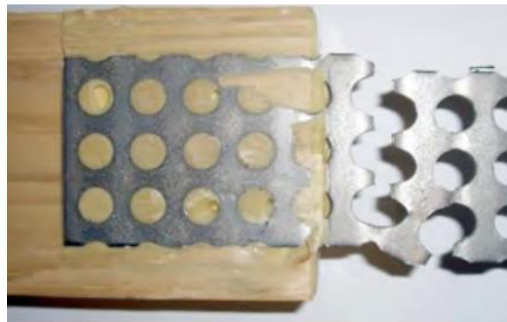
Figure 26: Tension test, hsk-connector

The research shows that these connections can be designed based on the load capacity and the stiffness of one adhesive dowel. Based on this, the authors suggest a characteristic load capacity of 1.2kN per dowel independent of the grain and number of adhesive dowels. Cyclic testing were performed in tension-tension with sinusoidal waveforms. The load was applied at frequencies between 3 and 10 Hz. A fatigue design is proposed with the formulas from EC5, with a=5 and b=2. This type of adhesive connectors allow new applications in timber design where timber can be used in configurations only known so far in steel and concrete.

3.16 Waveform Effect on Fatigue Behaviour of Laterally Loaded Nailed Timber Joints [13]

This research was conducted by Meng Gong, Ling Li and Ian Smith from the University of New Brunswick, Canada. Ph.D. Student Ling Li and Professor Meng Gong (earlier mentioned) are at the Department of Wood Science and Technology Centre. Ian Smith is a professor at the Faculty of Forestry and Environmental Management. Dr. Ian Smith has published over 200 technical articles on topics related to timber engineering, and is considered to be one of the leading experts on this topic in the world. Dr. Smith's book "Fracture and Fatigue in Wood" [4] was published by John Wiley and Sons in 2003. He has also published nine journal papers since 2002. Recognized as a leading expert worldwide on timber connections, his research results have been included in timber design codes in Canada, U.S., Europe, and the U.K.

This paper investigates the effect of different waveforms in fatigue testing on laterally loaded nailed timber joints. The topic of this research was to investigate the difference in nature of cyclic load situations caused by for example cyclones and earthquakes. Two load levels with two load frequencies were applied with different waveforms (repetitive square, triangular and sinusoidal).

The failure mode of the nailed timber joints were dominated by the mechanism of necking of nails or brittle fracture in the nails. Further, the fatigue life was found to be highly dependent on frequency and the waveform, where the square load cycle was the most damaging.

3.17 Fatigue Design of Wood-Concrete Composite Systems [34]

This chapter is including two papers from the authors Leander Bathon and Oliver Bletz-Mühldorfer from the World Conference on Timber Engineering in 2010 [35] and 2014 [34]. The papers are based on the same experimental research, but in the latest article, a proposal of design rule in respect to the EC5 is made.

Timber-concrete composite structures have good potential in structures like buildings and bridges. However, to build a bridge with this configuration a special approval is needed because of the limited research on the structural properties. The purpose was to gain information on the connection and the structural system. This way it enables bridges of the timber-concrete composite (TCC) system to be competitive in the market, and more bridges will possibly be constructed with this configuration.

Timber-concrete composite bridges of concrete and timber have many promising qualities. The bridge consists of a concrete slab supported by timber beams. With this configuration, timber is mostly subjected to tension while concrete is in compression. Concrete is well known for its favourable properties in compression, similar to timber showing great capacity in tension (parallel to grain). The components are placed to exploit the different behaviour and qualities of the materials in the best way. In addition, timber elements will make the construction lighter and will add to the aesthetical quality. In addition, the timber will be

protected from climate effects by the concrete slab. The theory is that the composite will give a structure with better properties with less sensitivity to cyclic load and deformations.

The composite structure is connected by a mesh of steel hbv-shear connectors. In order to provide a durable system for bridges, it is desirable to use this stiff but ductile connection. All fatigue and shear testing experienced failure in the steel connector.
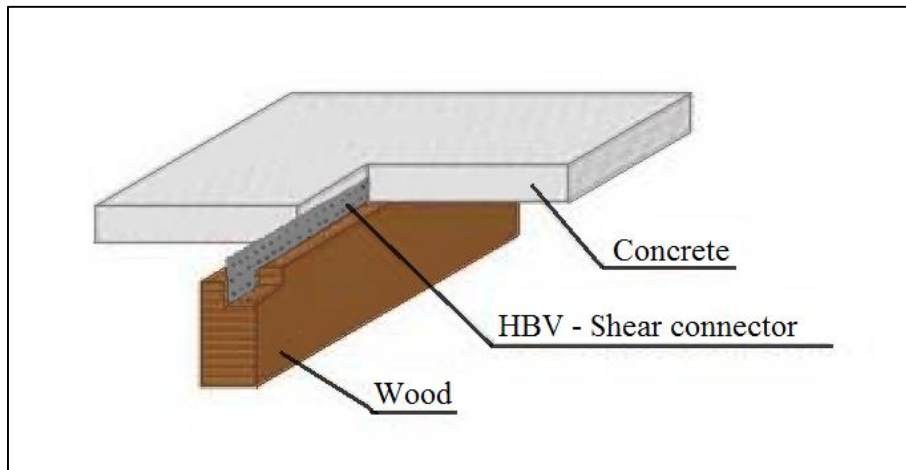
Figure 27: Composite system [35]

The shear connector shown in Figure 27 is a hbv-shear connector of steel S235. Almost half of this connector is bonded-in using adhesive in a 3.2mm wide channel 40mm deep. The other half of 50mm is cast into the concrete on the other side. To perform a design verification based on the rules in EC5, factors *a* and *b* need to be determined. In the paper it is stated that code approval of the hbv-shear connector shows *a*=2.5 and *b*=4. A fatigue design approach were presented for this connector in the composite system based on EC5 [11]:

$$a = 2.5$$
$$b = 4$$

$$k_{fat} = 1 - \frac{1 - R}{a(b - R)} \log(\beta N_{obs} t_L)$$

$$k_{fat} = 1 - \frac{1 - R}{2.5(4 - R)} \log N$$
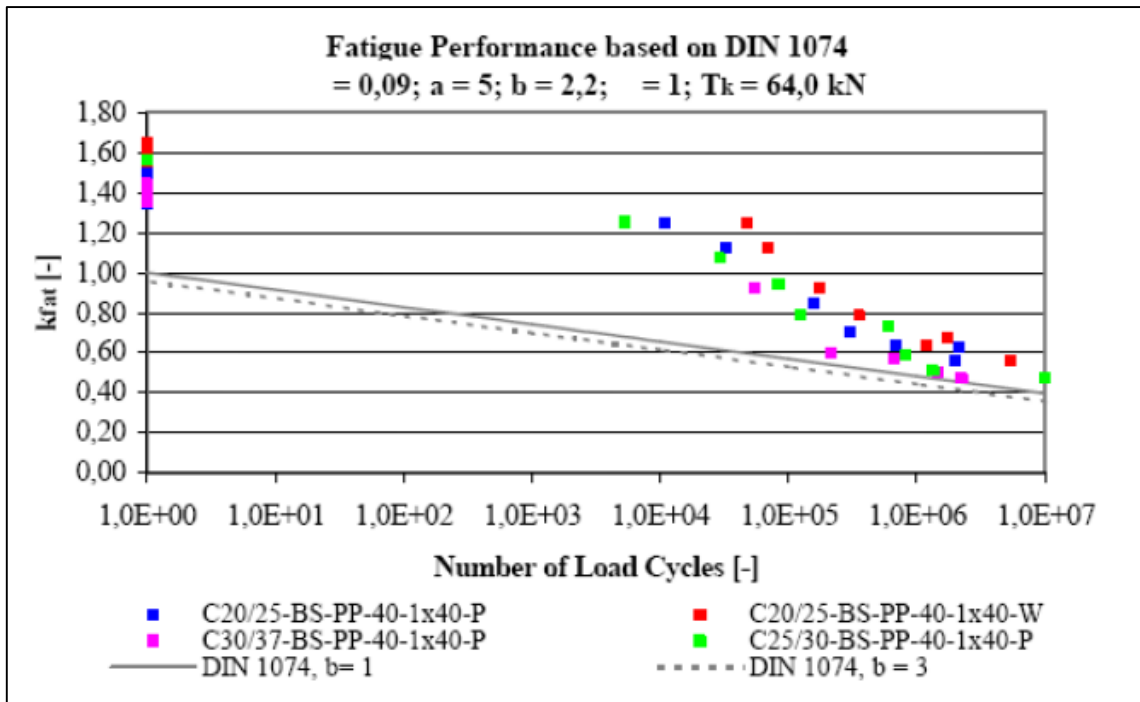
Figure 28: Results from fatigue testing on composite bridge compared to result from EC5

After performing 200 shear tests and 60 fatigue tests on the connection, the needed information to perform fatigue verification were obtained. The paper concluded that the verification with this connection in single span timber-concrete composite bridges is possible. The values from the design rule is conservative in comparison to the test results from the fatigue testing conducted (Figure 28).

3.18 Fatigue Strength of Timber-Concrete-Composite Bridges: Determination of a S-N-Line for the Grooved Connection and the "X-Connector" [36]

This is a paper by Pietro Aldi and Ulrike Kuhlmann. Pietro Aldi is a former research assistant at the Institute of Structural Design in the University of Stuttgart, Germany. Professor Ulrike Kuhlmann was named Professor of Steel and Timber Structures in 1995 at the University of Stuttgart and head of the Institute of Structural Design. She has conducted research on composite structures and fatigue, with experience from the industry on composite structures.

Fatigue testing of connectors used in timber-concrete composite structures is presented in this paper. The goal was to provide more information on how these connectors behave when subjected to fatigue loading, and to compare the results with the existing codes for timber and concrete. Further development of bridges with the TCC system are limited by the lack of knowledge on the interface between timber and concrete. The development of design rules might be expected to result in more small and middle span bridges built using this solution. The target was to derive an S-N-curve to use in fatigue verification of this type of structure.

38

Aldi and Kuhlmann summarised the data on the existing tests on the subject. However, it was acknowledged that a comparison would be difficult due to different properties of the materials, geometries and applied methods.

Figure 29: Specimen subjected to load [36]

Two connectors were tested: the "grooved connection" and the "x-connector". These connectors are regarded typical connections between timber and concrete, and show relatively high stiffness and strength values. For experimental testing, concrete class C30 and glulam GL32h was used in both configurations. The grooved connection consisted of a timber beam with casted-in concrete in the grooves. In these experiments, the notches were made with a length of 20cm. Crosswise glued-in rebars are called "x-connectors". In these experiments, the bars were bonded in at an angle of 45 degrees to the grain. The rebars were glued-in using a two-component epoxy adhesive.

Figure 30: Failure modes subjected to static load in grooved connections (left) and x-connectors (right) [36]

Ultimate load capacity in shear was determined with static load application. In the case of the grooved connection, a brittle failure occurred at maximum capacity after relatively small deformations. While for the x-connectors, a ductile behaviour was observed and the final failure was obtained by reaching ultimate tension stress in the rebars. Both failure modes are displayed in Figure 30. Results of each of the connections in mean from capacity, based on three push-out static tests:

- Grooved connector: 263.49kN
- X-connector: 226.39kN

Fatigue push-out tests were performed under load control with a sinusoidal waveform of 2-3Hz and with a load ratio of R=0.1. Three tests were conducted on each of the load levels with 75% and 50% of ultimate load on both connectors. In addition, both connections were tested at a third load level: notched connection at 41.7%, x-connector at 28.3%. Fatigue failure modes were observed similar to the static reference tests for each of the connections. These results were compared with nine three-point bending tests on beams with grooved connections, three in static testing and six in fatigue. These tests were conducted to support the simplified setup of the first set of tests. The influence of the duration of load seems to play a minor role for fatigue in this case, because traffic load is usually applied for a very short time.
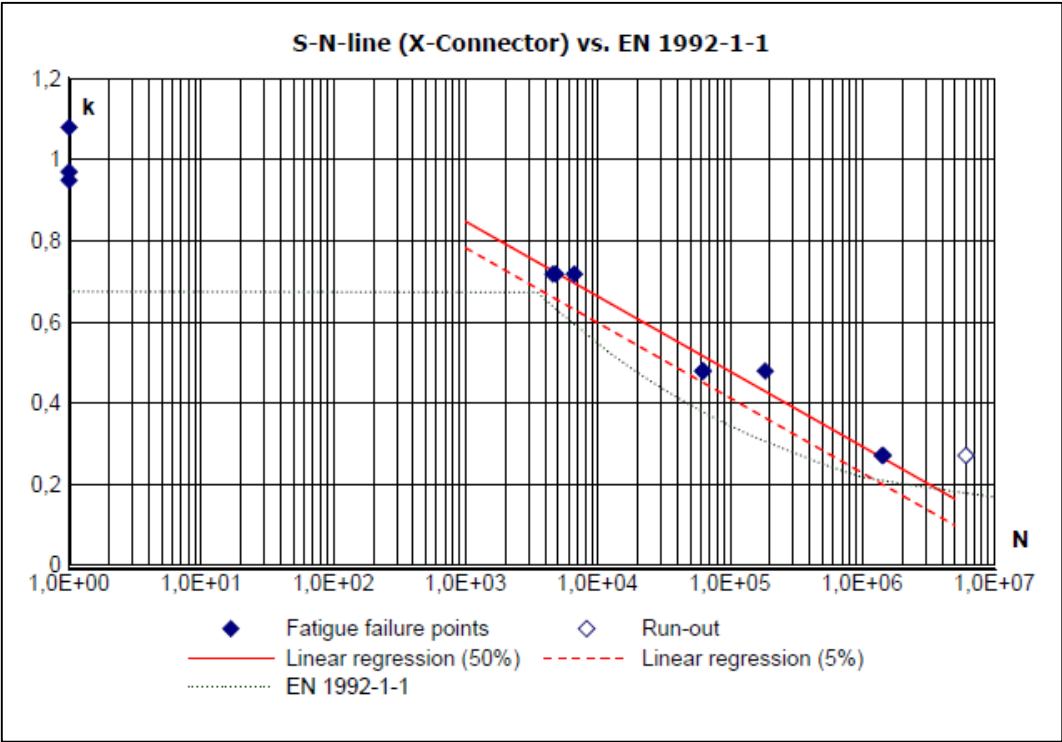
Figure 31: S-N curve from push-out test on x-connector

40
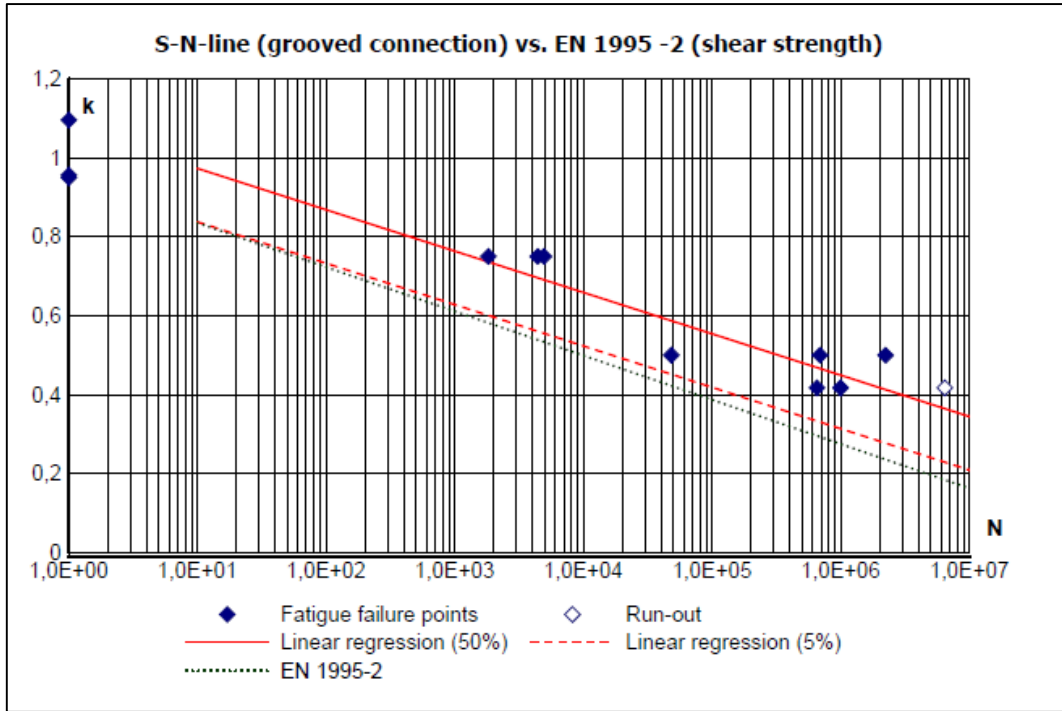
Figure 32: S-N curve from push-out testes on notched connections
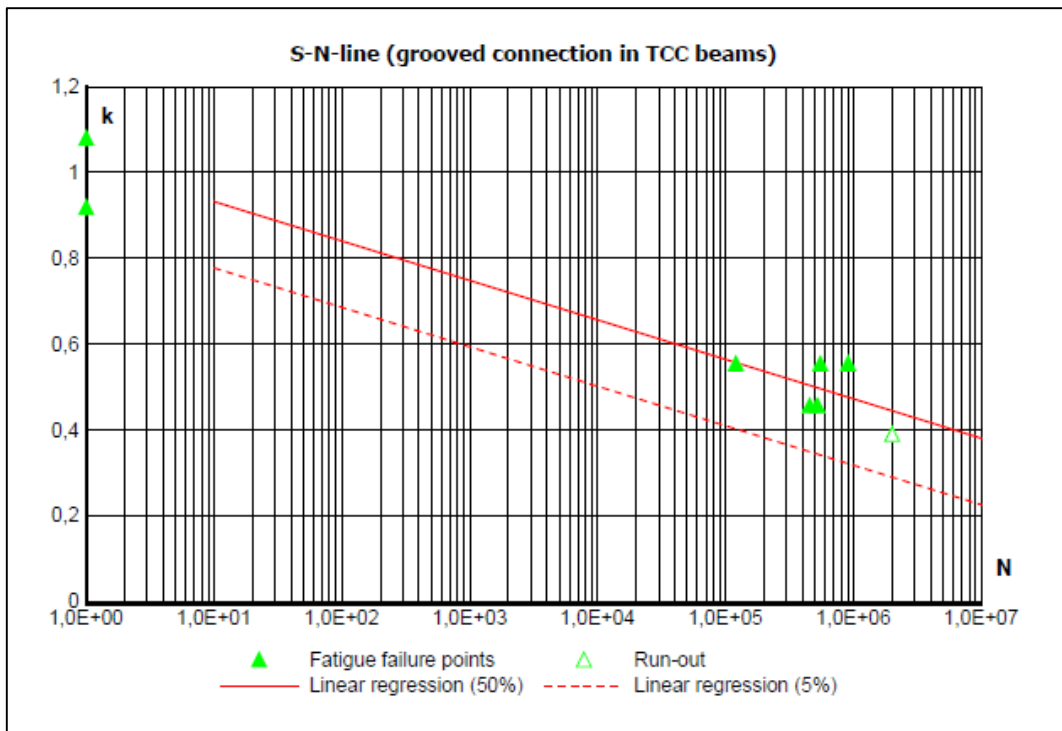
Figure 33: S-N-line for tested beams including the mean regression line and the 95% survival probability

3.19 Determination of Damage Equivalent Factors for the Fatigue Design of Timber-Concrete-Composite Road Bridges with Notched Connections [37]

This paper is connected to the paper presented in 3.18. The research is conducted by Katrin Stephan and Ulrike Kuhlmann at the Institute of Structural Design in the University of Stuttgart, Germany. Dipl.-Ing. Katrin Stephan is a research assistant and a guest lecturer at the university.

Due to the high stiffness and strength values and simplicity in construction, notched connectors are ideal for TCC bridges. Research so far have been conducted on pedestrian bridges. This paper investigates the possibility of using these shear connectors in larger vehicle bridges. For this report, two load models with different representing vehicles are used according to EC1 part 2. It were conclusion that S-N curves and simplified fatigue verification were needed for the economical application of TCC road bridges. Verification with different load applications should be performed to investigate the fatigue behaviour of the deck for different bridges.

3.20 Summary

When finding material to process for this thesis, material concerning connections, and especially axially loaded connections were prioritized. Some older papers from the 1990`s are also included since many of them have been republished. In general, fatigue of timber elements has been investigated over the last decades and currently a large variety of connections and composites are under investigation. This shows that there are an increasing focus and need for exploring behaviour during cyclic loading in timber elements. The use of timber in composite bridges is one of the structures that have initiated research on fatigue. These connections have different configurations from adhesive rods to notched connectors. In addition, research with simulated cyclone and earthquake load conditions suggest an increased use of timber structures. These papers were mainly focused on the ability in timber connections to dissipate energy. A connection must have ability to dissipate energy from large cyclic load when subjected to extreme conditions. This way the structure will not experience a complete failure without time to evacuate.

Many of the articles are authored and/or co-authored by the same researchers. This is because of the availability of the material, and may suggest that few people are big driving forces for this research. Literature found on fatigue in axially loaded connectors were sparse. No reports on threaded rods in HCF subjected at R=0.1 could be found. This makes direct comparisons between experimental results difficult. However, bonded-in rods with both rods of GFRP and steel are investigated in two different papers. These properties might be interesting to compare with present experimental testing, as they are competing solutions for use in similar connections. Stiffness during fatigue life is also an important parameter, which is worth investigating.

4 Laboratory testing

The laboratory testing was conducted to obtain information on fatigue failure in the glulam beam. With the network arch bridge as model, the primary goal is to gain information on how the connection will behave during static and cyclic load application. Fatigue of threaded rod is covered in EC3 [38]. A bridge will be subjected to cyclic loads with short duration, so the effect of duration of load will not be investigated. The design lifetime of abridge is usually 100 years. It is expected to withstand a high number of cycles at relatively low load levels during this time. That is why the investigation is aimed to provoke fatigue failure in HCF. This might provide important information, as there are little current test results on the HCF behaviour in this type of connection.

4.1 Materials

The finished specimens consisted of glulam elements with a threaded rod inserted at the top. Glulam elements were cut out of beams manufactured by Moelven Limtre AS. It was decided to test two types of specimens with different grain-to-rod angle. The hangers in a network arch bridge in reality will be inserted at many different angles. It was decided in discussion with the supervisors, that for this project it was sufficient to test specimens with two angles (90˚ and 45˚). The embedment depth of the rods were $20d_t$ =440mm. This is based on the estimated maximum embedment depth before experiencing steel failure instead of withdrawal of rod in static testing. The estimation was done based on experimental testing on withdrawal capacity conducted on similar axially loaded connections (Stamatopoulos 2016) [2].

4.1.1 Glulam

The network-arch bridge typically consists of glulam arches. Elements to test were cut out from glulam beams of two different geometries. This might influence test results, as the specimens will contain a different array of strength-class laminates. The first beam geometry was already available in the laboratory and were characterized by a large height. Two similar beams of this dimension were used to make 45-degree specimens. The second beam geometry was of a smaller height and ordered specially for the purpose of these tests. Glulam beams with these dimensions are easily accessed and cheap in comparison with the first type of beam. 90-degree specimens were made from two of these beams. All the specimens were made by technicians working in the laboratory according to provided illustrations with good accuracy (±10mm). The density at 12% moisture content have been estimated by the manufacturer to be 470 kg/m^3. The height of the beam might deviate +1/-0.5% from given dimensions. In addition, the moisture content can influence the size of the glulam.

Beam	Height	Width	Length	Wood	Class	Lamella height	Strong lamellas
	[mm]	[mm]	[mm]	(type)		[mm]	(each side)
90°	585	140±2	5000	Spruce	GL30c	45	3
45°	945	140±2	5000	Spruce	GL30c	45	4

The classification GL30c give information of the properties of the beam:

GL   Glulam

30   Bending capacity of the beam

c   Combined glulam

Combined glulam is made up of lamellas with different strength classes. The outer laminations are made of higher strength wood (T22), while the inner laminations are made of lower strength wood (T14 or T15). This solution places the strongest wood in the location of the largest stresses in the beam. The first beam had a large height, and it is required to have four strong lamellas at each side of the beam. At least h/6 on the top and the bottom of the beam must be made of stronger lamellas. For the second and lower beam, it is sufficient with three to meet the requirement. Glulam beams with different strength classes placed like this is called a combined glulam beam.
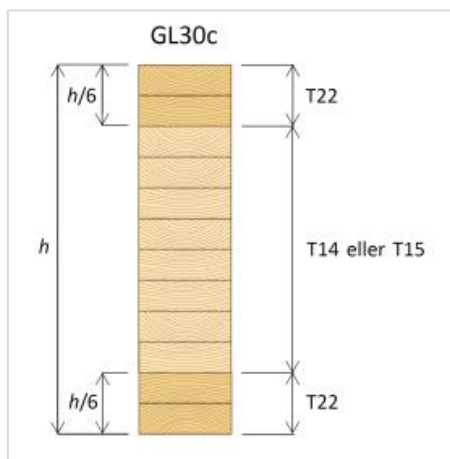
Figure 34: Requirements of the combined glulam beam [3] (left), picture end of second beam (right)

It is important to be aware of the location of stronger lamellas in the beam for these tests. Wood elements of different strength class have different properties, and the variation in the lamellas of the specimens can influence the test results. For increased homogeneity in test results, it is favourable with specimens of as similar properties as practically possible. The beams were cut in different ways to make the specimens, and a portion of the stronger

lamellas is removed in the process. The threaded rods are inserted into the specimen from the side where there are less strong lamellas.

The height of the specimens was first chosen based on available material in the laboratory. It was assumed that the largest beams would be used to make 90˚ specimens, and with a height of 945 mm two specimens could fit the embedment depth of 440 mm. 945/2 = 472.5 mm. However, the 90 degrees specimens were made from smaller beams. This solution was more practical as these beams are cheaper, and have a fast delivery time. Still, the height-dimension was sufficient for these tests and further used to make the glulam elements.

The length of the specimen was chosen based on the supports. The sufficient length was assumed 600 mm based on discussion with supervisors with experience from static testing of similar specimens [2](Stamatopoulos 2016). It was assumed sufficient to avoid plastic deformation in the wood below the supports, and still leave enough open surface surrounding the rod to avoid strengthening of the specimen. Calculations on the maximum stresses from the different supports on the timber surface is given in Annex D.

4.1.2 90˚ specimens

The 90˚ specimens were cut out of beams as shown in Annex E. and in Figure 35. The three strong 45mm lamellas are illustrated by the grey area in Figure 35. Not all of the stronger lamellas are cut of at the top of the specimen, with about 22mm at the point where the rod is inserted. Eight specimens were made from each beam, and the numbers on each beam depending on the original placement in the beam is shown in Figure 36. Specimens with numbers above 8 are following the same sequence (9 with similar location as 1 but in the next beam, 16 similar to 8 etc.). For 45˚ specimens from the second beam, the specimens were numbered from 25 to 32 due to an error.
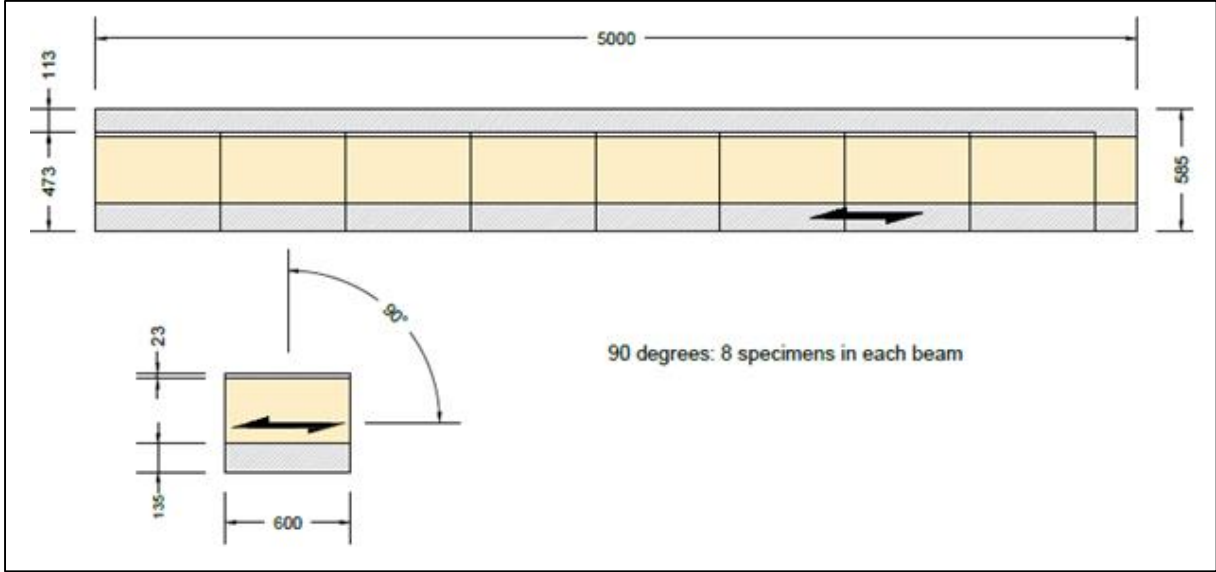
Figure 35: Plan of cutting the 90˚ specimens illustrating the strong lamellas, from Annex E

Figure 36: Cutting of specimens and numbering according to placement in the beam, 90˚

4.1.3 45˚ specimens

The 45˚specimens required more time to cut. As seen in Figure 37, the pattern is more complicated compared to 90˚specimens. The pattern was made to exploit the available surface in the best way and to limit the amount of waste material from the beam. Each of these beams could also fit eight specimens. The black line drawn on each specimen in Figure 38 were to mark the side in which the rod was inserted. Numbering were done similar to 90-degree specimens. The circular saw did not have sufficient diameter of the blade to cut the full thickness of the beam from one side. Consequently, the beam had to be turned and cut from both sides. This sometimes resulted in uneven surface at the top of the specimens, as the cuts from both sides were not equally deep. In retrospect, the possibility of ordering finished specimens from the manufacturer could have been investigated. This would have saved time in the initiating phase of the experimental testing, and the specimens would have less deviation.
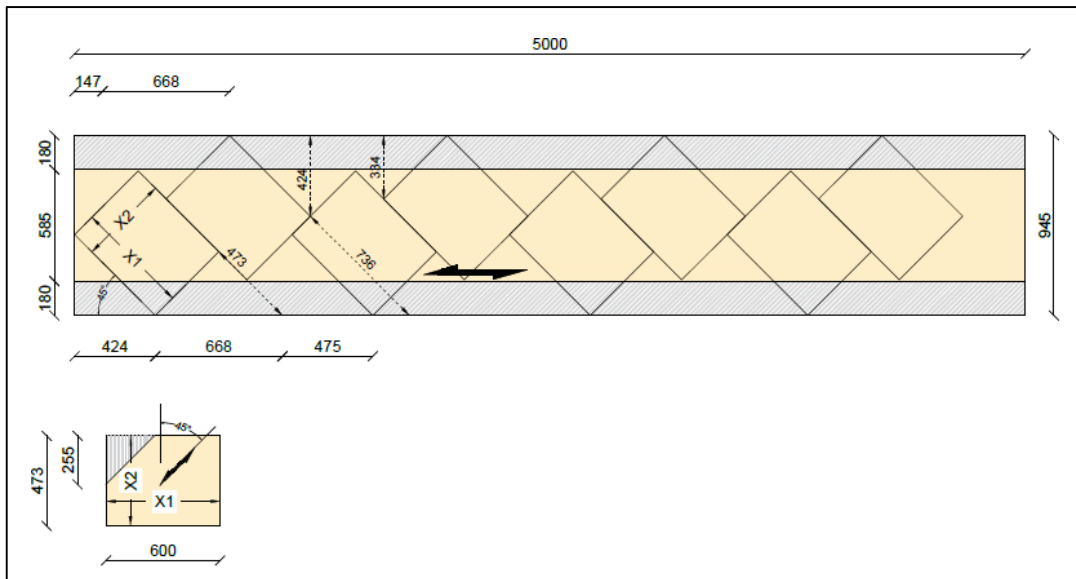
Figure 37: Plan of cutting the 45˚ specimens illustrating the strong lamellas, from Annex D

Figure 38: Numbering according to placement in the beam, 45˚

4.1.4 Steel rod

The investigated connection were in this case a threaded screwed-in rod embedded in a glulam element. As earlier mentioned, threaded rods might be ideal fasteners in connections suspending the deck of a network arch bridge to the glulam arch. These rods have displayed good stiffness and ductility properties in withdrawal. However, the fatigue properties are still largely unknown.

This particular threaded rod is threaded in both ends. The "top" of the rod consists of metric threads with geometry: M20. The "bottom" part consists of threads as shown in Figure 39, with 22mm outer diameter and 8mm pitch. These threads make up the largest part of the rod, and is the designed threads for insertion into wood. The inner diameter is slightly angled between pitches, with the slimmest part located in the middle with equal distance to threads. Full material data can be found in the datasheet, which is included in Annex A.
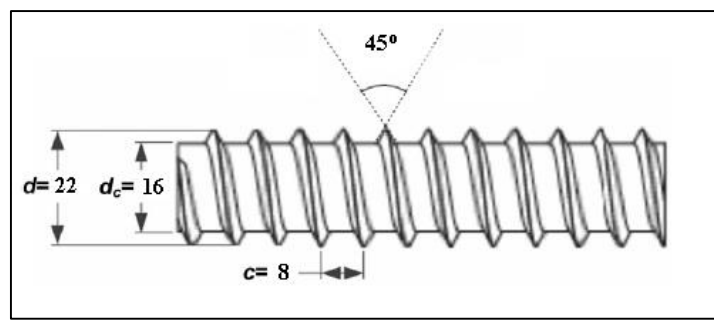
Figure 39: Threaded rod, dimensions

The machine is only capable of gripping the specimen by compressive force. Any plastic deformation from the grip would drastically decrease the capacity of the rod. A circular steel profile was specially made with internal M20 threads to protect the threaded rod. This circular profile was mounted on the top-part of the rod for the machine to grip during testing.

Table 8: Threaded rods, material data

	Max. diameter	Min. diameter	Yield limit	Ultimate limit	Tension capacity
	d, d_t	d_s, d_{min}	f_y	f_u	
	[mm]	[mm]	[N/mm^2]	[N/mm^2]	[kN]
M20	20	18	660	800 N/mm^2	203.6
Threads in wood	22	16.13	660	800 N/mm^2	163.5

Figure 40: Threaded rod side with M20 (left) and the threads designed for wood-insertion (right)

4.2 Finished specimens

With glulam elements cut with the right dimensions, rods were inserted at the top of the specimen at the side with least strong lamellas left. This was done to achieve specimen with a similar range of strength classes in the lamellas, see Figure 41. Threaded rods are inserted in the glulam elements previously described in 4.1.1. Prior to rod installation, the elements were pre-drilled with a diameter close the core diameter of the threaded rod (16.5 mm). Specimens were stored in a room at the standard conditions with relative humidity 65% and temperature 20 degrees.
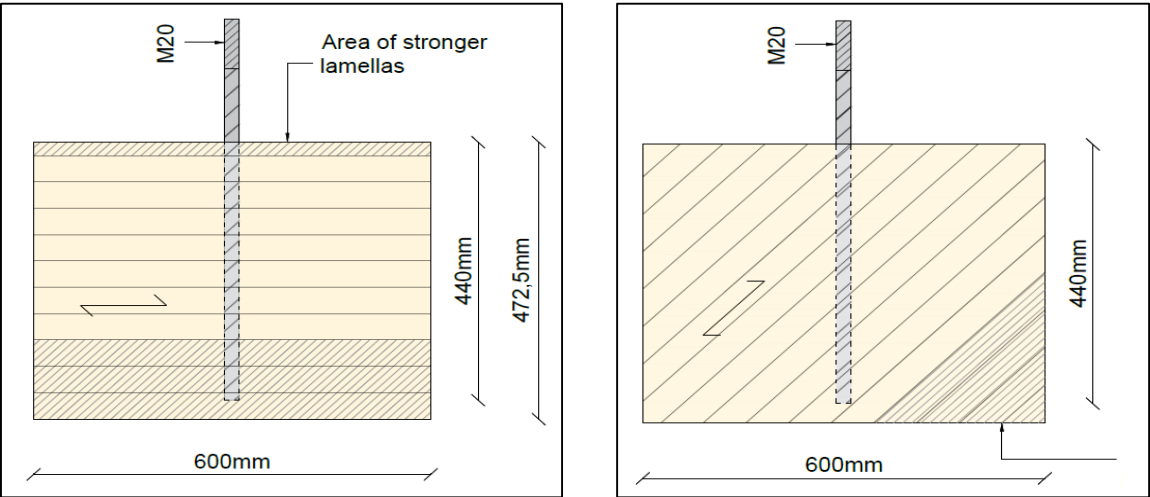
Figure 41: Specimens with 90-degree angle (left) and 45-degree angle (right)

4.3 Values of interest and instruments for measurements

4.3.1 Moisture and density

It is usually required to determine moisture content and density in timber elements according to ISO 3130. To save time the density and moisture were estimated with simplified methods. The density was calculated by using the dimensions of the specimen and weighing the pre-drilled element before insertion of the rod. The moisture content were measured at the surface of the specimen in the time before the start-up of the test after placement into the machine.

Procedure used for estimating moisture content:

> The moisture content was measured with the device at three different locations on the largest surface the specimen (not at the end where the fibres are cut or top and bottom). Defects in the wood might give misleading results, and values with too much deviation in respect to the others were therefore neglected. The mean value was derived from these results, and used as an estimate of the moisture content.

4.3.2 Relative humidity conditions

One challenge with testing wooden material is the fact that they are greatly affected by the moisture content. When the relative humidity and temperature conditions are changing, the moisture content in the wood will change accordingly. If subjected to relatively dry and warm conditions for a sufficient period, cracking of the timber may occur and affect the properties. Timber structures are divided into different climate classes according to the relative humidity and the average temperature defined by the environment the structure is expected to experience in its lifetime. EC5 [6] 2.3.1.3(2)P define the values of climate class 1: RH = 65% and 20 ˚C. EC5 states that the average moisture content for this climate class would not exceed 12% normally.

Figure 42: Rig before start-up, bowl with sponges and the humidity reader

The test rig is located in the laboratory hall, where the relative humidity is measured to be about 25% and the temperature is between 20˚C - 25˚C. As earlier mentioned, the finished specimens are conditioned at 20˚C with 65% RH when not being tested. However, cyclic testing can span over days and possibly weeks. It would be beneficial to make a similar stable environment with the desired conditions to keep the temperature and relative humidity close to the standardized values. To achieve this, a solution with a local environment in the test rig was tested. The rig was coated with a plastic sheet, which was fastened and sealed with duct tape at the openings. In an attempt to increase the relative humidity inside the rig, sponges in bowls with water were placed inside the plastic.

The relative humidity was measured during testing to monitor the conditions. From these measurements, it was soon evident that the solution with plastic and water bowls was ineffective. One problem might have been that the plastic sheet was not sealed properly. However, the biggest problem was that the test specimens did not stay in the rig for a long time. Because of problems concerning testing and setups, the longest test time in the rig for a specimen was just about 12 hours before failure or correction was required. The specimens had to be taken out of the rig with short time intervals, and the local environment did not have significant effect. It is assumed for these experimental tests that the specimens were not significantly affected by the dry and slightly hot air during the short period of testing. As an alternative to the wet sponges, the use of a humidifier could possibly have better effect. This solution would be more efficient in increasing the relative humidity, and the desired value of RH can be set on the humidifier. For conducting test over a larger span of time, this might be a practical and reliable solution. Because this system did not work properly, the end of the

specimens were applied moisture and covered with plastic. This was to ensure that no cracks at the ends developed, which might have interfered with results.

4.3.3 Temperature, steel rod

During cyclic testing, internal friction in the material might create heat. Especially at high load ranges, it is likely that the temperature of the rod will increase. If this temperature rises to a significant value, the heat can be conducted to the timber element. As earlier mentioned, wood is highly affected by temperature and relative humidity conditions. The wood surrounding the rod might become dry, which will influence the strength of the wooden material. Monitoring and cooling of the rod is needed as a counter measurement.

Figure 43: System to prevent heating of steel rod

A cooling device was installed on the threaded rod as shown in Figure 43. The temperature was monitored continuously throughout the duration of the tests. The system consisted of a copper tube entwined around the visible part of the threaded rod. A coolant with a constant temperature of -10 degrees were flowing through the tube constantly. Finally, the system was protected by a layer of an insulating material on the outside of the tube with the purpose of concentrating the cooling effect to the rod. The copper tube did not obtain ideal connection to the rod, and have the potential of a higher level of efficiency. Aluminium powder or thermal paste between the rod and the tube might improve the connection, but this solution was not tested here.

4.3.4 Test machines

The experimental tests were conducted with two different hydraulic test rigs in the laboratory at the Department of Structural Engineering, NTNU. The first machine had some problems with the hydraulic system. Oil poured down on the specimens in some of the tests conducted with this machine. It is possible that the results from tests subjected to oil are influenced, and this is later mentioned when presenting test results. After the static reference tests and the first cyclic test were conducted, it was decided to move the rest of the experimental testing to

another available machine. It would be too time consuming and expensive to fix the problem in the time left for this thesis. The calibration forms are added in Annex J.

Table 9: Test machine info

Number	Name	Capacity	Comment
1	Schenk Trebel Universal	1000 kN	Oil leakage
2	Instron	500 kN	

Figure 44: First (left) and second (right) test machine

4.3.5 Test order

Static reference test:

> The specimens were chosen at random with a random number generator in excel. However, a new number was generated if the specimens had location next to each other in the original beam. Only two static tests were conducted with each of the rod-to-grain angles. That is why it might be favourable to test specimens with different locations in the beam, preferably from different beams.

Fatigue test:

> The order were chosen by the order they were placed in the climate room. It was assumed that all specimens were going to be tested, and the order of testing would not matter. During start up and conducting tests, it was soon evident that the testing is time consuming. In addition, some problems were encountered and this made it difficult to complete the testing on all specimens.

4.3.6 Displacement transducers

Linear variable differential transducers (LVDT) were installed on the threaded rod embedded in the wooden specimen. Transducers were mounted on the rod as close to the wooden surface as possible. The relative displacement between the rod and the centre point in the glulam element was measured. The first 10 minutes of each tests were logged at 50 Hz. After the initial phase, the data were logged at time intervals during the course of the test until failure. During the static testing and the first two cyclic tests, transducers with push rods were used. Due to the risk of these transducers being damaged during cyclic testing from friction, they were replaced by laser transducers.

Two displacement transducers were used if possible, one on each side of the specimen to eliminate distortions from the results. Some problems with logging were encountered with both transducer types. The push-rods were at times influenced by the support on the rod not being properly fastened sideways, which caused a stop and restart of the test to correct the position. The laser transducers had some problems with the connections, and only one was working and logging during some of the tests. The last test on the defected test rig with the oil spill only have one of the lasers producing valid position logging. Oil on the surface of the laser distorted the readings.

The support fastened on the threaded rod could not always be placed at the wood surface. l_1 is the distance between the supports and the glulam surface. For specimens with $l_{eff}=330mm$, the displacement transducers could not be installed in the centre of the glulam element because of conflict with the steel profile in the setup. For these tests, the transducer was installed 165mm from the top of the specimen. This distance was the largest without risking damage to the transducers during testing.

Figure 45: LVDT, laser (left) and push rod (middle), support to the rod (right)

4.3.7 Specimen I. D.

The specimens are marked with an I.D. number based on information concerning the geometry of the specimen. The placement in the glulam beam, the nature of the load conditions of the test (static or cyclic) and the rod-to-grain angle. When the load condition or the rod-to-grain angle is changed, the numbers of the load conditions restart.

S90-2-s1:

S90	=	Specimen with 90 degrees grain direction
2	=	The placement in the beam
s1	=	Static testing, first test with this geometry (90˚)

4.4 Setup

To enable testing of the specimens, a frame to counteract the axial force on the threaded rod is needed. Unwanted movement should be prevented as much as possible. The purpose was to enable failure in the timber element at the given load levels. A push-pull configuration was chosen, where the rig is pulling at the rod while the frame is supporting the specimen at the top. The frame has to be able to withstand the forces without risk of deformations.

The setup had be changed continuously as problems were discovered. Illustrations with correct dimensions are provided in Annex F. Fatigue on axially loaded threaded rods are an uncharted area, and no similar test reports are found on the subject with similar rod-to-grain angle. Therefore, there are no existing standardized test methods yet. From the literature chapter, axially loaded bonded-in rods are tested with $0˚$ grain direction. Similar threaded rods are tested in LCF range with $0˚$ grain direction. With this rod-to-grain angle, the supports would not be influencing the test in the same way, and often a pull-pull configuration was used with one stronger rod on one side [27](Bainbridge 2002). Fractures would involve pulling out of the grain surrounding the rod with not much effect on the timber element. However, with $α=90˚$ some development of cracking along the length of the glulam element is expected. Cracks will form along the weak plane in the wood, and in this case along the fibres. When pulling at the rod, it will result in splitting of the wood and this crack should get sufficient area to propagate without interruption. This way the most realistic failure mode is obtained.

Different solutions on how to conduct fatigue testing were evaluated and tested. Setups were designed based partly on simple rough calculations and in discussion with supervises connected to this thesis. The design of the setup had to be changed many times during the process of testing. Each of these setups will be presented and the purpose is to document the performance on these testing procedures. Future development of the test will be made easier to predict and conduct.

Table 10: Parts for the frame

Type	Dimensions	Use
Steel square hollow section	120x120x10mm	Top of test specimen, distributing forces to the specimen. Holes are to suspend to support with threaded rods.
Threaded rods	M25	Suspending the square hollow section to the stationary support
Round profile (Support held by the machine)	D=240mm	Machine gripping the smallest diameter, while steel profiles are fastened with bolts (M20)
Steel profiles	500x100x50mm	Fastened to the round profile and suspended to the square hollow sections with the threaded rods (M25)
Steel plates	140x140x10mm	To distribute forces at the end of both sides of the rods on the specimen
L-profile	100x50x8mm	To distribute forces along the length of the specimen
Half circle steel profile	140x25mm Max height: 5mm	To level out forces between square hollow profiles and the steel plates
Circular steel profile	M20	Circular steel part to screw onto the top of the threaded rod in the specimen, and gripped by the machine. This allows for gripping and pulling of rod without plastic deformation.

Figure 46: Parts used in setup

Setups are numbered chronologically in respect to testing from first to last:

Setup 1

> Setup 1 was used as the first test and the dummy test. All the other setups were developed from this one. Hollow profile were distributing the forces to the glulam surface at both sides of the rod.

Setup 2

> L-profiles were placed underneath the rectangular hollow profile. The forces are distributed along the length of the beam, and failure parallel to the grain in 45-degree specimens are prevented.

Setup 3

> Two cyclic tests at the same time, mirroring each other in the test machine. This setup was gripped by the threaded rod at each side.

Setup 4

> The L-profiles were cut to open the area around the threaded rod. This were to open up surface surrounding the rod for the fracture to propagate freely.

57

Setup 5

L-profiles were replaced by rectangular steel plates to distribute the forces similar to Setup 1. Plates of 140x140x10 increases the area of Setup 1. In addition, relatively small half-circle profiles (5mm high and 25mm wide) were introduced between the square hollow sections and the plates on both sides. The uneven loading caused by the uneven surface of the specimen were better distributed.

Setup 6

Similar to Setup 2 with new uncut L-profiles, long enough to span all 600mm. It is no longer possible to use the half circle profiles, as the L-profiles does not cover the full width of the specimen.
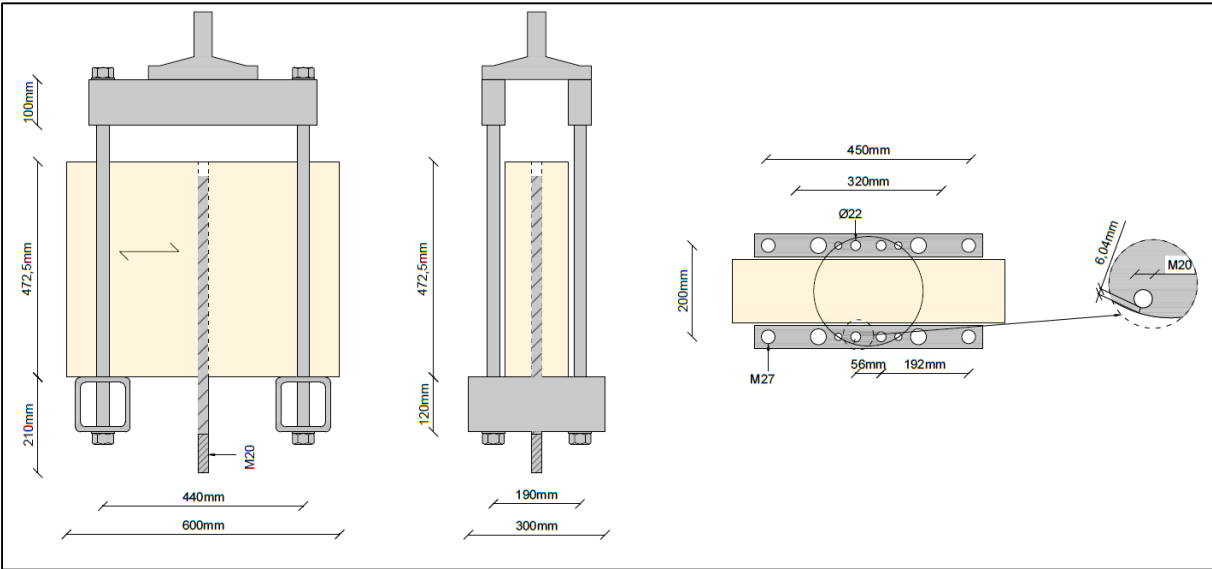
Figure 47: Setup 1, front (left) side (middle) and from above showing the placement of the support (right)

Setup	Used on	Pro	Con
1	S90-2-s1 S90-15-s2 S45-2-s1	- Good surface to distribute the force to the glulam element	- Allows failure along the grains for S45
2	S45-7-s2 S45-5-s3 S90-11-d3	- Good surface to distribute the force to the glulam element - Is able to hold the 45° specimen without in-grain failure	- Might interfere with the test result, as the surface covered by the support is large
3	S90-9-d1 S90-10-d2	- Better efficiency, can run two tests at the same time.	- Difficult to get accurate measurements after first failure - The frame is not fastened in the machine, giving the specimens more room to move.
4	S90-12-d4 S90-8-d5	- God open space around the threaded rod, making the fibres free to move	- Bad surface to counteract forces on the glulam element
5	S90-14-d6 S90-1-d7	- Eliminates some of the effect from distortions in the frame, making the steel rods last longer	- Can't be used on 45° degree specimens
6	S45-27-d1 S45-6-d2 S45-4-d3 S45-26-d4 S45-25-d5 S45-30-d6	- Is able to hold the 45° specimen without in-grain failure - Similar to setup 2, with longer L-profiles	- Might interfere with the test result, as the surface covered by the support is large

4.5 Static load procedure

There are already conducted some experimental testing regarding withdrawal strength on threaded rods [2]. However, the threaded rods used in the present study are of a different type with larger diameter. Two static tests were conducted to obtain some results to compare with the existing research and to establish a static reference capacity. The amount of tests are not enough to get a good and stable result, but here it is assumed enough if the test results does not deviate too much from each other. The cyclic testing is time consuming, so the static testing is not prioritized. They can be supported with the results from similar tests in «Withdrawal properties of threaded rods embedded in glued-laminated timber elements» [2]. The testing was conducted according to EN 26891:1991 [39], which is a standardized

guidance on the testing of joint in timber structures made with mechanical fasteners. The maximum withdrawal force has to be estimated.

$$F_{est} = f_{w.est} \cdot \pi \cdot d \cdot l_{eff} \tag{18}$$

F_{est} Estimated maximum static failure load

d Rod diameter

$f_{w.est}$ Estimated withdrawal strength

l_{eff} The depth the threaded rod is inserted into the specimen

α Angle between insertion of rod and grain direction

Equation (18) will give a conservative estimate of the maximum withdrawal capacity. The shear stress values from withdrawal testing in [1] (Stamatopoulos & Malo 2015) are mainly in the area 4-6 N/mm^2. Using the middle value here, 5 N/mm^2. The value for the load procedure do not need great accuracy as long as the failure does not happen before 0.7 $F_{est.}$

$$F_{est} = \pi * 22 \text{ mm} * 5 \text{ N/mm}^2 * 440 \text{ mm}$$

$$F_{est} = 152.05 \text{ kN} \approx 150 \text{ kN}$$

If the test results deviates more than 20% from the estimated value, it is recommended that the load level should be adjusted accordingly. The critical point is to decide the force so that $F_{ult} > 0.7 \, F_{est.}$ If the failure happens before the machine is changed from load controlled to displacement controlled, the failure will happen suddenly and there is a risk of the machine being damaged. After switching to displacement controlled load application, the maximum capacity is reached at a point. After the max capacity is reached, logging continues until the load has dropped to 50% of the ultimate load.
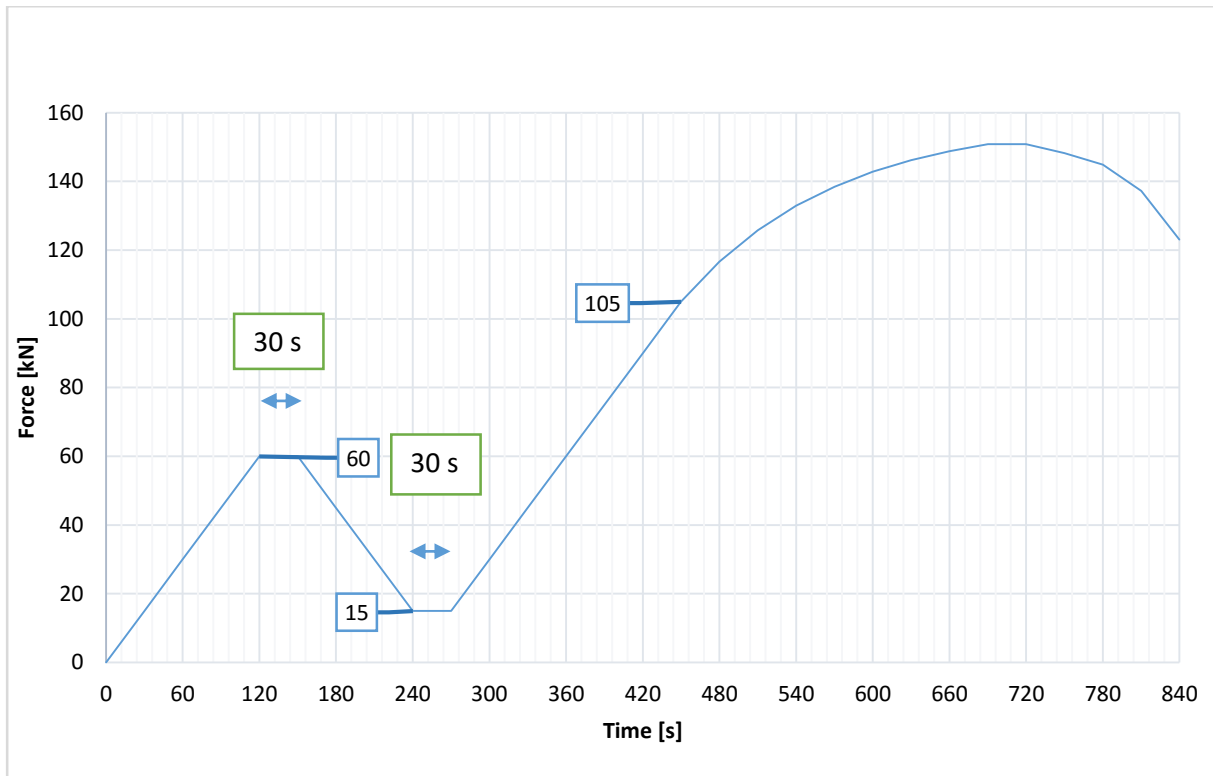
Figure 48: Load applied during the static test

Load procedure, Figure 48:

1. The load is applied at a rate of 0.2 F_{est} per minute until 0.4 F_{est} is reached after 2 minutes. F_{est} = 150kN assumed in this case.
2. At 0.4 F_{est} = 60kN the load is maintained for 30 seconds.
3. Then the specimen is unloaded at the same rate as in pt.1 until reaching 0.1 F_{est} after 1.5 minutes.
4. The load is maintained, 30 seconds.
5. Now the load is increased again with the same speed at in pt.1.
6. Reaching the load of 0.7 F_{est}, the load application changes from load controlled to displacement controlled. This means that instead of a constant increase of load, the machine will increase the load with a constant rate of slip. The displacement is constantly increasing. In this way, the machine will safely obtain fracture in the specimen. The danger with load control at the point of fracture is that the machine will not be able to detect the limit value that signals the end of the test fast enough. It might in this case make a "jump" upwards at the ultimate load. This might damage the machine.

61

4.6 Cyclic load procedure

The cyclic testing is conducted with tension-tension sinusoidal load application R=0.1. The stress ratio was chosen to simulate a connection with dead load subjected to cyclic tension forces. The intention was to test one embedment depth and change the load range on the specimens. However, due to problems in achieving fatigue failure in withdrawal of the rod at some load levels, another embedment depth was also investigated. As earlier mentioned, the first embedment depth was chosen based on experience from testing in withdrawal capacity [1] and in discussion with supervisors.

1.	$l_{eff} = 20 \cdot d_t = 440 \; mm$	
2.	$l_{eff} = 15 \cdot d_t = 330 \; mm$	

When the decision of introducing another embedment depth was made, all 32 specimens had already been made with 440mm screwed-in length. It would be difficult to unscrew the rods without damaging them, as it would require gripping of the upper threads. The solution was to cut out the top 110mm from the glulam specimen. It was important to get a smooth surface along the top without any markings from the saw as they could initiate premature cracking. The timber surrounding the rod was carefully removed. First vertical cuts were made on both sides of the rod avoiding contact. The "plug" left after this is removed by hand with a handsaw.
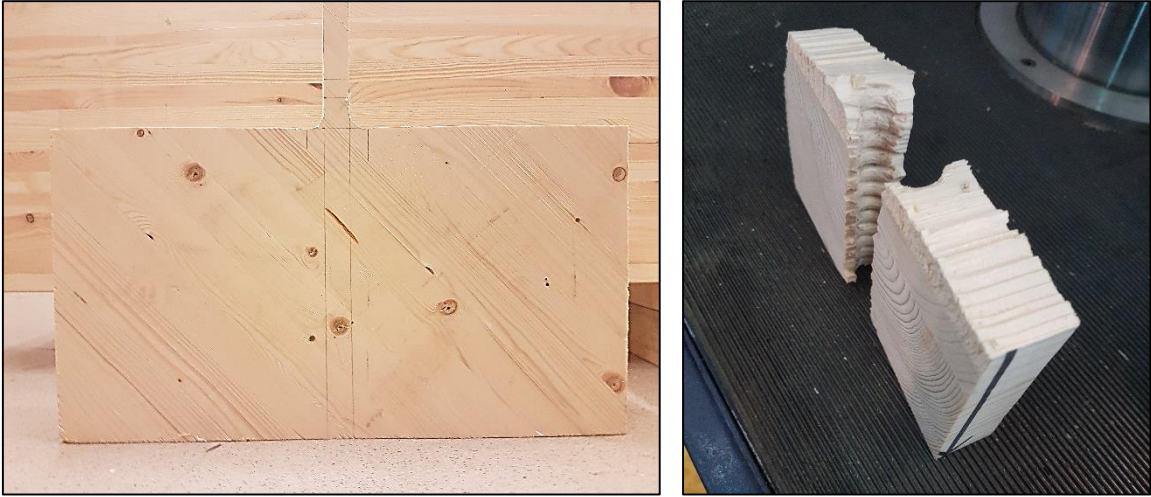
Figure 49: Specimen with new screwed-in length (left), removed part surrounding the rod (right)

4.6.1 Test procedure

The static reference load was derived from the results obtained from the two sets of static reference tests. These values were used to calculate the normalized load ranges. They were also used to estimate the withdrawal capacity of 330mm screwed-in length by assuming linear relationship with respect to embedment. This way, more static reference tests were avoided when a new embedment depth was introduced. The stress levels were calculated with the formulas in chapter 2.2. Calculation concerning this chapter are added in Annex D. The specimen was slowly applied load manually until reaching mean load and then cycles were applied at 2.5 Hz. The only exception is during the initiating phase of test S90-11-d3, the first dynamic test. Here, the cyclic load was started at 0.1 Hz and increased to 2.5 Hz within the first 10 minutes. If experiencing steel failure, another grip was taken on the rod when possible and the test was restarted.

Table 12: Load levels from Annex D

Load level	α	l_{eff}	F_{ref}	Δf	F_{max}	F_{min}
nr.		[mm]	[kN]	[mm]	[kN]	[kN]
1	90°	440	157	0.675	118	11.8
2	90°	440	157	0.54	94	9.4
3	90°	330	117.8*	0.54	71	7.1
4	45°	330	138.8*	0.675	104	10.4
5	45°	330	138.8*	0.54	83	8.3
6	45°	330	138.8*	0.585	90	9

*Estimate, linearly scaled with changed l_{eff}

The load level was decided in order to obtain fatigue failure in the HCF range. Table 3 in "Fatigue strength of dowel joints in timber structures" [18] were used loosely as a guideline for what number of cycles to expect from different load ranges. This is a report on fatigue in dowel joints and it is not directly transferable to this type of connection. The first tests were conducted at large load levels in order to get failure fast. The next load levels were chosen based on the first set of tests and decreased in accordance with Table 3 in "Fatigue strength of dowel joints in timber structures" [18].

5 Results - Static testing

Table 13: Results static reference tests, from Annex H

Specimen	Moisture	Weight	Density		Maximum force		Setup
I.D.		W	ρ	l_1	F_{ult}	Δ_{max}	
[name]	[%]	[kg]	[kg/m³]	[mm]	[kN]	[mm]	[nr.]
S90-2-s1	9.8	16.845	433.85	0	159.22	3.37	1
S90-15-s2	10.8	16.83	431.55	0	155.18	3.62	1
S45-2-s1*	11.3	18.27	465.74	0	118.93	0.82	1
S45-7-s2	12.8	19.67	498.23	9.5	188.03	3.16	2
S45-5-s3	12.5	19.55	491.45	12.5	182.15	2.85	2

*The result from this test is not included as reference withdrawal capacity, irrelevant failure mode

Special events during testing:

Specimen S90-2-s1

> This is the first specimen to be tested and therefore the "dummy test". The results from this test are used since there is not much time to conduct tests. The specimen was taken out of the climate room and was placed in the rig four days before test start. This resulted in some superficial cracking at the ends. The reason for the delay was that displacement transducers were wrongly mounted, and a new solution had to be designed. Oil from the machine had also been dripping from the machine onto the top surface of the specimen. Ideally, the machine should be repaired or replaced at this point. It was discussed, but no test rigs were vacant at the time. Therefore assuming the influence from the oil will not influence the test result very much.

Specimen S45-2-s1

> This specimen failed at 118kN wait failure along the grains 45 degrees to the rod. This result is therefore not used in establishing a reference withdrawal strength. In reality, this failure mode would not be possible. In an arch, the fibres are uncut with the rod inserted at an angle. Results are included in the graphs.
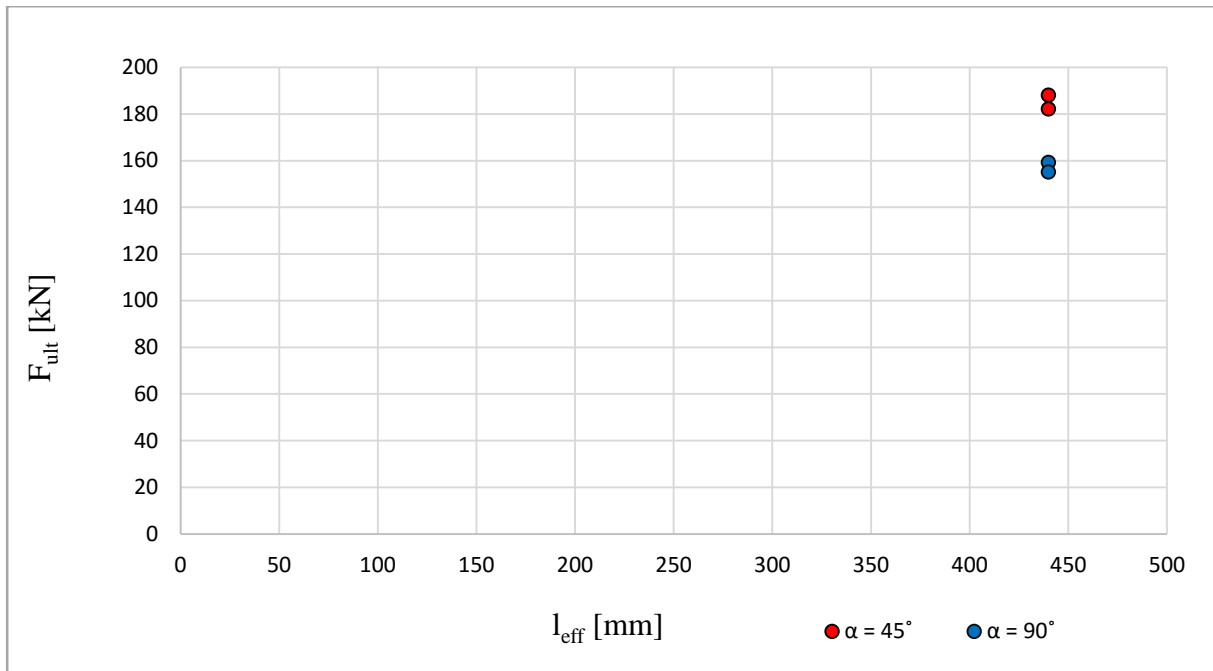
Figure 50: Withdrawal capacity, static reference tests

Table 14: Results static tests - mean values

Specimen	F_{ref}	St. Dev.	C. o. V.	Density	Displacement at F_{max}
[I.D.]	[kN]	[kN]	[-]	[kg/m^3]	[mm]
S90-x-sx	157.2	2.02	0.013	432.7	3.50
S45-x-sx*	185.1	2.94	0.016	494.8	3.01

*Without results from S45-2-s1

Table 14 provides a summary of the results on two static tests on each of the grain directions. As seen in the table, the deviation is small. Supporting values from similar test results in "Withdrawal stiffness of threaded rods" [1] are used as supplementing values when the static tests are evaluated. Extended values with information obtained from experiments are given in Annex H. The density of the two types of tests have large variation, and the mean value is calculated to be 464 kg/m^3. The high value of variation might be caused by the different long time storage the beams were subjected to before the specimens were made. As mentioned, 45-degree specimens originates from beams available in the laboratory which had been stored at an ideal environment for a longer period (RH=60% and T=20ºC). While the beams for making 90-degree specimens, were ordered later from the manufacturer (Moelven AS), and had recently been under transport. The difference in moisture can also be contributed to the difference in laminate classes. A larger beam will have more high-strength lamellas, which would make them more dense and heavy.
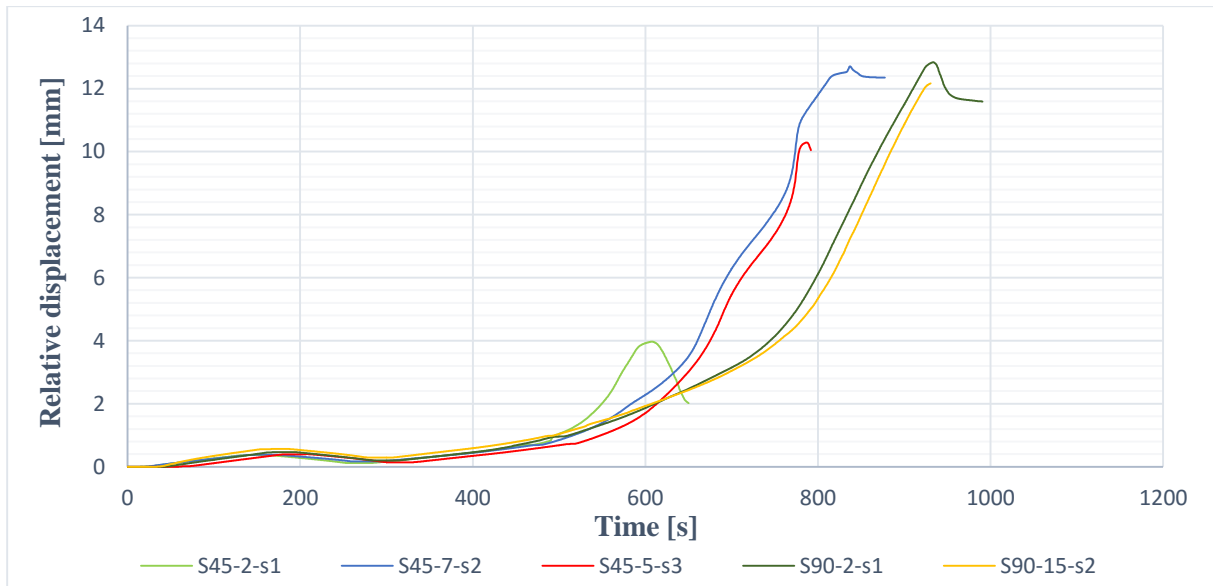
Figure 51: Development of displacement, static test
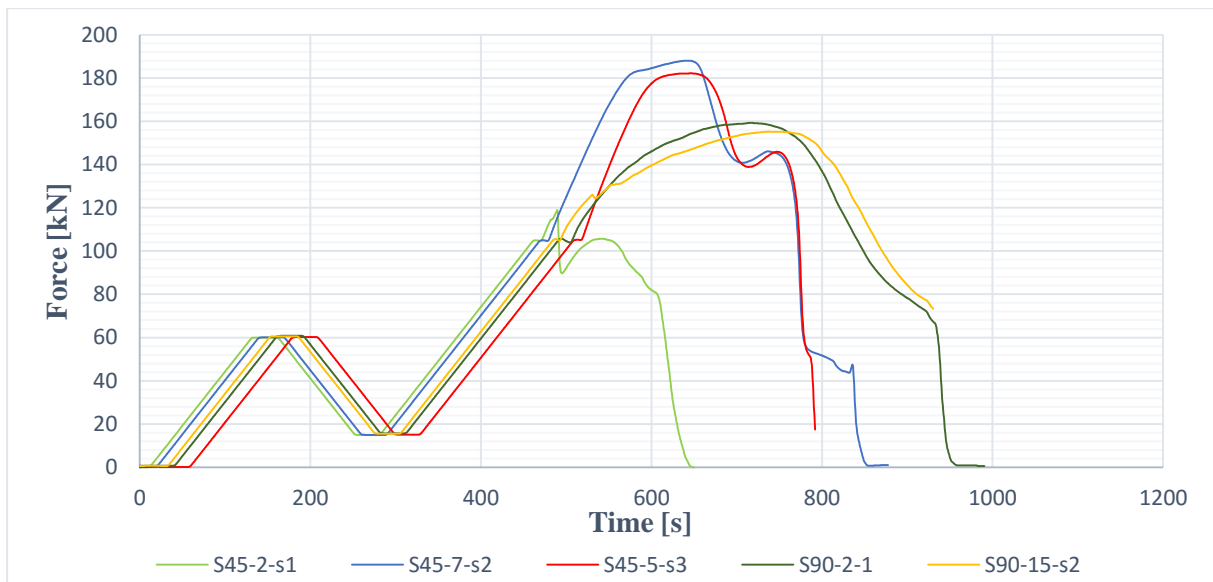
Figure 52: Development of force, static test

The two specimens on both S90 and S45 are behaving in a similar way. However, according to experimental observation 45-degree specimens are stronger. The difference in withdrawal capacity is 28kN, which is rather large. This might be also be caused by the difference in structure of the glulam elements.

Figure 51 and Figure 52 are displaying the force and displacement during the load application. The time count in the graphs start at logging, which is why the graphs have similar shape but are shifted in respect to each other when plotted with time. At 105kN, there is a small delay in continued load application caused by manually changing between load controlled and displacement controlled load application.

66
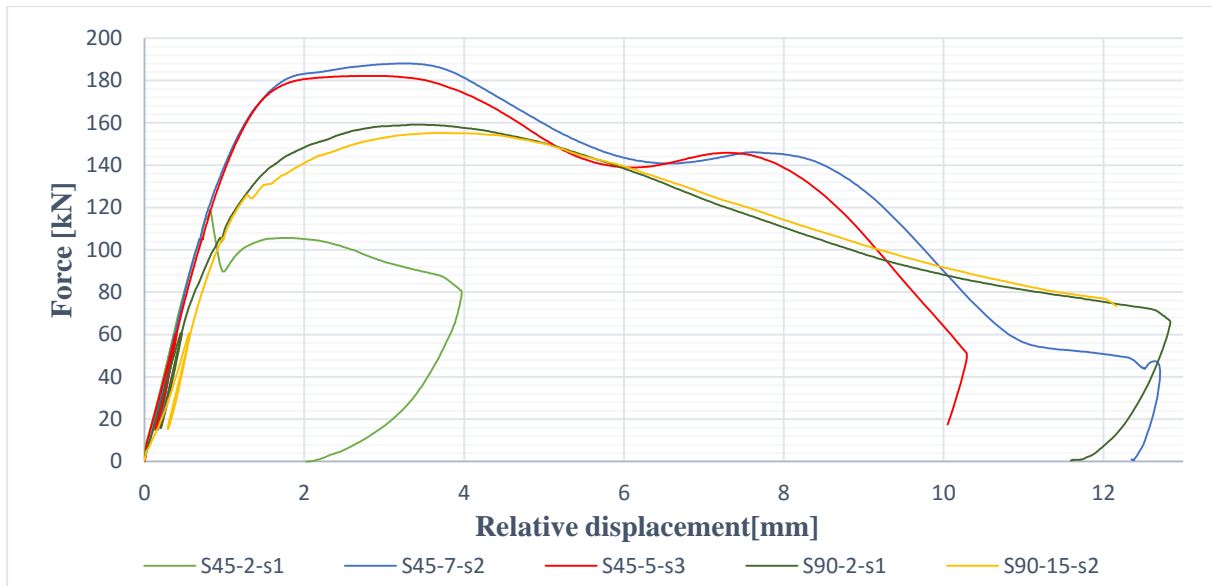
Figure 53: Stiffness during static load procedure

The failure for the 90˚ specimen is not very brittle, and the force is slowly descending over a span of several millimetres. While the 45˚ specimen experiences a slightly different drop in capacity after failure relative to the 90˚ specimens. Both specimen plateaus at max force while pulling the rod 2mm relative to the wood. The result from S45-2-s1 shows similar behaviour to the other tests until fracture. Then the failure is highly brittle, which is corresponding well with the failure mode observed with splitting along the fibres.

When only considering the 45˚ static test, the graphs stabilizes after the initial drop in a "valley" at about 75 % of the max force after 6mm relative displacement. After this, it actually experiences an increase in strength before the final the drop to complete failure. A similar observation is made in the paper on lagscrewbolts [19] (M. Gong et al. 2004) for 0˚ rod-to-grain angles. A "holding capacity" was obtained at the slip equal to the pitch of the rod. The difference in the two observations is that the valley is reached for the lagscrewbolts at slip equal to pitch, while in present testing, the final drop occurs when slip equals pitch (8mm). The 45˚ specimens also display less drop in load capacity after first failure. With these results, this might show a possibility of the 45˚ withdrawal tests to have the mixed failure characteristics of both 0˚ and 90˚ tests.

67

5.1 Failure modes

Most specimens subjected to static loading failed due to withdrawal of the rods. In general, the rods were pulled out with fracture in the wood surounding the threads embedded in the glulam.

At specimen with 90˚ rod-to-grain angle, cracking in the form of splitting along the fibres is observed to propagate along the length of the specimen. These cracks reached the end of the specimen, and are caused by forces imposed by pulling the fibres. The fibres between the pitches along the embedded part of the rods are broken. This results in splitting as the fibres are pushed outwards from the rod in the horisontal directions. At the surface the full fibres are pulled along with the thread. The fibres are splitted parallel to the grain, and large pieces are still whole. This is because the fibres are not held back similar to deeper in the glulam element.

For the 45 degree specimens, the fibres at the surface were pulled along with the thread at the surface. This is because the capacity along the fibres are much smaller than perpendicular to the fibres. Under this pulled out piece, the grains are longer and capacity in local breaking of the fibres along the rods are smaller than in splitting along fibres.

Table 15: Visual observations from static reference tests

90˚	45˚
- Fibres between the threads are "broken" with the pulling of the rod - Cracking along the length of the specimen to the end of specimen	- Fibres from between the threads pulled up with the rod - No cracking along the length - Pulled up fibres at the top of the specimen

No yielding or damage of the threaded rod was observed in any of the static tests. The tensile capacity of the steel rod is calculated to be 163.5 kN. Since failure happened at the interface between the outer threaded diameter of the rod and the wood, the capacity is larger than expected. The manufacturer of steel will always deliver goods of larger capacity to stay in the 95%-fractile. This is why the given capacity can be assumed to be conservative and the steel rod will most likely have more capacity.
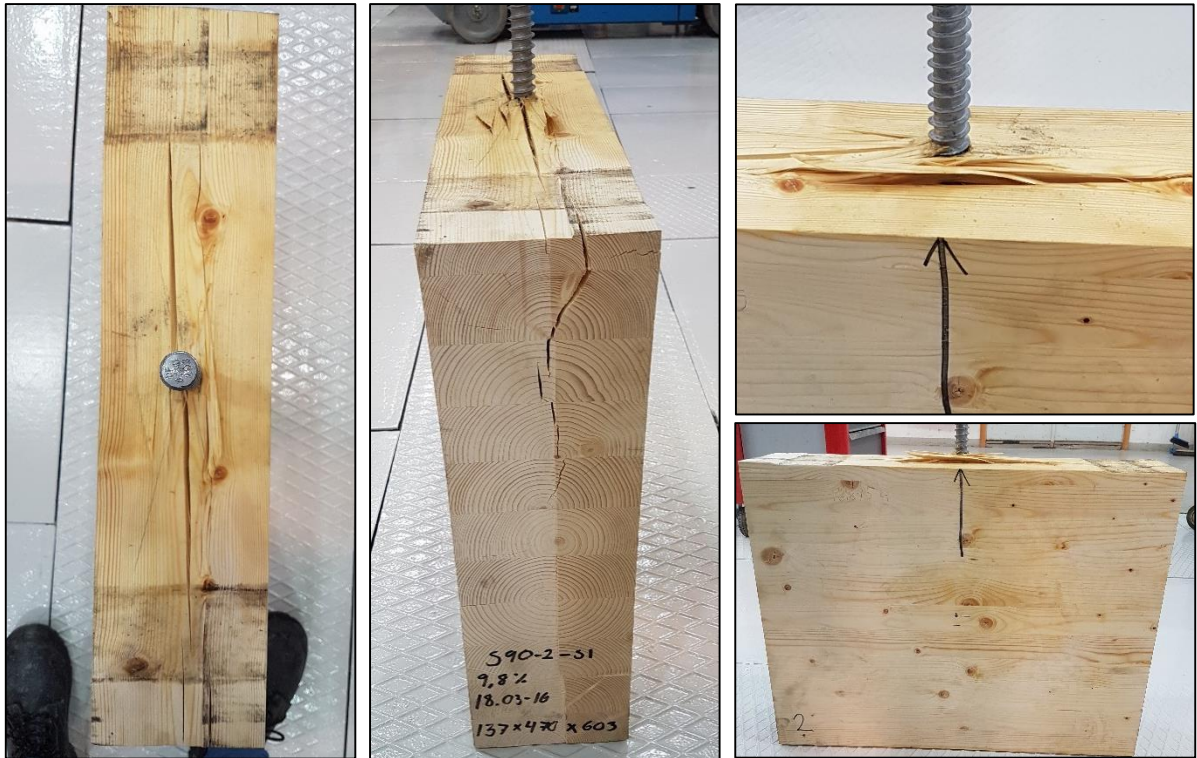
Figure 54: Failure of S90-2-s1
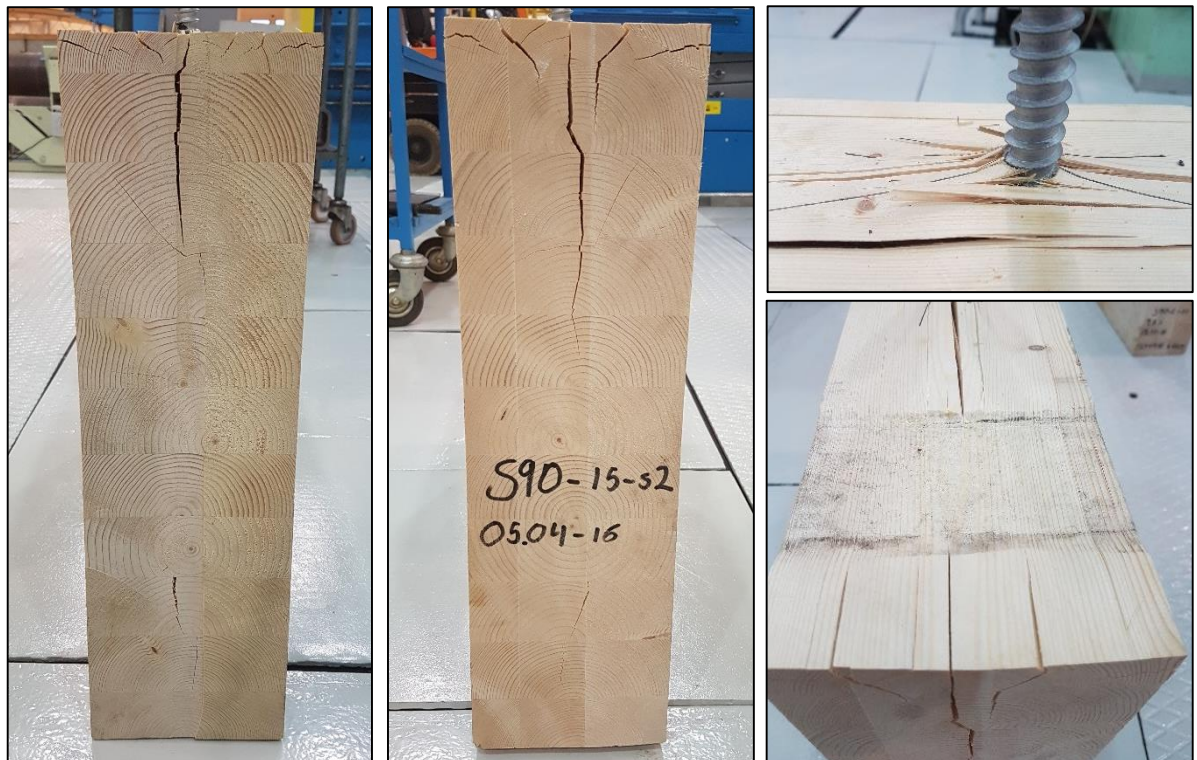
Figure 55: Failure of S90-15-s2

Figure 56: Failure of S45-7-s2 (above) and S45-5-s3 (below)

Failure mode of S45-2-s1:

The failure mode that was obtained is not desired during these tests. The fracture is parallel to the grain direction, 45 degrees to the threaded rod. Wood is weak in tension perpendicular to the fibres. With the stresses concentrated at the supports, the failure happens along the support. The threaded rod is pulling the fibres and lifting it, making the fracture parallel to grain direction. In reality, the fibres would not be cut and the threaded rods would be installed in a long beam (arch). Because of space and economic advantages, the specimen is small to look at the effects. To counteract this failure mode, another support system is used on the other 45˚ specimens that will distribute the force along the length of the top of the specimen (setup 2).

Figure 57: Failure mode of S45-2-s1

5.2 Previous experimental results

The experimental results were compared to the test results in "Withdrawal capacity of threaded rods embedded in timber elements" [1].

Table 16: From Table 1 in "Withdrawal capacity of threaded rods embedded in timber elements " [1]

Specimen	$P_{u.mean}$	St. Dev.	C. o. V.	Density
[I.D.]	[kN]	[kN]	[-]	[kg/m³]
S90-450-(1-5)	139.2	7.4	0.05	486
S60-450-(1-5)	141.7	4.5	0.03	476
S30-450-(1-5)	144.6	13.3	0.09	475

A possible linear relationship between the area of the interface surface between the outer threads the withdrawal strength is investigated. The difference in rod diameter and the embedment depth has to be taken into account. Linearly scaling the values for withdrawal strength in Table 16 to obtain compatibility with present testing:

$$P_l = P_{u.mean} * \frac{l_0}{l_{eff}} \tag{19}$$

$$P_{l.d} = P_l * \frac{d_0}{d_t} \tag{20}$$

71

P_l Maximal withdrawal force from Table 16 linearly scaled from l_{eff}=450mm to l_{eff}=440mm

$P_{l.d}$ Maximal withdrawal force from Table 16 linearly scaled from l_{eff}=450mm to l_{eff}=440mm and d_t=20mm to d_t=22mm

$$P_l = P_{u.mean} * \frac{440 \text{ mm}}{450 \text{ mm}}$$

$$P_{l.d} = P_l * \frac{22 \text{ mm}}{20 \text{ mm}}$$

Table 17: Linearly scaled values with new rod and embedment depth

Specimen	$P_{u.mean}$	P_l: l_{eff}=440 mm	$P_{l.d}$: l_{eff}=440 mm and d=22 mm	F_{ref}
[I.D.]	[kN]	[kN]	[kN]	
S90-450-(1-5)	139.2	136.1	149.7	157.2
S60-450-(1-5)	141.7	138.6	152.5	185.1
S30-450-(1-5)	144.6	141.4	155.5	(S45)

Comparing the withdrawal capacity $P_{l.d}$ from Table 17 and F_{ref} from Table 14, the values that are scaled from 90° rod-to-grain tests are similar. The deviation can be explained by the scatter, and the number of tests conducted here are not sufficient. Since 45° rod-to grain tests are not conducted in this report, it is assumed that the value can be compared with the value between 30° and 60°. The experimentally conducted withdrawal forces from these two types of tests are similar. However, the difference between the scaled values are deviating about 20kN from the tests presently conducted, which is almost similar to the deviation in respect to 90° specimens. This is supporting the earlier theory of stronger lamellas in the 45° specimens. The reference withdrawal strength used to calculate the cyclic load level is therefore chosen as the mean values from present static testing.

5.3 Analytical evaluation

This chapter includes evaluation of the static test properties with some analytical and empiric models. Relevant models are presented and at the end, the results are compared with the experimental results.

5.3.1 Eurocode 5 – Part 1-1 [6]

Withdrawal strength capacity of screws (outer screwed in diameter >12mm) is mentioned in EC5-1-1 section 8.7.2(5) [6] . Formula (21) is numbered as (8.40a) in EC5-1-1.

$$F_{ax,\alpha,Rk} = \frac{n_{ef} f_{ax} d * l_{ef}}{1.2 \cos^2 \alpha + \sin^2 \alpha} \left(\frac{\rho_k}{\rho_a}\right)^{0.8} \tag{21}$$

$F_{ax,\alpha,Rk}$ Characteristic withdrawal capacity of screw.

n_{ef} Effective number of screws.

$f_{ax,k}$ The characteristic withdrawal parameter perpendicular to grain direction.

d Diameter of the threads.

l_{ef} The embedment depth of the threaded rod in the timber.

α The angle between grain direction and the insertion of the threaded rod.

ρ_k The characteristic density (for GL30c: 390 kg/m^3).

ρ_a The density with connection to $f_{ax,k}$.

NS-EN 14592 [40] chapter 6.3.4.3 states that:

"For screws the characteristic withdrawal parameter $f_{ax,k}$ the result shall be declared on one or more characteristic timber densities or on other types of timber products, either directly by testing in accordance with EN 1382 or declared by calculation according to the relevant equations given in EN 1995-1-1."

For threaded rods of these dimensions (d > 12 mm), the equation from EC5-1-1 to estimate the withdrawal parameter is not valid. The parameter could be given from the manufacturer of the threaded rods, but in this case, the required tests have not been conducted and the information is limited. The expression from DIN 1052 [41] can be used to estimate the characteristic withdrawal parameter.

5.3.2 DIN 1052 [41]

According to DIN 1052, the withdrawal strength can be estimated from an equation that is independent of the grain angle with respect to the embedment direction. A restriction is imposed, and the validity of the equations requires that the condition 45˚<α< 90˚ is met. Instead of using the characteristic value for density, the middle value were used when comparing results. The density between the two different specimens were relatively large.

$$F_{ax.Rk} = f_{1.k} \cdot l_{ef} \cdot d \tag{22}$$

$$f_{1.k} = 70 \cdot 10^{-6} \cdot \rho_k{}^2 \tag{23}$$

5.3.3 Analytical model from "Withdrawal capacity of threaded rods embedded in timber elements" [1]

The theory were developed and is described in a report (Stamatopoulos and Malo 2015) [1] made in connection with the doctoral thesis of Haris Stamatopoulos from 2016 [2]. The theory is based on a model of an axially loaded connector embedded in a timber element from (Jensen et al. 2001) [17]. This theory is based on Volkersen theory from 1938.

The assumption from (Jensen et al. 2001) [17] is that all the shear deformation will occur in an infinitely thin layer defined in the glue between the connector and the wood, and the glue will deform linearly. The connector and the surrounding wooden material is assumed to be in constant axial stress. For screwed-in connectors without adhesive, the assumption of the infinitely thin layer from (Jensen et al. 2001) [17] is no longer valid. The shear deformation is therefore assumed to be happening in a finitely defined shear zone located between the wood and the outer surface of the threaded rod. Pure uniform axial stresses are allocated to another zone of the wood with a defined cross sectional area. The displacement is the equal to the relative displacement between the connector and the timber element.

$$\delta(x) = u_s(x) - u_w(x) \tag{24}$$

$\delta(x)$ Displacement of the shear zone.

$u_s(x)$ Displacement of the connector.

$u_w(x)$ Displacement of the wood.

Where x is the distance from the entering point of the threaded rod to the considered point, shown in Figure 58.
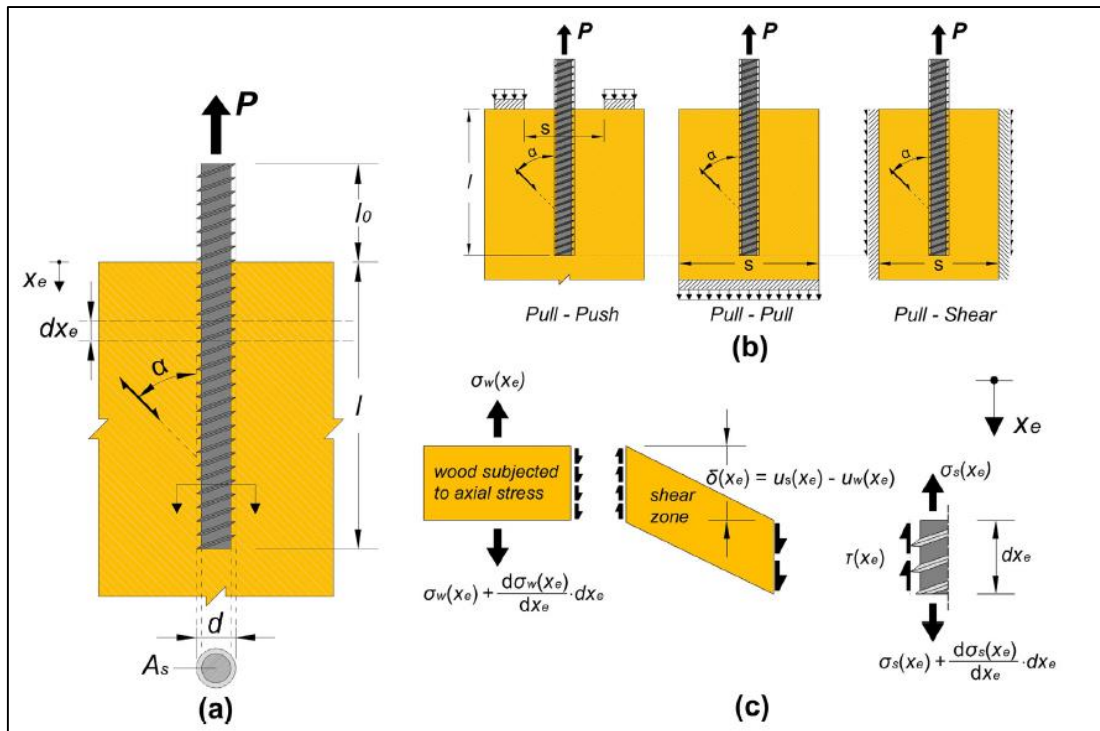
Figure 58: Modell of axially loaded connector [1]
(a) geometric features, (b) loading conditions and (c) stress state of an infinitesimal slice dx_e

The shear stress versus displacement behaviour is modelled with an idealized bi-linear constitutional law. This separates the curve into two different zones: elastic and post-elastic behaviour. The equivalent shear-stiffness parameters for the elastic and the fracture zone are denoted Γ_e and Γ_f respectively. They define the slopes of the two zones. This theory is described with the following equations:

$$\tau(x) = \Gamma_e \cdot \delta(x) \qquad\qquad \delta(x) \leq \delta_e = f_w/\Gamma_e \qquad (25)$$

$$\tau(x) = f_w - \Gamma_f \cdot (\delta(x) - \delta_e) \qquad \delta(x) > \delta_e = f_w/\Gamma_e \qquad (26)$$

Where f_w is the elastic withdrawal strength and δ_e is the maximal elastic displacement of the shear zone.
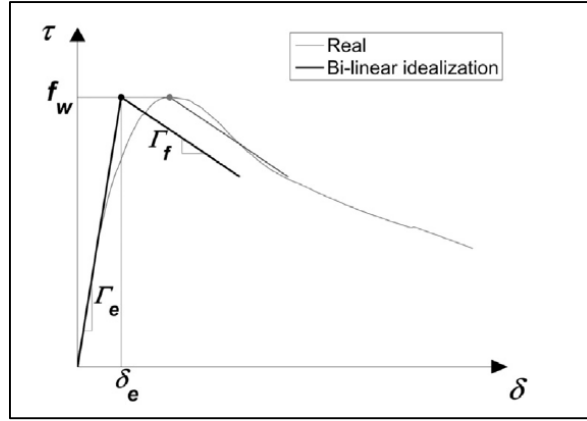
Figure 59: Real and idealized bi-linear τ-δ curve. Fig. 2 in [1]

This theory results in an expression for the based on equilibrium from Figure 58 and boundary conditions concerning the pull-shear condition from Figure 58(b):

$$\frac{P}{\pi \cdot d \cdot l \cdot f_w} = \frac{\sin(m \cdot \omega \cdot \lambda)}{m \cdot \omega} + \frac{\tan((1-\lambda)\omega) \cdot \cos(m \cdot \omega \cdot \lambda)}{\omega} \tag{27}$$

$$f_{w.\alpha} = \frac{4.35}{0.91 \cdot \sin^2 \alpha + \cos^2 \alpha} \tag{28}$$

$$m_\alpha = \frac{0.332}{1.73 \cdot \sin \alpha + \cos \alpha} \tag{29}$$

$$\Gamma_{e.\alpha} = \frac{9.35}{1.5 \cdot \sin^{2.2} \alpha + \cos^{2.2} \alpha} \tag{30}$$

$f_{w.\alpha}$, $\Gamma_{e.\alpha}$ and m_α are equations based on regression derived from experimental values conducted with the smallest embedment depth (100mm). The equations are used as an estimate. The parameter m is a measure of the brittleness of the shear zone, while λ is the dimensionless fracture length parameter:

$$m = \sqrt{\frac{\Gamma_f}{\Gamma_e}} \tag{31}$$

$$\lambda = \frac{l_f}{l} \tag{32}$$

76

l_f is the fracture zone length of the shear zone and l is the embedment depth. Assuming for simplicity that the shear zone will be entirely in the fracture domain ($\lambda \approx 1$) for simplicity. Inserted into the expression above, the withdrawal capacity can be calculated:

$$P = \frac{\sin(m \cdot \omega)}{m \cdot \omega} \cdot \pi \cdot d \cdot l \cdot f_w \tag{33}$$

5.3.4 Comparison of values

Note that different mean density values have been used and that is why the 45° rod-to-grain angle calculations have more capacity when this value is used. Values linearly scaled for both different diameter and embedment.

	DIN 1052	DIN 1052	EC51-1	Theory [1]	Scaled values [1]	Present testing
ρ	Char.	Mean	Mean	-	488	433/495
F(90)	103.06	127.04	127.04	145.4	149.7	157.2
F(45)	103.06	166.03	150.94	138.5	154*	185.1

*Mean value of scaled 60° and 30°

6 Results - Cyclic testing

It was decided to start the cyclic testing with 90° grain-to-rod specimens. After some tests was completed, it was evident that the process would take too much time to complete all the specimens. Specimens were altered as earlier mentioned to include a new embedment depth.

Table 18: Results fatigue testing, values from complete table in Annex I

Specimen	E. depth	Load level	Max load	Moisture	Weight	Density	Cycles, timber failure	Cycles, steel failure
	l_{eff}	f_{max}	F_{max}		W	ρ	N	N
	[mm]		[kN]	[%]	[kg]	[kg/m^3]		
S90-2-s1	440	1,01	159,22	9,8	16,845	433,85	0,25	
S90-15-s2	440	0,99	155,18	10,8	16,83	431,55	0,25	
S45-7-s2	440	1,02	188,03	12,8	19,67	465,74	0,25	
S45-5-s3	440	0,98	182,15	12,5	19,55	498,23	0,25	
S90-9-d1	440	0,75	118	9,9	17,76	463,08	0	
S90-10-d2	440	0,75	118	9,4	17,87	465,95	0	
S90-11-d3	440	0,75	118	10,5	17,34	442,75	27026	
S90-12-d4	440	0,75	118	10,7	17,38	446,60	20550	16919
S90-8-d5	440	0,75	118	10,1	17,196	441,87	16960	16725
S90-14-d6	440	0,60	94	10,6	16,91	429,62	79033*	46982
S90-1-d7	330	0,60	71	10,8	16,852	425,04	464845*	98414
S45-27-d1	300	0,824	104	12,0	19	479,22	8178	
S45-6-d2	330	0,75	104	12,0	19,58	493,85	15619	
S45-4-d3	330	0,75	104	11,8	19,16	483,25	21994	
S45-26-d4	330	0,75	104	11,6	19,2	484,26	17979	
S45-25-d5	330	0,60	83,3	12,1	19,3	486,78	91289*	91289
S45-30-d6	330	0,65	90,2	11,7	18,5	466,61	75517	45721

*Terminated without timber failure

78

Special events during testing:

S90-9-d1 & S90-10-d2

Test specimens S90-9-d1 and S90-10-d2 were tested with setup 3. The test was started by slowly applying load until mean value of the cycle is reached, and then the load cycle was applied at 0.1 Hz. However, it was apparent shortly after this that the test should be terminated. By visual inspection of the movement, the specimens were found to be pushing against each other. This resulted in friction, which imposed forces in the horizontal direction to the specimens. The test was terminated at 72 cycles. These specimens were placed in the climate room and not tested further.

S90-11-d3

The first test to proceed to failure and the "dummy test" for fatigue testing. The frequency of loading was slowly increased from 0.1Hz to the final 2.5Hz during the first ten minutes. This was to investigate and monitor how fast the machine would be able to apply the load without problems. The machine might have difficulties if the displacements are too large. The distance the machine has to move to apply the given load cycles require a large amount of oil capacity.

This specimen had been taken out and placed in the rig four days before start up. There was some problems with the displacement transducers, and the intended start had to be postponed. Some visible cracks formed at the end of the beams during this time. In addition, oil from the machine had been spilling onto the specimen.

S90-12-d4

The displacement was measured from the L-profiles relative to the threaded rod, because of a misunderstanding in communication. This was the first test where laser transducers was used. The logging of data was restarted at 445 cycles because the computer stopped logging. After the steel failure, no cooling system was mounted on the threaded rod and temperature slowly increased.

Following temperatures were measured:

16919 cycles: 26.8°C (Start-up)
18000 cycles: 29.2°C
19800 cycles: 34.6°C
20550 cycles: 36.2°C (Steel failure)

S90-8-d5

This test was run until experiencing steel failure. It was then discovered that the machine had started leaking oil, and the continued test had to be moved to another machine in the laboratory. The test was restarted at the new machine. However, a fracture along the fibres underneath one of the supports (L-profiles) had developed and the test was terminated after few cycles. This might indicate that the new set up impose too large forces along the grains in the 90˚ specimen. Due to this observation, another setup was developed. Another possible factor could be that the oil worsened the already developed crack. There was some time where the new machine was prepared, and the oil could be absorbed by the timber.

S90-14-d6

First test conducted at next load level and setup 5 was used. This setup is designed with the purpose of removing some of the forces in the horizontal direction that might contribute to steel failure. There is no possibility of testing more than one more time after this failure because of the space between the machine and the setup. The test was terminated after steel failure number two.

S90-1-d7

In an effort to obtain fatigue failure as withdrawal of the rod from the timber element on the next load level, a new embedment depth was introduced. The threaded rod does not have enough capacity to withstand enough cycles, and will be experiencing fatigue failure in the steel. With less embedment depth, failure in timber might be obtained sooner. In addition, the load range will be lowered, giving the threaded rod longer fatigue capacity. With more of the rod exposed, the machine can grip the rod four times. The test was terminated at 464845 cycles after three restarts.

S45-27-d1

After the test was conducted, it was found that the specimen was cut with lower embedment depth than intended. This was due to an error in measurement when cutting the original sample. The load is therefore too high in respect to estimated withdrawal capacity. This resulted in failure at LCF.

S45-25-d5

When the specimen was observed during testing, signs of horizontal forces were spotted. The specimen moved horizontally inside the frame with the cycles. This might have caused the unusual location of steel failure, which was obtained for this specimen. This was the only occurrence of steel failure in the rod close to the wooden surface. The test was terminated after first steel failure, as the remaining part of the rod was embedded in the timber element.

S45-30-d6

Obvious moment forces were observed from horizontal movement during this test as
well. However, steel failure happened close to the round steel profile near the grip as
usual.

Table 19: Density of specimens subjected to cyclic load

Specimen	Moisture content	Density	St. Dev.	C. o. V.
[I.D]	[%]	[kg/m^3]	[kg/m^3]	[-]
S90-x-dx	10,50	442,75	15,37	0,0347
S45-x-dx	11,9	483,8	9,10	0,0188

Table 19: Density of specimens subjected to cyclic load display the mean moisture content
and density form specimens tested with cyclic load application. The density for specimens
with lowered embedment depth were estimated with the original values for the geometry of
the specimen. The specimens were weighed before altering, and therefore the density had to
be calculated with the original measurements. The specimens were assumed to be b=140mm,
h=472mm and L=600mm before removing the top 110mm layer of glulam to achieve
l_{eff}=330mm. The mean density from static tests were calculated for α=90° and α=45° equal to
432.7kg/m^3 and 494.8kg/m^3 respectively. The gap between these values have decreased with
more values, however there is still a notable difference. Specimens with 45-degree rod-to-
grain angle had larger density.

6.1 Failure modes

Steel failure was obtained for all but one of specimens with 90˚ rod-to-grain angle. The tests
conducted on 45˚ specimens at lower load level (<75%) also lead to failure in steel. The
fracture surface showed typical fatigue failure for steel, with the propagation starting at one
side of the area with the final tearing of the material at the other side (Figure 60). The rods
were subjected to bending from movement of the timber element. The frame of the setup
enabled horizontal movement of the glulam element, which could be observed visually during
cyclic load application. The rod was connected to the machine in a rigid grip, which created
bending in the rod. All but one of the steel failures were located at the rod where were gripped
by the machine.
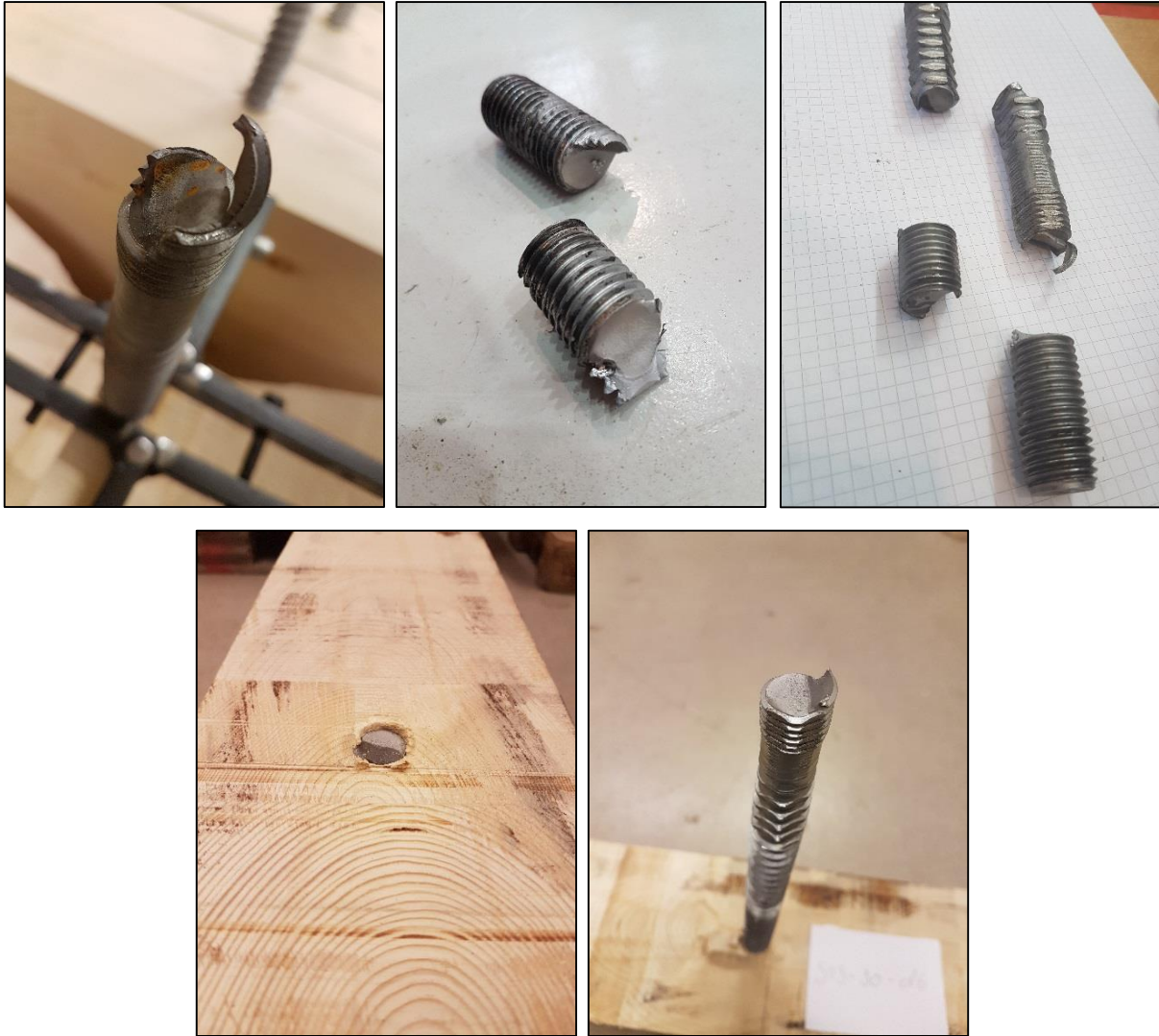
Figure 60: Steel failure

Fatigue failure of timber in this connection were observed similar to the failure mode for the static reference tests. However, some difference in crack development horizontally for the 90˚ specimens where observed. When subjected to cyclic load, the crack did not develop along the full length of the top of the specimen. The crack was less developed, and there were no evidence of splitting along fibres at the end of the specimens. In general, the fatigue failure mode showed more tearing of fibres with less "smooth"-surface pieces of wood pulled out. The static failure mode was more characterized by splitting and larger pieces of wood tearing. This supports the observations from "Fatigue Behaviour of Lagscrewbolted Timber Joints" [19].

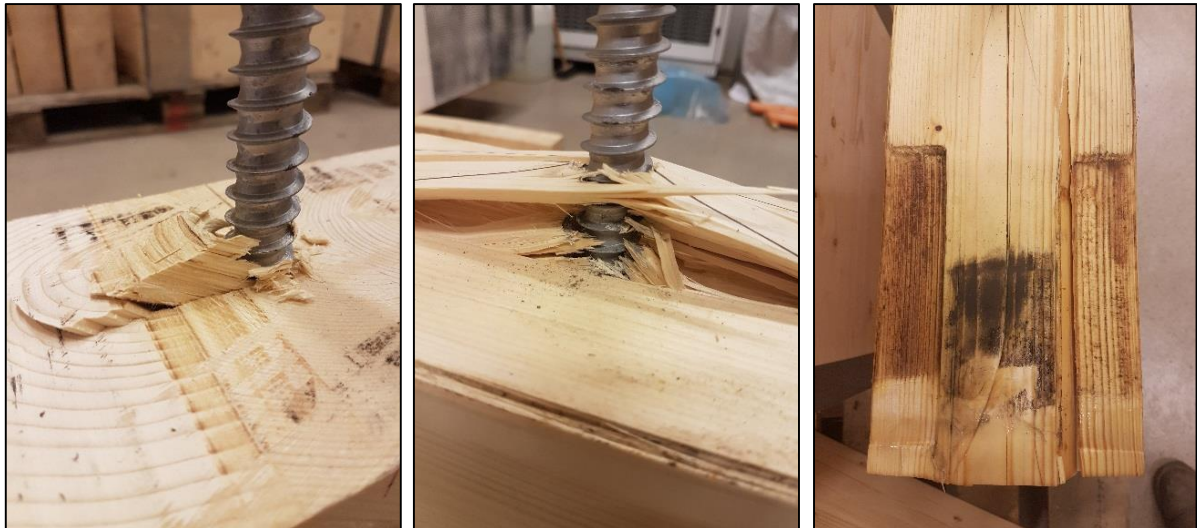*Figure 61: Fatigue failure of timber: S45-26-d4 (left), S90-12-d4 (middle), S90-8-d5 (right)*

Two failure modes were unexpected. For specimen S90-8-d5 a different failure mode of timber occurred. The wood failed from compression imposed by the supports (altered L-profiles). The surface area of the support to distribute the compression forces in the push-pull configuration was found to be insufficient. Relatively large plastic deformation was observed due to the forces imposed by the supports were observed for this specimen. One other specimen were tested under similar conditions with the same setup and load application, without developing the same large deformation at the surface of the specimen. This might suggest that the specimen have been influenced by the oil at the top surface, which it were subjected to for a longer period. However, in compliance with calculations, this lead to the conclusion that the altered L-profiles did not have enough surface. This setup was therefore changed.

The other surprising failure occurred in specimen S45-25-d5, shown bottom left in Figure 60. This is a steel failure, located near the surface of the timber element. This was the only specimen tested on 60% load level for 45˚ specimens. The embedment depth was 330mm and more of the rod were exposed (longer arm for the moment). Relatively large movement was observed during testing, which might have caused the different location of steel fatigue failure.

6.2 Steel failure

After experiencing the first fatigue failure of steel in S90-12-d4, a check of fatigue capacity for the threaded rods were made according to EC3 part 1-9 [38]. Figure 62 illustrates the first two load levels used in cyclic testing on 90˚ specimens with embedment depth 440 mm. The graph display the relationship between applied force range and the number of cycles before fatigue failure of the steel. Point A is the capacity of the threaded rod subjected to the largest load level used on 90˚ specimens. In this case, the largest load range was at 106.2kN. The threaded rods have the capacity of withstanding about 4000 cycles. The second line (B) represent the calculated value of fatigue capacity for the rods during the second load range. At this load range of 84.8kN, it were estimated to be able to endure 7000 cycles. The first obtained steel failures of all specimens are plotted in the graph. The specimens with failure in the threaded rod were subjected to load ranges at a high enough values to cause fatigue failure according to the Eurocode.
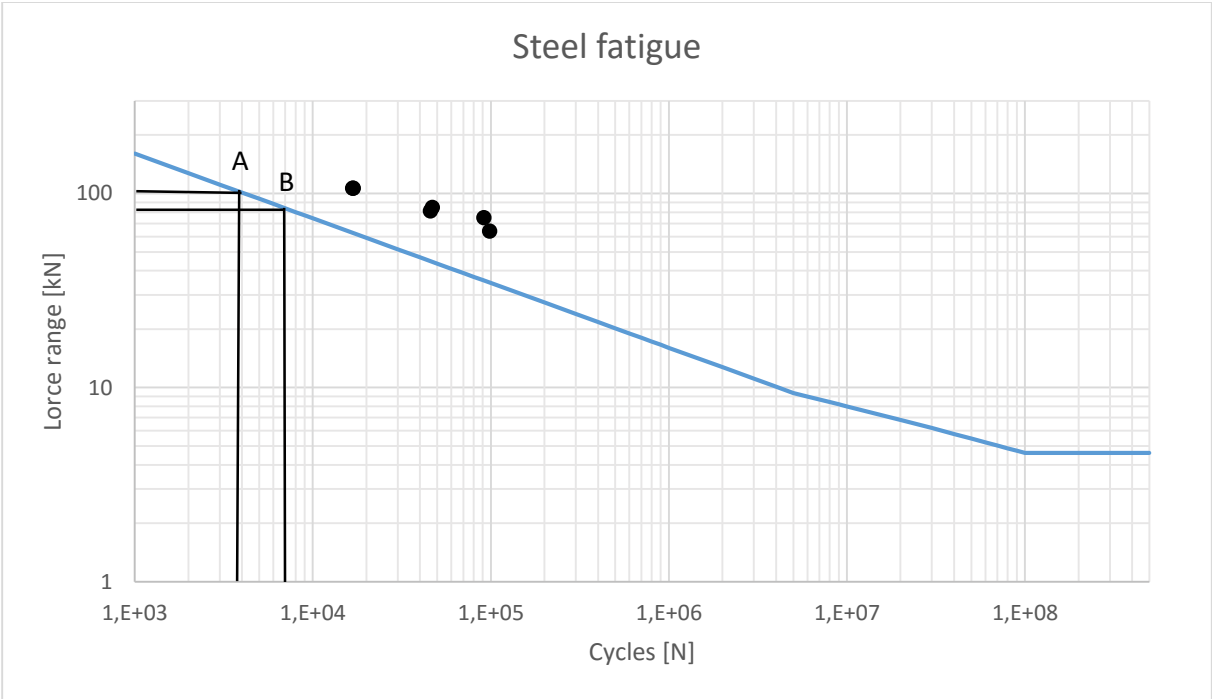
Figure 62: Cycles to failure in steel with the applied force range.

Eurocode 3 part 1-9 [38] is a design guide to ensure stability and mechanical resistance of structures and structural elements subjected to cyclic loading. It is therefore a fair assumption that the actual capacity is a bit higher and that the graph will display conservative values. Some of the increased capacity might also be contributed to the hardening by rolling of the threads in the screw. Calculations concerning the capacity of the threaded steel rod (static and fatigue) are included in Annex C.

6.3 S-N curve
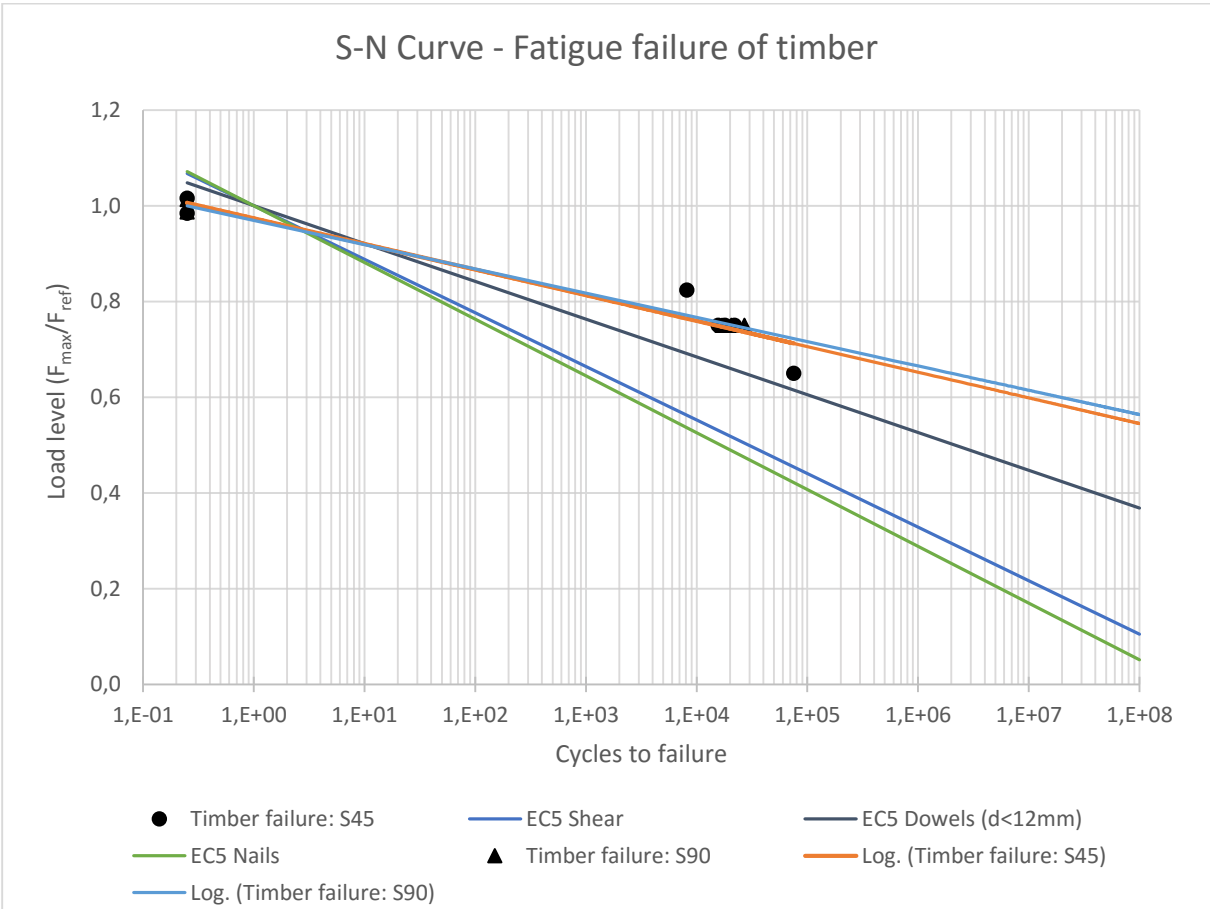
Figure 63: S-N curve and EC5 requirements

The S-N curve was derived from the obtained values of specimens experiencing in fatigue of timber. Many of these specimens had already obtained steel failure and had to be restarted to obtain fatigue failure of rod withdrawal from timber element. It has to be noted that one test for 90˚ specimens failed in timber compression, and one 45˚ specimen was by accident subjected to load level resulting in LCF. Both results were included to make the S-N curves for each of the rod-to-grain angles. Static reference loads are included, plotted with 0.25 cycles. This is the number of cycles from the start in one cycle until reaching its first peak. This is the best representation of static load application. The design values for dowels, nails and structure elements in shear from EC5 part 2 [11] are plotted with the S-N curves for the different specimens.

By observation of the S-N curve, the regression lines (trend lines) are remarkably similar for the two rod-to-grain angle specimens. The values obtained for different embedment depth and grain angles but with the same load level, are placed relatively close to each other in the plot. S-N curves for each of the rod-to-grain angle specimens are also added in Annex I. The equation for the regression lines for the two specimens are:

$\alpha = 90°$ $\qquad\qquad\qquad\qquad y = -0.022 \ln(x) + 0.9694$

$\alpha = 45°$ $\qquad\qquad\qquad\qquad y = -0.023 \ln(x) + 0.9738$

As the testing were more time consuming as first assumed, a limited number of test results were obtained. The S-N curves derived from a limited plot will have a large amount of uncertainty, and consequently will be more sensitive to each result. More tests need to be conducted for a variety of load levels and rod-to-grain angles to gain more certainty in information on this connection. Here, the curve were mainly derived from fatigue tests conducted with normalized maximum load range of 67.5%.

6.4 Relative displacement, first cycles

The stiffness during fatigue life is valuable information. The changes in behaviour and properties are important to investigate. For dowel joints, the bolts are installed in pre-drilled holes with larger diameters, and an initial slip is observed in the connection before reaching full capacity. The displacement during the first set of data points were used to investigate if a similar effect could be observed in the connection with screwed-in joints.

The curves in Figure 64 and Figure 65 were made by plotting the difference in displacement at maximum and minimum force. The actual maximum and minimum displacement were observed to often occur after the force switched direction when passing a peak. This value were estimated to occur 0.02-0.06s after passing of a peak. This means that the actual relative displacements were larger than illustrated in Figure 64 and Figure 65. However, it is assumed to be a good enough estimate here with the similar shape of the plot.
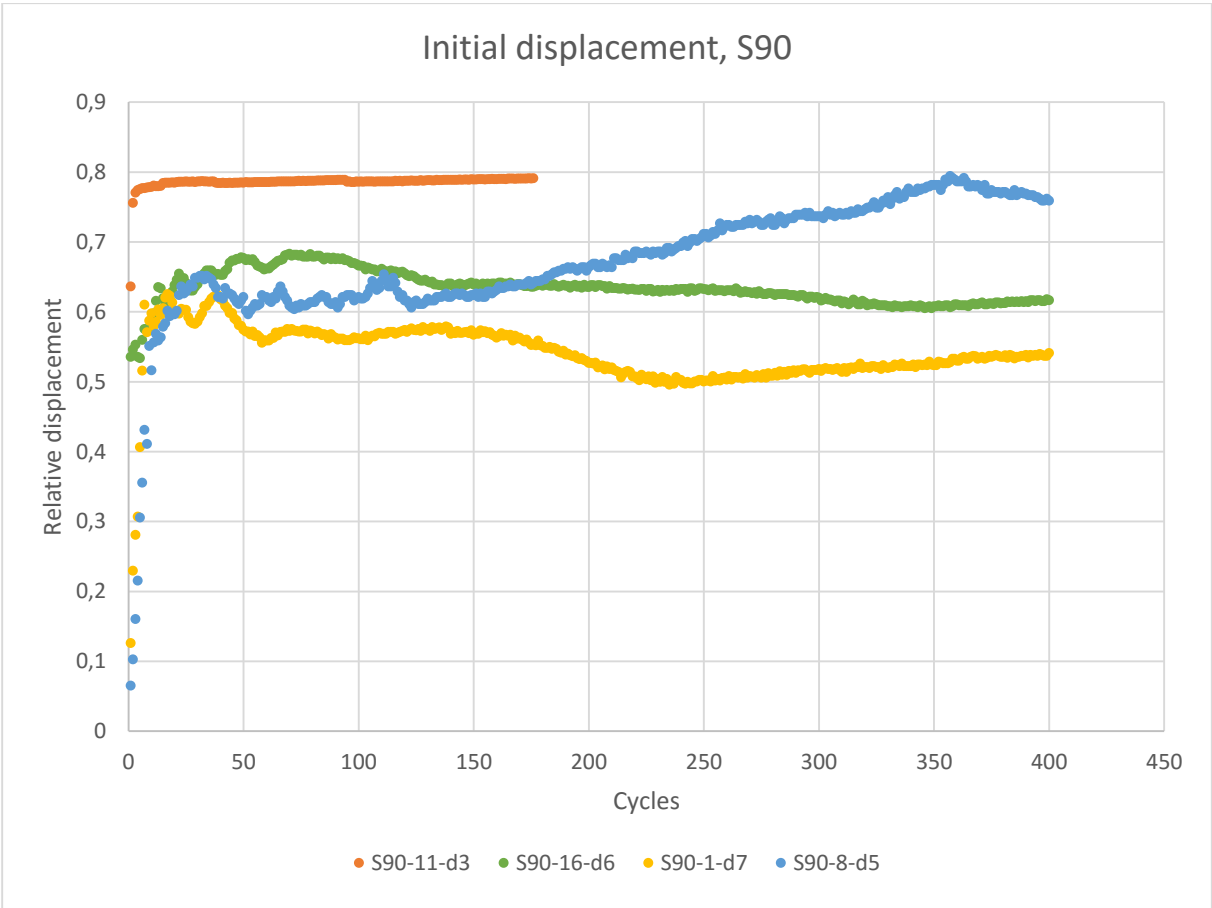

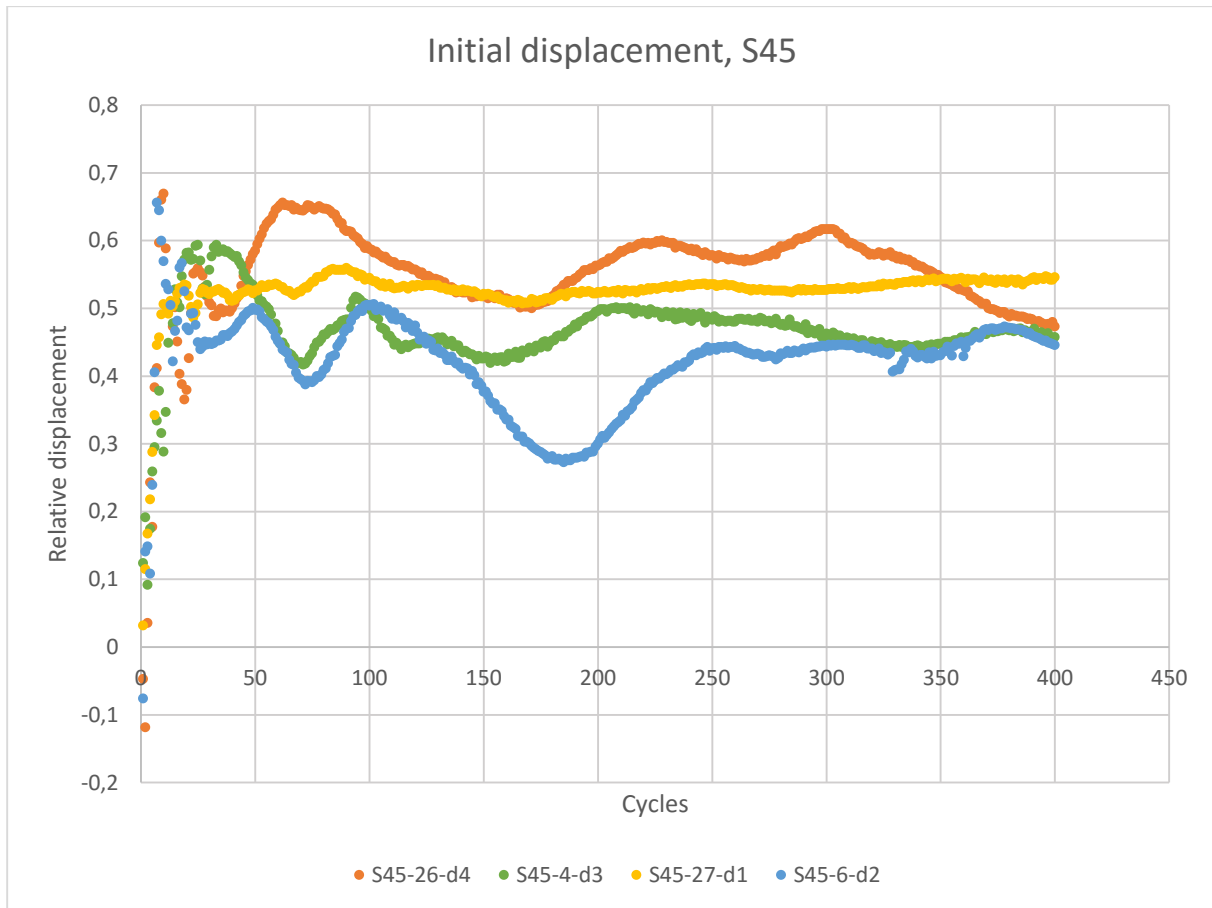*Figure 64: Displacement during the initial phase, S90*

Figure 65: Displacement during the initial phase, S45

In Figure 64, the relative displacement in the cycle is displayed. The displacement range between maximum and minimum force for each cycle is plotted for the first 400 cycles of the tests. The red curve represents the first test, S90-11-d3, which have less data plots. This particular test was subjected to load cycles at 0.1 Hz. A lower amount of cycles were applied during the first 10 minutes, and consequently the logged peak values were fewer. The plot shows an overall similar behaviour. In the first few cycles, the rod is "setting" into the wood. In addition, the machine have to run a small amount of cycles before reaching the actual maximum and minimum peak loads of the cycle. However, the line soon flattens and the displacement is more or less continuous for 90-degree specimens. S90-16-d6 and S90-1-d7 are similar, and the gap can be explained by the difference in load application. Both are at f_{max}=0.6, but S90-2-d7 have less embedment depth with a lowered reference load. The difference in S90-11-d3 and S90-8-d5 might be explained by the difference in frequency, as they are subjected to similar load level. From the literature, larger displacements and more damage will occur with lower frequency. It has to be noted that one displacement transducer were non-functional during test of S90-8-d5. Figure 65 shows the plot for 45˚ specimen. The curves show in general larger variations in comparison with results from 90˚ specimen. This might indicate a difference in behaviour when the rod is inserted at different rod-to-grain angles. However, this plot also show the tendency to flatten after the first 250-300 cycles imposed on the specimen.

7 Summary and conclusion

7.1 Summary of experimental testing

A total of five specimens were tested for establishing static reference load in withdrawal. One failed in splitting, and was not included to establish the static reference load. The results obtained from 90˚ specimens showed good compatibility with calculations conducted with different analytical estimates. The static withdrawal capacity also showed good fit with linearly scaled previous results in respect to different rod diameter and embedment depth. 45˚ specimens did show larger capacity in withdrawal than expected. A larger volume of stronger wood lamellas in the specimen might explain this. A higher measured density in the 45˚ specimens supports this theory.

Cyclic tests were conducted on thirteen specimens, two of which were terminated after few cycles and not counted in the results. Five specimens with α=90˚ and six specimens with α=45˚ constitutes valid test results. Steel failure was observed in six of the specimens, while failure in withdrawal was obtained for eight of the specimens. Some of the specimens experienced both failure modes as the test was restarted after experiencing steel failure.

The number of completed tests were limited by several expected and unexpected problems. Due to the fact that there have been little, or no equivalent testing on these connections in fatigue, it was expected that some (unexpected) practical problems could be met. Additional problems were also disclosed by elements not connected to the experimental setup or specimen. The first test machine had a defected hydraulic system and were almost constantly leaking oil. This caused delay in testing when repairs was needed, and when the tests had to be moved to a new machine. Displacement logging proved to be problematic as well. Different displacement transducers (both laser and rod) had connection problems. In addition, the computer sometimes stopped logging and saving data during testing, which had to be resolved by a computer restart.

The setup used in these experimental tests were changed and improved during the course of testing. It was developed based on previous experience from experimental tests conducted on similar specimens subjected to static axial load application (Stamatopoulos, 2016) [2]. The objective for these tests was to obtain and observe fatigue failure of rod withdrawal from the timber element. When it became evident that steel failure would most likely occur before withdrawal, different setups were tested to strengthen the steel capacity by eliminating unwanted movement during load application. In addition, a shorter embedment depth was introduced to increase steel capacity and lower withdrawal capacity of glulam in fatigue. Fatigue failure of timber still proved to be difficult to obtain, especially at lower load levels.

The steel failure was observed for all but one test conducted on specimens with 440mm embedment. With lowered load level, the difference in fatigue capacity between steel and timber withdrawal seemed to increase. The introduction of 330mm embedment depth proved to be effective in decreasing this gap, and for 45˚ specimen no steel failures were observed at 0.75 normalized maximum load level.

As earlier mentioned, less embedment depth will lower the withdrawal capacity of the timber element. However, for this connection, a lowered embedment depth will not be used to practical solutions. Lowered embedment depth would not exploit the full static rod withdrawal capacity. This solution were used to enable observation of the fatigue behaviour in withdrawal. Steel capacity can be increased by preloading or with a surface treatment to eliminate micro fractures at the surface of the rod. Better setup might also contribute to a longer fatigue life in the steel of the threaded rod. The horizontal movement in the rod contributes to crack initiation, and needs to be eliminated.

7.2 Summary of literature

The existing literature is sparse for axially loaded connectors in timber elements. These properties are therefore still largely unknown, and an increased amount of research are currently being conducted that involves timber and timber connectors. Recent research papers conducted for connections and composites were prioritized in this paper, along with available information found in textbooks. TCC bridges are one of the structures currently contributing to increased research on timber connections subjected to fatigue load conditions. Several solutions for concrete-timber connections have been investigated. The use of timber in the rotor blades in windmills have also prompted research on fatigue in wood when subjected to different load combinations.

All research papers found on fatigue in axially loaded rods (bonded-in and screwed in), was inserted at a 0˚ rod-to-grain angle. Failures in bonded-in connectors using adhesive components were found to sometimes be experiencing brittle and sudden failures. Threaded rods however, show relatively ductile and stable behaviour until failure (both static and fatigue).

Important information from literature:

- A simplified method for fatigue design in timber bridges are described in EC5 part 2, Annex A [11]. This verification requires values for coefficients *a* and *b*. Table A.1 in EC5 part 2 does not include values for axially loaded threaded rods.
- Static withdrawal capacity for threaded rods can be estimated by EC5. Alternatively, a newly developed theory with the use of a bi-linear constitutive law can be applied with good prediction (Stamatopoulos et al., 2015) [1].
- For fatigue testing, a fatigue limit is thought to exist for wood and connections [4]. It is somewhat disputed, but in general it seems acceptable as a working hypothesis.
- The fatigue strength can be considered a linear decaying function of the logarithm of the number of cycles in accordance with the classical work of Wöhler (Malo, 2002) [18]. Fatigue strength increases with decreased load level.
- The use of normalized maximum stress as fatigue strength parameter seems more reasonable than the use of normalized stress range (which is common for steel) (Malo, 2002) [18]. EC5 part 2 currently use normalized maximum stress.
- Fracture morphology in cyclic loading differs from static withdrawal of LSB (lagscrewbolts) (Gong et al., 2004) [19].

- Reversed load cycles are most severe on axially loaded wood laminates in fatigue. Pulsating compression is more damaging in fatigue than pulsating tension (Bonfield et al., 1991) [14].
- Stress versus strain hysteresis loops can be used to observe damage accumulation in wood composites (Hacker, 2001) [25].
- The fatigue performance tend to depend on moisture content and density (Ansell, 2003) [15].
- Bonded-in rods can experience more failure modes than threaded rods. The interfaces between layers in the connection might limit the capacity in both fatigue and withdrawal. Different adhesives in bonded-in rods have proved to behave fundamentally different. The choice of adhesive is important, and similar connections might display an array of failure modes. (Bainbridge et al., 2002) [27].
- Bonded-in GFRP rods are influenced by adhesive thickness in fatigue, and the failure mode when subjected to axial cyclic load was found to be dependent on rate of loading (Madhousshi et al., 2004) [28].
- The ability to dissipate energy when subjected to cyclic load is an important property in areas with the possibility of experiencing seismic forces (Gong et al., 2004) [19].
- Fatigue in timber joints are highly affected by frequency and waveform. Square waveforms are found to be most damaging (Gong et al., 2008) [13].

7.3 Conclusion and proposal for future work

The number of tests conducted for this paper are not sufficient to make any firm conclusions based on the results. More tests should be conducted to ensure a larger certainty in the test results. However, some tentative observations were made despite of this. The observations might indicate a tendency in the behaviour. With more tests conducted, they could be refuted.

The existing fatigue design verifications from Eurocode 5 part 2 were compared to the obtained test results for fatigue. With no coefficients for threaded rods, values for most similar connections of load situations were used. In comparison with the experimental values, the design limit for dowel connections showed best fit for both specimen geometries. In general, the regression lines derived for both rod-to-grain angles showed similar behaviour. These lines were derived from a small scatter plot, and are highly influenced by each of the test results.

The capacity of the steel rod seems to be the limiting factor for this connection in fatigue capacity. For most of the specimens, it was only after lowering embedment depth that fatigue in withdrawal of rod were obtained without first experiencing steel failure. At 0.75 normalized max load level, specimens with $\alpha=90°$ seemed to have similar capacity in both steel and rod withdrawal. One of three specimens experienced no steel failure, while the other two tests achieved rod withdrawal shortly after restart of the test. With lowered load level, no withdrawal of rod was obtained. One test was restarted three times with no rod withdrawal achieved, indicating that the steel capacity decays at a higher rate than withdrawal capacity for lowered load levels. No tests were conducted on 45˚ specimens with 440mm embedment. However, these tests indicate the same behaviour as 90° specimens in fatigue. With lowered

embedment depth, none of these specimens subjected to 0.75 normalized max load level experienced steel failure. However, with lowered load level, steel failure proved to be the limiting capacity in fatigue for 45˚ specimens as well.

It might be suggested that fatigue failure, in withdrawal of rod in axially loaded rods embedded in timber, will be more relevant as the rod to grain angle is lowered towards zero. This observation is based on the fact that in similar previous research on fatigue in axially loaded rod connectors, are conducted at 0° angle. From these experimental tests, timber failure can be achieved even at lower load levels. As previously mentioned, it is difficult to obtain this failure mode for the specimens used here. This might imply that for HCF of timber screwed-in connections in axial loading will not occur before steel failure for $\alpha=45°-90°$. This is observed with condition that embedment depth is chosen to achieve maximum static withdrawal capacity. At these two angles with static load application, the withdrawal of the rod is the limiting property. When observing HCF behaviour however, the steel capacity seems to limit the fatigue life of this connection.

More tests will have to be conducted to gain better information on the behaviour of this connection. The number of test results needs to be increased, and a less sensitive S-N curve is desirable. Specimens with different geometries and subjected to a larger variety of load levels will gain a better base to make observations on. Tests should also be conducted on specimens with a larger length to investigate if the supports arrested any crack development along fibres or influenced the results in any way. With a better and upgraded setup conducted on larger glulam elements, the results might prove to be more easily obtained. Experience from these tests showed that small introduced improvements proved efficient.

For future work, numerical models should be developed to investigate the behaviour of this connection. Simulations with cyclic load application will validate experimental tests, and support any future conclusions. Currently, the fatigue behaviour of threaded rods as connectors for hangers in bridge arches are still highly uncertain. Hopefully, more experimental tests will be conducted in the future. With a larger set of test results, one might reach a more durable conclusion.

Literature list

[1] H. Stamatopoulos and K. A. Malo, "Withdrawal capacity of threaded rods embedded in timber elements," *Construction an Building Materials,* vol. 94, pp. 387-397, 2015.

[2] H. Stamatopoulos, Withdrawal properties of threaded rods embedded in glued-laminated timber elements, Trondheim: Doctoral thesis at NTNU, 2016.

[3] Norske Limtreprodusenters Forening, Limtreboka, 2015.

[4] I. Smith, E. Landis og M. Gong, Fracture and Fatigue in Wood, Chichester: John Wiley & Sons Ltd, 2003, pp. 123-154.

[5] S. Thelandersson and H. J. Larsen, Timber Engineering, Chichester: John Wiley & Sons, Ltd, 2003.

[6] Standard Norge, NS-EN 1995-1-1:2004+A1:2008+NA:2010, Eurocode 5: Design of timber structures - Part 1-1: General - Common rules and rules for buildings, 2004.

[7] S. Tschudi-Madsen, "Store Norske Leksikon," 21 November 2015. [Online]. Available: https://snl.no/Urnes_stavkirke. [Accessed 1 06 2016].

[8] P. Tveit, "The Network Arch," March 2014. [Online]. Available: http://home.uia.no/pert. [Accessed 15 May 2016].

[9] PLAN Arkitekter AS, «PLAN Arkitekter,» [Internett]. Available: http://plan.no/project/tynset-bru/. [Funnet 1 June 2016].

[10] Balke, Hilde (Statens Vegvesen), "Bruseksjonen Region Øst: Hedmark, Oppland, Akershus, Oslo og Østfold," in *Brukonferansen 2014*, 2014.

[11] Standard Norge, NS-EN 1995-2:2004+NA:2010, Eurocode 5: Design of timber structures - Part 2: Bridges, 2004.

[12] M. P. Ansell, "Fatigue Design for Timber and Wood- Based Materials. Timber Engineering STEP 2: E22/1– E22/8.," 1995.

[13] M. Gong, L. Li and I. Smith, "Waveform Effect on Fatigue Behaviour of Laterally Loaded Nailed Timber Joints," in *World Conference on Timber Engineering*, Miyazaki, 2008.

[14] P. W. Bonfield og M. P. Ansell, «Fatigue properties of wood in tension, compression and shear,» *Journal of Materials Science ,* vol. 26, pp. 4765-4773, 1991.

[15] M. P. Ansell, «Fatigue of wood and wood panel products,» i *Fatigue in Composites*, Woodhead Publishing, 2003, pp. 339-360.

[16] O. Volkersen, "Die nietkraftverteilung in zugbeanspruchten nietverbindungen mit konstanten laschenquerschnitten," in *Luftfahrtforschung 15*, 1938, pp. 41-47.

[17] J. L. Jensen, A. Koizumi, T. T. Y. Sasaki and Y. Lijima, "Axially loaded glued-in hardwood dowels," in *Wood science and Technology*, 2001, pp. 73-83.

[18] K. A. Malo, "Fatigue Strength of dowel Joints in Timber Structures," Norwegian University of Science and Technology, Trondheim, 2002.
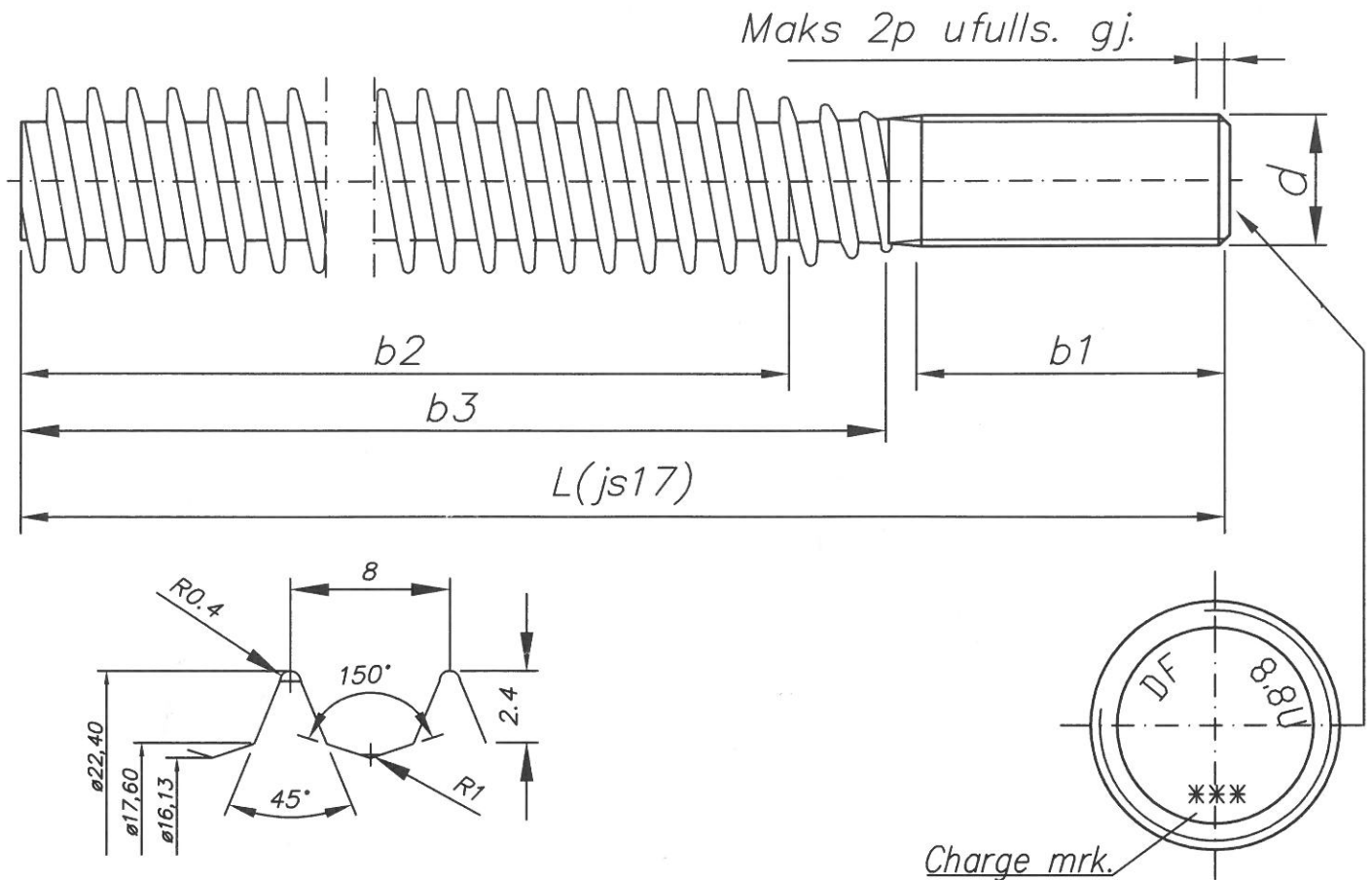
[19] M. Gong, K. Komatsu and M. Nakatani, "Fatigue Behaviour of Lagscrewbolted Timber Joints," in *World Conference of Timber Engineering*, Lahti, 2004.

[20] University of New Brunswick, «Faculty of Forestry and Environmental Management: People,» [Internett]. Available: http://www.unb.ca/fredericton/forestry/people/gong.html. [Funnet 2 June 2016].

[21] University of Bath, «Department of Mechanical Engineering: Our people,» [Internett]. Available: http://www.bath.ac.uk/mech-eng/people/ansell. [Funnet 1 June 2016].

[22] University of Bath, «Department of Architecture and Civil Engineering: Our people,» [Internett]. Available: http://www.bath.ac.uk/ace/people/bonfield/. [Funnet 1 June 2016].

[23] I. P. Bond og M. P. Ansell, «Fatigue properties of jointed wood composites,» *Journal of Materials Science,* vol. 33, pp. 2751-2762, 1998.

[24] University of Bristol, «Aerospace Engineering about: people,» [Internett]. Available: http://www.bris.ac.uk/engineering/departments/aerospace/people/ian-p-bond/about.html. [Funnet 1 06 2016].

[25] C. L. Hacker og M. P. Ansell, «Fatigue damage and hysteresis in wood-epoxy laminates,» *Journal of Materials Science ,* vol. 36, pp. 609-621, 2001.

[26] R. J. Bainbridge, C. J. Mettem, K. Harvey and M. P. Ansell, "Fatigue Performance of Bonded-In Rods In Glulam, Using Three Adhesive Types," in *CIM-W18/33-7-12*, Delft, 2000.

[27] R. Bainbridge, C. Mettem, K. Harvey and M. Ansell, "Bonded-in rod connections for timber structures - development of design methods and test observations," in *International Journal of Adhesion & Adhesives*, Elsevier Science Ltd., 2002, pp. 47-59.

[28] M. Madhoushi and M. P. Ansell, "Experimental study of static and fatigue strengths of pultruded GFRP rods bonded into LVL and glulam," in *International Journal of Adhesion & Adhesives 24*, Elsevier Ltd., 2004, pp. 319-325.

[29] M. Madhoushi and M. P. Ansell, "Fatigue and cyclic loading of moment-resisting structures connected using glued-in GFRP rods," in *8th World Conference on Timber Engineering*, Lahti, 2004.

[30] M. Madhoushi and M. P. Ansell, "Behaviour of timber connections using glued-in GRFP rods under fatigue loading. Part I: In-line beam to beam connections," in *Composites - Part B: Engineering*, Elsevier Ltd., 2008, pp. 243-248.

[31] M. Madhoushi and M. P. Ansell, "Behaviour of timber connections using glued-in GRFP rods under fatigue loading. Part II: Moment-resisting connections," in *Composites - Part B: Engineering*, Elsevier Ltd, 2008, pp. 249-257.

[32] A. Lokaj and K. Klamonová, "Round timber bolted joints exposed to stsic and dynamic loading," in *Wood Research 59 (3)*, Bratislava, SDVÚ, 2014, pp. 439-448.

[33] L. Bathon, O. Bletz-Mühldorfer, J. Schmidt and F. Diehl, "Fatigue design of adhesive connections using perforated steel plated," in *World Conference on Timber Engineering*, Quebec City, 2014.

[34] L. Bathon and O. Bletz-Mühldorfer, "Fatigue design of wood-concrete-composite system," in *Wood Conference on Timber Engineering*, Quebec City, 2014.

[35] L. Bathon and O. Bletz-Mühldorfer, "Fatigue of single span wood-concrete-composite bridges," in *World Conference on Timber Engineering*, Riva del Garda, 2010.

[36] P. Aldi og U. Kuhlmann, «Fatigue strength of timber-concrete-composite bridges: Determination of a S-N-line for the grooved connection and the "X-connector",» i *World conference on timber engineering*, Riva del Garda, 2010.

[37] K. Stephan og U. Kuhlmann, «Determination of damage eqivalent factors for the fatigue design of timber concrete-composite road bridges with notched connections,» i *World Conference on Timber Engineering*, Quebec City , 2014.

[38] Standard Norge, NS-EN 1993-1-9:2005+NA:2010, Eurokode 3: Prosjektering av stålkonstruksjoner - Del 1-9: Utmattingspåkjente konstruksjoner, 2005.

[39] Standard Norge, EN 26891:1991, ISO 6891:1983 Timber structures - Joint made with mechanical fasteners - General principles for the determination of strength and deformation characteristics, 1991.

[40] Standard Norge, NS-EN 14592:2008+A1:2012, Trekonstruksjoner - Festemidler av dybeltype, 2012.

[41] DIN 1052. Entwurf, Berechnung und Bemessung von Holzbauwerken - Allgemeine Bemessungsregeln und Bemessungsregeln für den Hochbau, Berlin: Beuth Verlag GmbH, 2010.

[42] H. Larsen and V. Enjily, "Practical design of timber structures to Eurocode 5," Thomas Telford Limited, London, 2009.

[43] J. Ambrose and P. Tripeny, Simplified Design of Wood Structures, Hoboken: John Wiley & Sons, Inc, 2009.

[44] C. O. Clorius, M. U. Pedersen, P. Hoffmeyer and L. Damkilde, "Fatigue damage in Wood," in *International COST 508 Wood Mechanics Conference*, Stuttgart, 1996.

[45] Standard Norge, NS-EN 1993-1-8:2005+NA:2009, Eurokode 3: Prosjektering av stålkonstruksjoner - Del 1-8: Knutepunkter og forbindelser, 2005.

[46] P. K. Larsen, Dimensjonering av stålkonstruksjoner, Oslo/Trondheim: Akademika forlag, 2013.

[47] T. Nilsen, "Utmattingskapasitet av dybelforbindelser I trekonstruksjoner," NTNU, Trondhein, 1998.

[48] Standard Norge, NS-EN 1991-2:2003+NA:2010, Eurokode 1: Laster på konstruksjoner - Del 2: Trafikklast på bruer, 2003.

Annex A

Datasheet threaded rods

DOKKA FASTENERS

Vår ref / Our ref Hilde Loeng	Dato / Date 11. April, 2016	Sertifikatnr. / Certificate No. **548122**
Kunde / Customer NTNU/ Kjell A.Malo / Odd Nerdal	Produksjonsordrenr / Production Order no. 548122	Salg-eksp.-no Sales-exp. No 161513
Institutt for konstr.teknikk, Port 1 Rich.Birkelandsv.1a, 7491 Trondheim	Kundens ref./ Customers ref. 117319	
NORGE	Kundens tegning / Customer drawing	

Kund.det.nr./ Customer part no.	Artikkelnr., benevning / Part no., part name 77 pcs Stud bolt, M20 x 1900, cl. 8.8 , DFS 1626

Omfang / extent

INSPECTION CERTIFICATE   EN 10204 - 3.1

It is hereby certified that the products covered by this certificate has been tested and is compliant with the requirements of the order.

Product standard DFS 1626 pos.1

Mechanical properties: ISO 898-1:2013, Cl. 8.8.

Threads: M. tol. cl. 6az. ISO 965-4:1998, before hot dip galv.

Product marking: DF 8.8U 122

Foreskrevet materiale / Prescribed material acc. to ISO 898-1	Levert materiale / Supplied material GERDAU 32 CrB4

MATERIALANALYSE / CHEMICAL COMPOSITION

Charge nr.	C	Si	Mn	P	S	Cr	Ti	B	Al	Cu
176201	.33	.20	.82	.009	.003	1.09		.0033		.15
Analysekrav / min	.30	.12	.70			1.05		.0020		
Specification max	.34	.25	.90	.015	.015	1.20		.0050		.25

VARMEBEHANDLING / HEAT TREATMENT

Hardened and tempered

MEKANISKE EGENSKAPER / MECHANICAL PROPERTIES

Prøve på ferdig produkt / test on manufactured product	Krav / Specification		Prøveres. / Test results		Prøveantall / Number .of samples	Anmerkning / Note
	Min.	! Max	Min.	! Max		
Zn belegg / Zncoating μm						
Strekkfasthet/Tensile strength **Rm N/mm²**						
$R_{p0.2}$ på hel bolt / $R_{p0.2}$ on full size bolts **N/mm²**						
Hardhet / Hardness **HB**	250	331	264	277	5	Average 271
Spesiell strekkprøving / Special tensile test Strekkfasthet/Tensile strength **Rm N/mm²**	830		938	966	3	Prøvestaver iflg. / Test pieces acc to Ø 12.6
Flytegrense / Yield stress **Rel $Rp_{0.2}$ N/mm²**	660		855	889	3	
Forlengelse / Elongation **A_5 %**	12		14	15	3	
Kontraksjon **Z %**	52		62	65	3	Average 63
Skårslagprøve / Impact test **kV 300 Joule**						Prøvestaver iflg. / Test pieces acc to EN 10045-1
Slagseighet / Impact strength **Joule**	27 J		121	138	3	Test pieces: 10x10x55 Single values: 138 – 121 – 131 J
Prøvetemperatur / Test temp. **°C**	- 20°					

Kvalitetskontrollavdeling / Quality Control Department

Hilde Loeng

Phone: 61 11 30 30   Fax: 61 11 30 03

Maks 2p ufulls. gj.

b2

b3

b1

L(js17)

d

R0.4

8

150°

2.4

ø22,40

ø17,60

ø16,13

45°

R1

DF 8.8U

***

Charge mrk.

Gjenger: M, tol kl. 6az iflg DF-SP-693-51 før vfz. ISO 965-4(6az)
Mek. egensk. iflg. ISO 898-1:2013 kl 8.8.
Form og beliggenhetstol ifl DIN ISO 4759-1 utf. kl. B
Overflate: Varmforsinkes ISO 10684, høytemp skal benyttes (530-560°C)

Pos.nr.	1		2		3		4		5	
Gjenge d	M20									
P	2.5									
	min	maks	min	maks	min	maks	min	maks	min	maks
Materialdiam.	17,966	18,050								
b1	90	95								
b2	1750	—								
b3	—	1800								
L	1892,5	1907,5								
Bruddgr. N/mm2	830									
Flytegr. N/mm2	660									
Forlengelse, A5%	12									
Slagseighet J.	27									
Test temp.°C.	−20									
Kunde	NTNU									
Kundetegn.	Mail 16.12.15									

Stk. antall	Gjenstand	Pos.nr.	Materiale	Emnesm?l—Modell nr.	Netto Vekt—kg	Tegn.nr.—Anmerkninger

Forandr.

AVDELING: _____

Gruppe SALGSVARER

Undergr. _____

Delgruppe _____

TITTEL: Pinbolt, spes. gjenger for tre
i ene enden. NTNU

Målestokk
—

Dato Navn
Tegn. 16.12.15 T.Låksrud

Kontr.

Godkj. 16/12-15 EL.

Erstatn. for:

DOKKA FASTENERS

DFS-1626-1

Erstattet av:

For 1 stk.

Annex B

Threaded rod: EC3 part 1-9

Steel fatigue - EC3 part 1-9

Force range [kN]

Cycles [N]
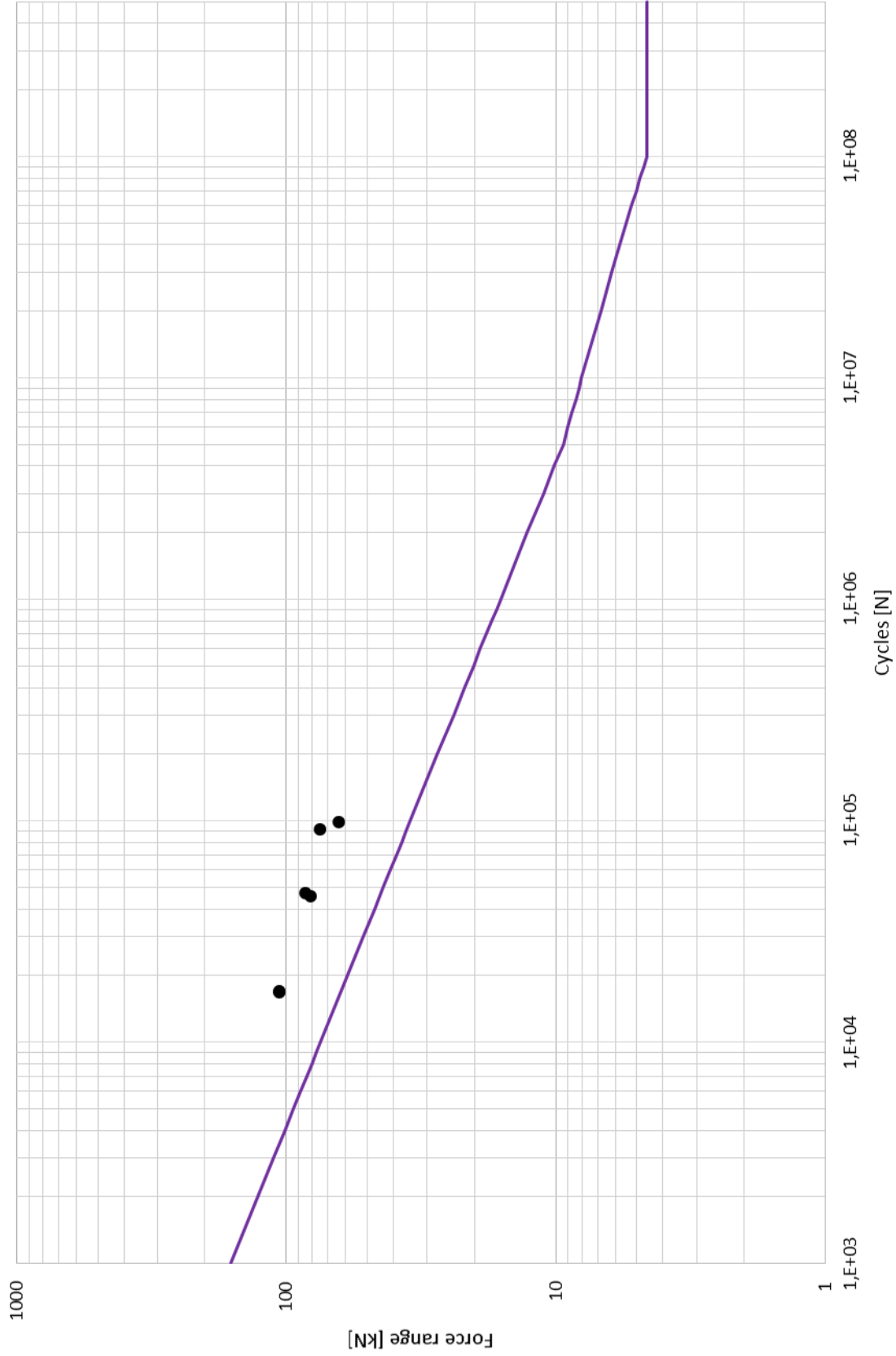
Annex C

Mathcad: Steel capacity

Capacity assessment of threaded rods

Data:

$F_{ref.90} := 157 \ kN$ Static reference load, 90 degrees. 440 mm embedment.

$F_{ref.45} := 185.1 \ kN$ Static reference load, 45 degrees. 440 mm embedment.

$d := 20 \ mm$ Diameter thread, metric rod.

$d_s := 18 \ mm$ Shear diameter, metric rod.

$A_s := \left(\dfrac{d_s}{2}\right)^2 \cdot \pi = 254.469 \ mm^2$

$d_t := 22 \ mm$ Outer diameter threaded screwed-in glulam

$d_{min} := 16.13 \ mm$ Minimum diameter rod: *Annex A*

$A_{min} := \left(\dfrac{d_{min}}{2}\right)^2 \cdot \pi = 204.342 \ mm^2$

$f_{ub} := 800 \ \dfrac{N}{mm^2}$ *NS-EN 1993-1-8, Table 3.1*

Maximum capacity in tension, steel failure

$F_{t.max} := f_{ub} \cdot A_{min} = 163.474 \ kN$

$F_{t.s} := f_{ub} \cdot A_s = 203.575 \ kN$

Fatigue - According to NS-EN 1993-1-9:2005+NA:2010

Fatigue failure in steel at the upper threaded part M20 at the grip of the machine:

Detail category 50:

$\Delta\sigma_C := 50 \ \dfrac{N}{mm^2}$ *NS-EN 1993-1-9, Table 8.1*

This is the reference fatigue strength range at 2 million cycles. No size effect.

$m := 3$ Assuming N<5000000 cycles   *NS-EN 1993-1-9, 7.1 (2)*

$N_C := 2 \cdot 10^6$

Load level 1, 90 degrees:

$$F_{max} := 118 \ kN$$

Maximum load in the cycle

$$F_{min} := 11.8 \ kN$$

Minimum load in the cycle

$$\sigma_{max} := \frac{F_{max}}{A_s} = 463.711 \ \frac{N}{mm^2}$$

Maximum stress in the cycle

$$\sigma_{min} := \frac{F_{min}}{A_s} = 46.371 \ \frac{N}{mm^2}$$

Minimum stress in the cycle

$$\Delta\sigma := \sigma_{max} - \sigma_{min} = 417.34 \ \frac{N}{mm^2}$$

Stress range

Number of cycles before fatigue failure in the threaded rods according to EC3:

$$\Delta\sigma_R := \Delta\sigma = 417.34 \ \frac{N}{mm^2}$$

$$N_R := \frac{\Delta\sigma_C{}^m \cdot N_C}{\Delta\sigma_R{}^m} = 3439$$

NS-EN 1993-1-9, 7.1 (2)

Load level 2, 90 degrees:

$$F_{max} := 94 \ kN$$

Maximum load in the cycle

$$F_{min} := 9.4 \ kN$$

Minimum load in the cycle

$$\sigma_{max} := \frac{F_{max}}{A_s} = 369.397 \ \frac{N}{mm^2}$$

Maximum stress in the cycle

$$\sigma_{min} := \frac{F_{min}}{A_s} = 36.94 \ \frac{N}{mm^2}$$

Minimum stress in the cycle

$$\Delta\sigma := \sigma_{max} - \sigma_{min} = 332.457 \ \frac{N}{mm^2}$$

Stress range

Number of cycles before fatigue failure in the threaded rods according to EC3:

$$\Delta\sigma_R := \Delta\sigma = 332.457 \ \frac{N}{mm^2}$$

$$N_R := \frac{\Delta\sigma_C{}^m \cdot N_C}{\Delta\sigma_R{}^m} = 6804$$

NS-EN 1993-1-9, 7.1 (2)

Annex D

Mathcad: Calculations timber element and fatigue load level

Stresses on timber surface

- For estimation of support surface

Data:

$l := 600 \; mm$ Length specimen.

$b := 140 \; mm$ Width specimen.

$h := 475 \; mm$ Height specimen.

$d := 22 \; mm$ Diameter thread.

$l_{eff} := 20 \cdot d = 440 \; mm$ Embedment depth.

$f_w := 5 \; \dfrac{N}{mm^2}$ Withdrawal strength of the glulam beam, estimation.

$f_{c.90.g.k} := 2.5 \; \dfrac{N}{mm^2}$ Compression strength, glulam GL 30c.

Max force before withdrawal of the threaded rod:

$F_{max} := \pi \cdot d \cdot l_{eff} \cdot f_w = 152.053 \; kN$

Estimation of withdrawal capacity. Used to determine load in static reference testing.

$F_{est} := F_{max} = 152.053 \; kN$

Calculated maximum force for set ups, static compression

Set up 1:

Two rectangular hollow sections (120x120x10).

$l_s := 120 \; mm$ Support dimention on both sides of the rod.

$F_{max.1} := f_{c.90.g.k} \cdot b \cdot l_s \cdot 2 = 84 \; kN$

$F_{max.1} > F_{est} = 0$

Plastic deformations is possible

<u>Set up 2:</u>

Two L-profiles (100x50x8) along the length of the top of the specimen.

L-profile:

$b := 50 \; mm$

$s := 8 \; mm$

$r_1 := 9 \; mm$

$b_s := b - s - r_1 = 33 \; mm$ Support dimention on both sides of the rod.

$F_{max.1} := f_{c.90.g.k} \cdot l \cdot b_s \cdot 2 = 99 \; kN$

$F_{max.1} > F_{est} = 0$

The capacity is increased, but not enough.

<u>Set up 4:</u>

Two L-profiles (100x50x8) along the length of the top of the specimen. Cut out around the location of the threaded rod(35x240).

Cut out part:

$b_c := 35 \; mm$ Dimention of the cut out part

$l_c := 240 \; mm$ on both sides of the rod.

$F_{max.1} := f_{c.90.g.k} \cdot l \cdot b_s \cdot 2 - f_{c.90.g.k} \cdot l_c \cdot b_c \cdot 2 = 57 \; kN$

The capacity and the area is decreased by 42%.

<u>Set up 5:</u>

Two steel plates(140x140x10) at the top of the specimen under the rectangular hollow sections.

$F_{est} := F_{max} = 152.053 \; kN$

Steel plate:

$b_s := 140 \; mm$ Support dimention on both sides

$l_s := 140 \; mm$ of the rod.

$F_{max.1} := f_{c.90.g.k} \cdot l_s \cdot b_s \cdot 2 = 98 \; kN$

Calculated load levels, fatigue

Data:

$$F_{ref.90} := 157 \ kN$$

Maximum static reference force, 90 degrees

$$F_{ref.45} := 185.1 \ kN$$

Maximum static reference force, 45 degrees

$$d_s := 18 \ mm$$

Shear diameter, *Annex A*

$$A_s := \left(\frac{d_s}{2}\right)^2 \cdot \pi = 254.5 \ mm^2$$

Annex A

$$d_t := 22 \ mm$$

Outer thread diameter, *Annex A*

Load level 1

$$\alpha := 90$$

Grain to rod direction

$$l_{eff} := 440 \ mm$$

Embedment depth

$$R := 0.1$$

Stress ratio

$$f_{max} := 0.75$$

Maxmum stress

$$\Delta f := f_{max} \cdot (1 - R) = 0.7$$

Stress range

$$F_{max} := \frac{\Delta f \cdot F_{ref.90}}{0.9} = 118 \ kN$$

Maximum force in the cycle

$$F_{min} := 0.1 \ F_{max} = 11.8 \ kN$$

Minimum force in the cycle

$$F_m := \frac{F_{max} + F_{min}}{2} = 64.8 \ kN$$

Mean force of the cycle

$$F_a := \frac{F_{max} - F_{min}}{2} = 53 \ kN$$

Force amplitude

$$\sigma_{max} := \frac{F_{max}}{A_s} = 462.7 \ \frac{N}{mm^2}$$

Max. stress in threaded rod

$$\sigma_{min} := \frac{F_{min}}{A_s} = 46.3 \ \frac{N}{mm^2}$$

Min. stress in threaded rod

Load level 2

$\alpha := 90$

Grain to rod direction

$l_{eff} := 440 \ mm$

Embedment depth

$R := 0.1$

Stress ratio

$f_{max} := 0.6$

Maxmum stress

$\Delta f := f_{max} \cdot (1 - R) = 0.5$

Stress range

$F_{max} := \dfrac{\Delta f \cdot F_{ref.90}}{0.9} = 94 \ kN$

Maximum force in the cycle

$F_{min} := 0.1 \ F_{max} = 9.4 \ kN$

Minimum force in the cycle

$F_m := \dfrac{F_{max} + F_{min}}{2} = 51.8 \ kN$

Mean force of the cycle

$F_a := \dfrac{F_{max} - F_{min}}{2} = 42.4 \ kN$

Force amplitude

$\sigma_{max} := \dfrac{F_{max}}{A_s} = 370.2 \ \dfrac{N}{mm^2}$

Max. stress in threaded rod

$\sigma_{min} := \dfrac{F_{min}}{A_s} = 37 \ \dfrac{N}{mm^2}$

Min. stress in threaded rod

Load level 3

$\alpha := 90$

Grain to rod direction

$l_{eff} := 330 \ mm$

Embedment depth

$R := 0.1$

Stress ratio

$f_{max} := 0.6$

Maxmum stress

Assuming linear relationship between the embedment depth and the withdrawal strength in the glulam beam. Scaling static result from 440mm to 330mm.

$F_{ref.90} := 157 \ kN$

$$F_{ref.90.330} := F_{ref.90} \cdot \frac{15 \; d_t}{20 \; d_t} = 117.8 \; kN$$

New reference load with less embedment depth.

$$\Delta f := f_{max} \cdot (1 - R) = 0.5$$

Stress range

$$F_{max} := \frac{\Delta f \cdot F_{ref.90.330}}{0.9} = 71 \; kN$$

Maximum force in the cycle, load level 3.

$$F_{min} := 0.1 \; F_{max} = 7.1 \; kN$$

Minimum force in the cycle, load level 3.

$$F_m := \frac{F_{max} + F_{min}}{2} = 38.9 \; kN$$

Mean force of the cycle

$$F_a := \frac{F_{max} - F_{min}}{2} = 31.8 \; kN$$

Force amplitude

$$\sigma_{max} := \frac{F_{max}}{A_s} = 277.6 \; \frac{N}{mm^2}$$

Max. stress in threaded rod

$$\sigma_{min} := \frac{F_{min}}{A_s} = 27.8 \; \frac{N}{mm^2}$$

Min. stress in threaded rod

Load level 4

$$\alpha := 45$$

Grain to rod direction

$$l_{eff} := 330 \; mm$$

Embedment depth

$$R := 0.1$$

Stress ratio

$$f_{max.4} := 0.75$$

Maxmum stress

$$F_{ref.45} = 185.1 \; kN$$

$$F_{ref.45.330} := F_{ref.45} \cdot \frac{15 \; d_t}{20 \; d_t} = 138.8 \; kN$$

New reference load with less embedment depth.

$$\Delta f := f_{max.4} \cdot (1 - R) = 0.675$$

Stress rate

$$F_{max} := \frac{\Delta f \cdot F_{ref.45.330}}{0.9} = 104.1 \; kN$$

Maximum force in the cycle, load level 1.

$F_{min} := 0.1 \; F_{max} = 10.4 \; kN$

Minimum force in the cycle, load level 1.

$\Delta F := F_{max} - F_{min} = 93.7 \; kN$

Load range

$F_m := \dfrac{F_{max} + F_{min}}{2} = 57.3 \; kN$

Mean force of the cycle

$F_a := \dfrac{F_{max} - F_{min}}{2} = 46.9 \; kN$

Force amplitude

$\sigma_{max} := \dfrac{F_{max}}{A_s} = 409.2 \; \dfrac{N}{mm^2}$

Max. stress in threaded rod

$\sigma_{min} := \dfrac{F_{min}}{A_s} = 40.9 \; \dfrac{N}{mm^2}$

Min. stress in threaded rod

Load level 5

$\alpha := 45$

Grain to rod direction

$l_{eff} := 330 \; mm$

Embedment depth

$R := 0.1$

Stress ratio

$f_{max.5} := 0.6$

Maxmum stress

$F_{ref.45.330} := F_{ref.45} \cdot \dfrac{15 \; d_t}{20 \; d_t} = 138.8 \; kN$

New reference load with less embedment depth.

$\Delta f := f_{max.5} \cdot (1 - R) = 0.54$

Stress ratio

$F_{max} := \dfrac{\Delta f \cdot F_{ref.45.330}}{0.9} = 83.3 \; kN$

Maximum force in the cycle, load level 1.

$F_{min} := 0.1 \; F_{max} = 8.3 \; kN$

Minimum force in the cycle, load level 1.

$\Delta F := F_{max} - F_{min} = 75 \; kN$

Load range

$F_m := \dfrac{F_{max} + F_{min}}{2} = 45.8 \; kN$

Mean force of the cycle

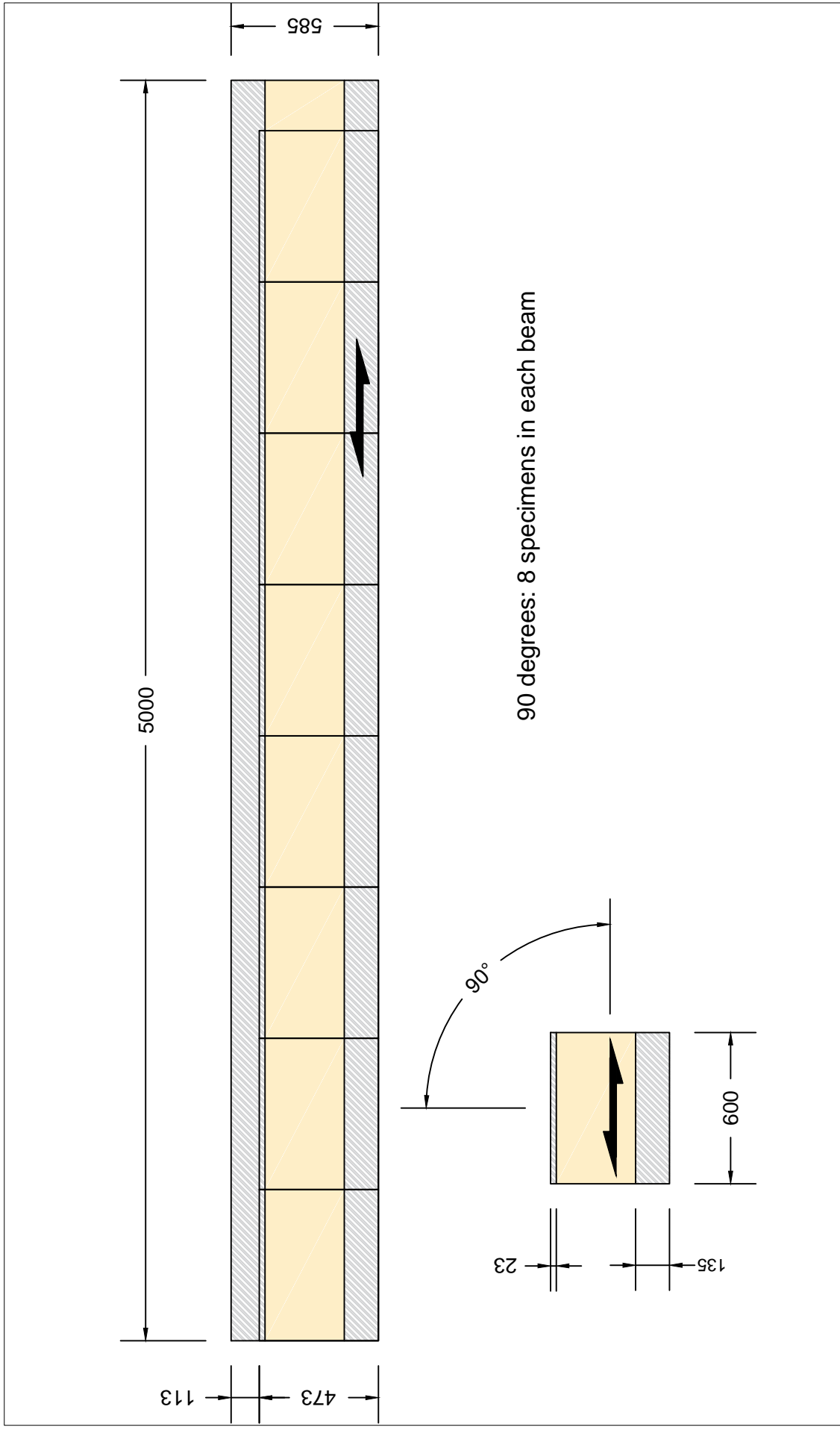$$F_a := \frac{F_{max} - F_{min}}{2} = 37.5 \ kN$$

Force amplitude

Load level 6

$\alpha := 45$

Grain to rod direction

$l_{eff} := 330 \ mm$

Embedment depth

$R := 0.1$

Stress ratio

$f_{max.6} := 0.65$

Maxmum stress

$$F_{ref.45.330} := F_{ref.45} \cdot \frac{15 \ d_t}{20 \ d_t} = 138.8 \ kN$$

New reference load with less embedment depth.

$\Delta f := f_{max.6} \cdot (1 - R) = 0.585$

Stress ratio

$$F_{max} := \frac{\Delta f \cdot F_{ref.45.330}}{0.9} = 90.2 \ kN$$

Maximum force in the cycle, load level 1.

$F_{min} := 0.1 \ F_{max} = 9 \ kN$

Minimum force in the cycle, load level 1.

$\Delta F := F_{max} - F_{min} = 81.2 \ kN$

Load range

$$F_m := \frac{F_{max} + F_{min}}{2} = 49.6 \ kN$$

Mean force of the cycle

$$F_a := \frac{F_{max} - F_{min}}{2} = 40.6 \ kN$$

Force amplitude

Annex E

AutoCad: Glulam elements

All dimensions in [mm].

Cutting of the glulam beams, 90 degrees

585

5000

90°

90 degrees: 8 specimens in each beam

600

473
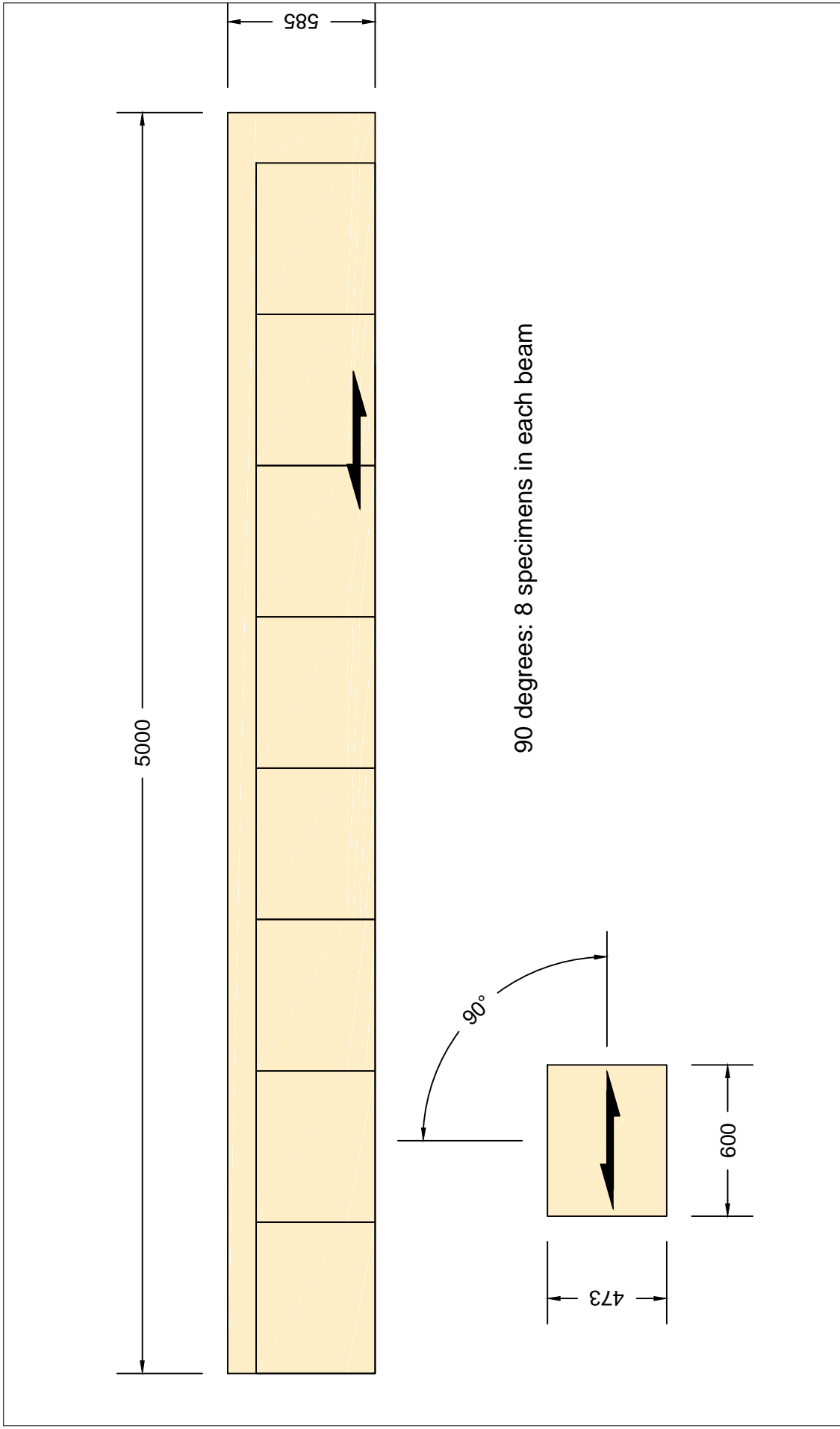
Placement of strong lamellas, 90 degrees

585

5000

113

473

90°

90 degrees: 8 specimens in each beam

600

23

135

Specimens with 90 degrees grain direction.

140mm

Area of stronger lamellas

472,5mm

440mm

M20

600mm

M22 embedded in the timber. Predrill 16.5 mm

M22

140mm

23mm

45mm

135mm

Cutting of the glulam beams

945

5000
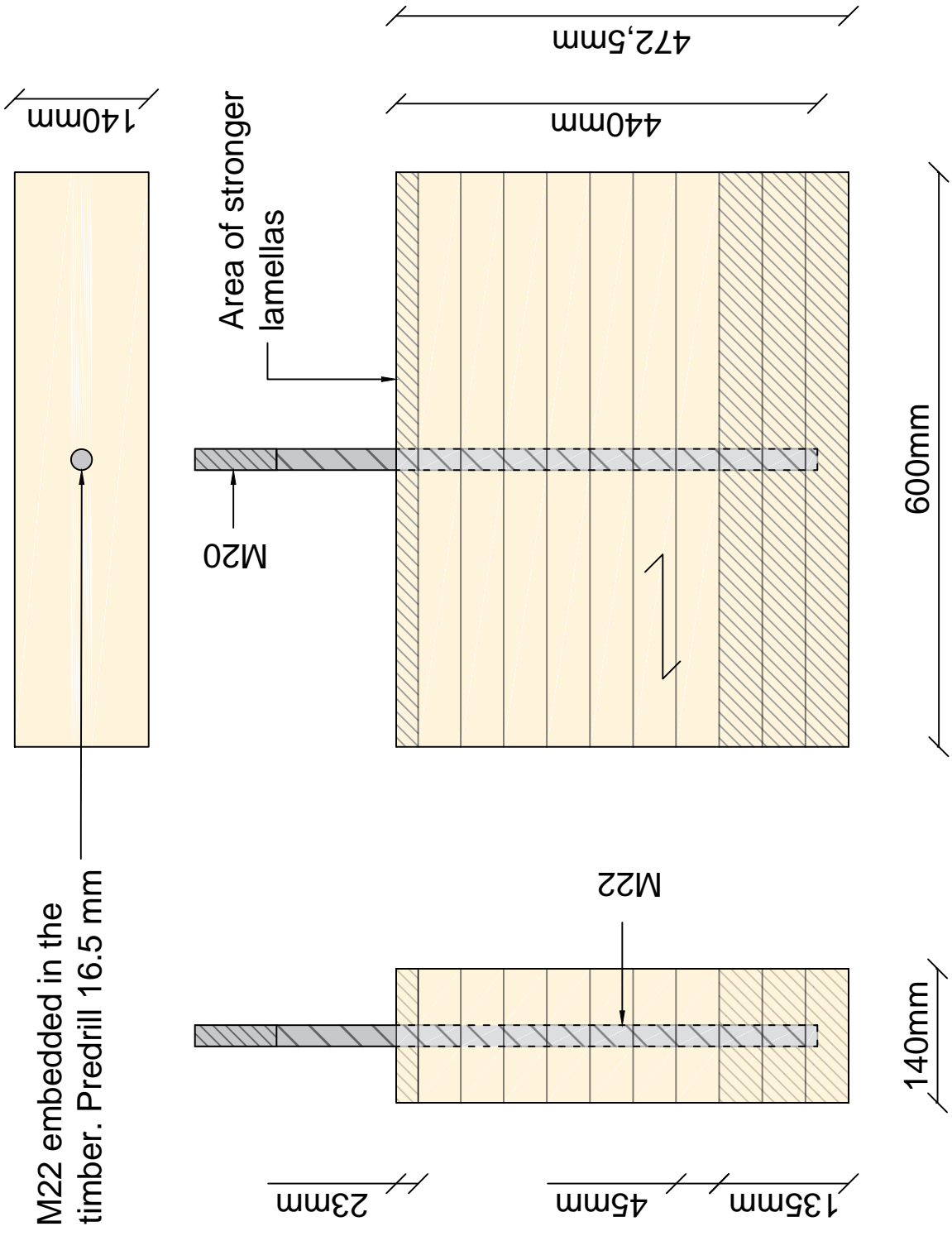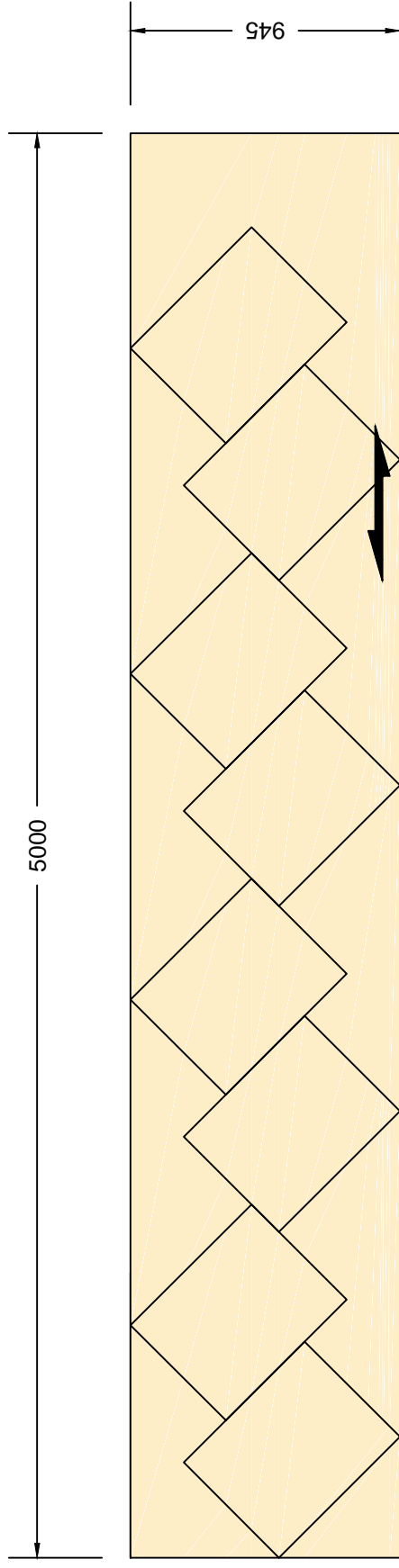
45 degrees: 8 specimens each beam

45°

473

600

Cutting of specimens, 45 degrees

945

5000

147

668

668

668

334

187

424

736

136

475

473

668

424

264

209

X2

X1

45°

521

424
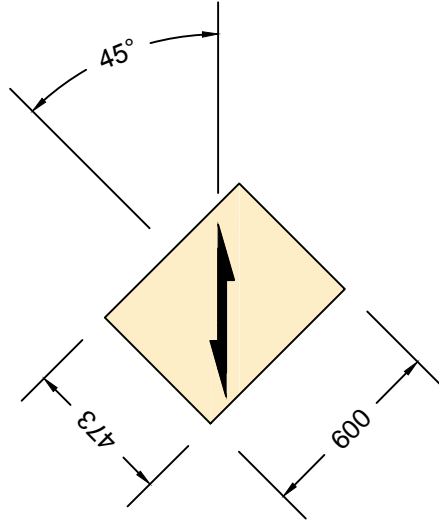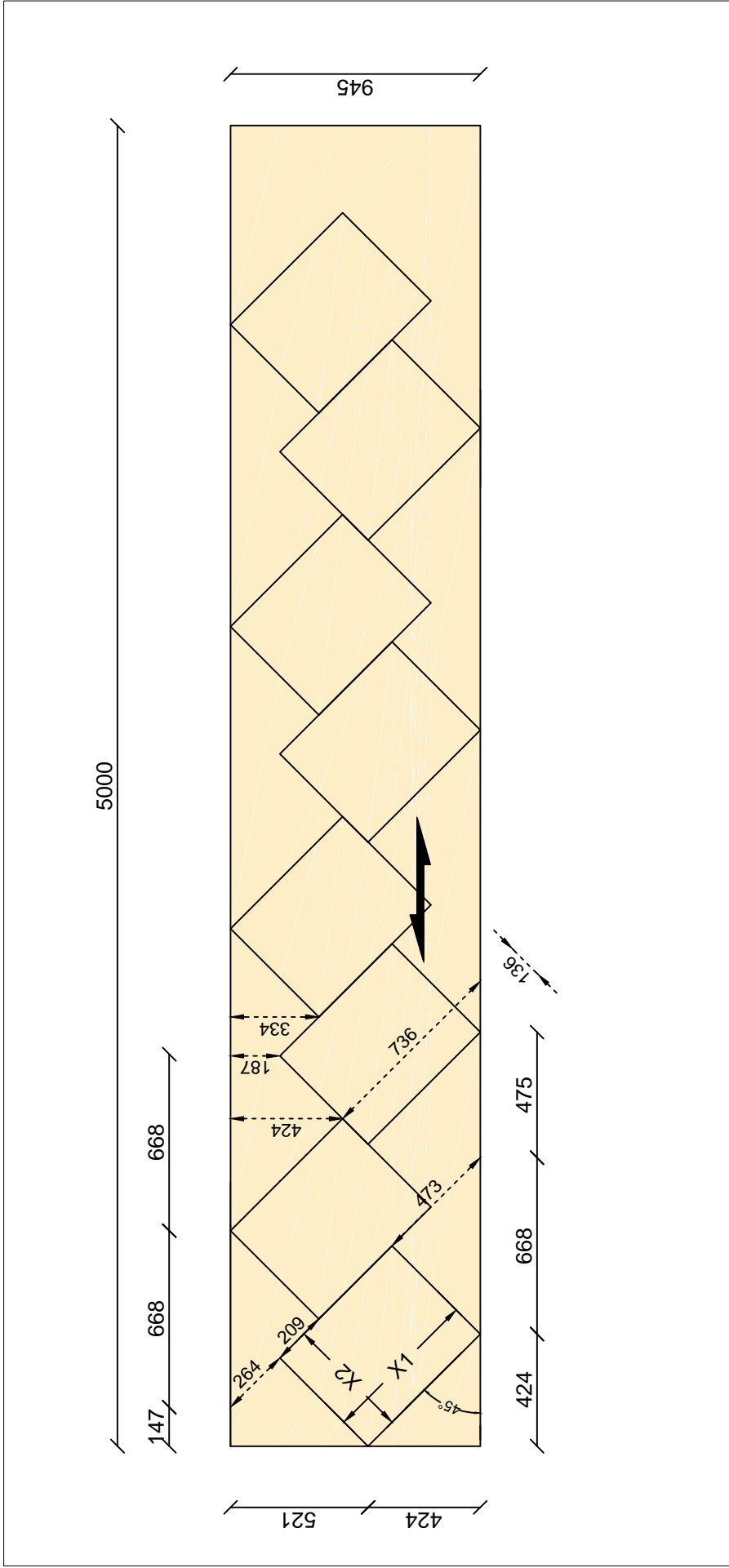
Cutting of specimens, 45 degrees
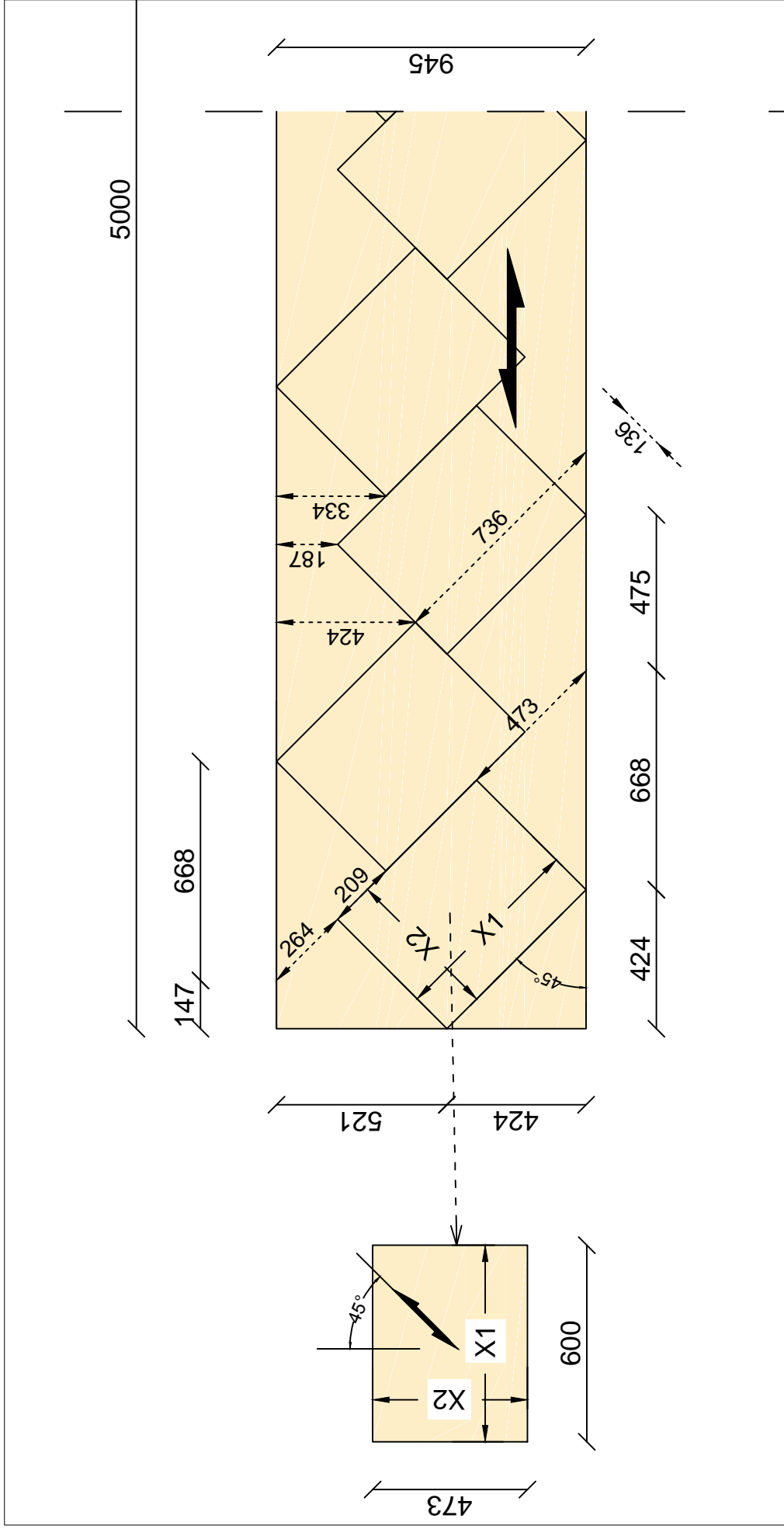
Stronger lamellas, placement in beam
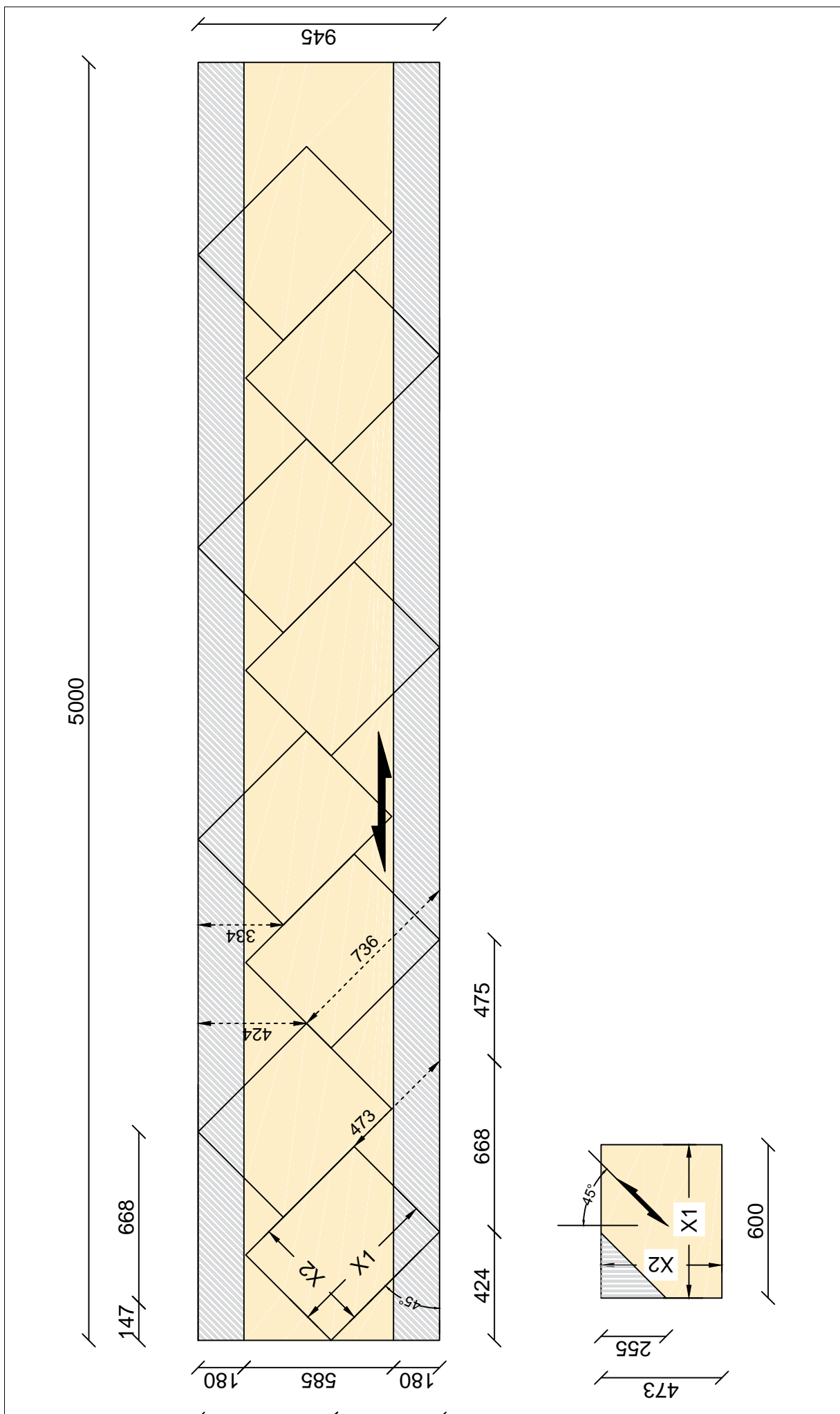
Specimens with 45 degrees grain direction.

140mm

M22 embedded in the
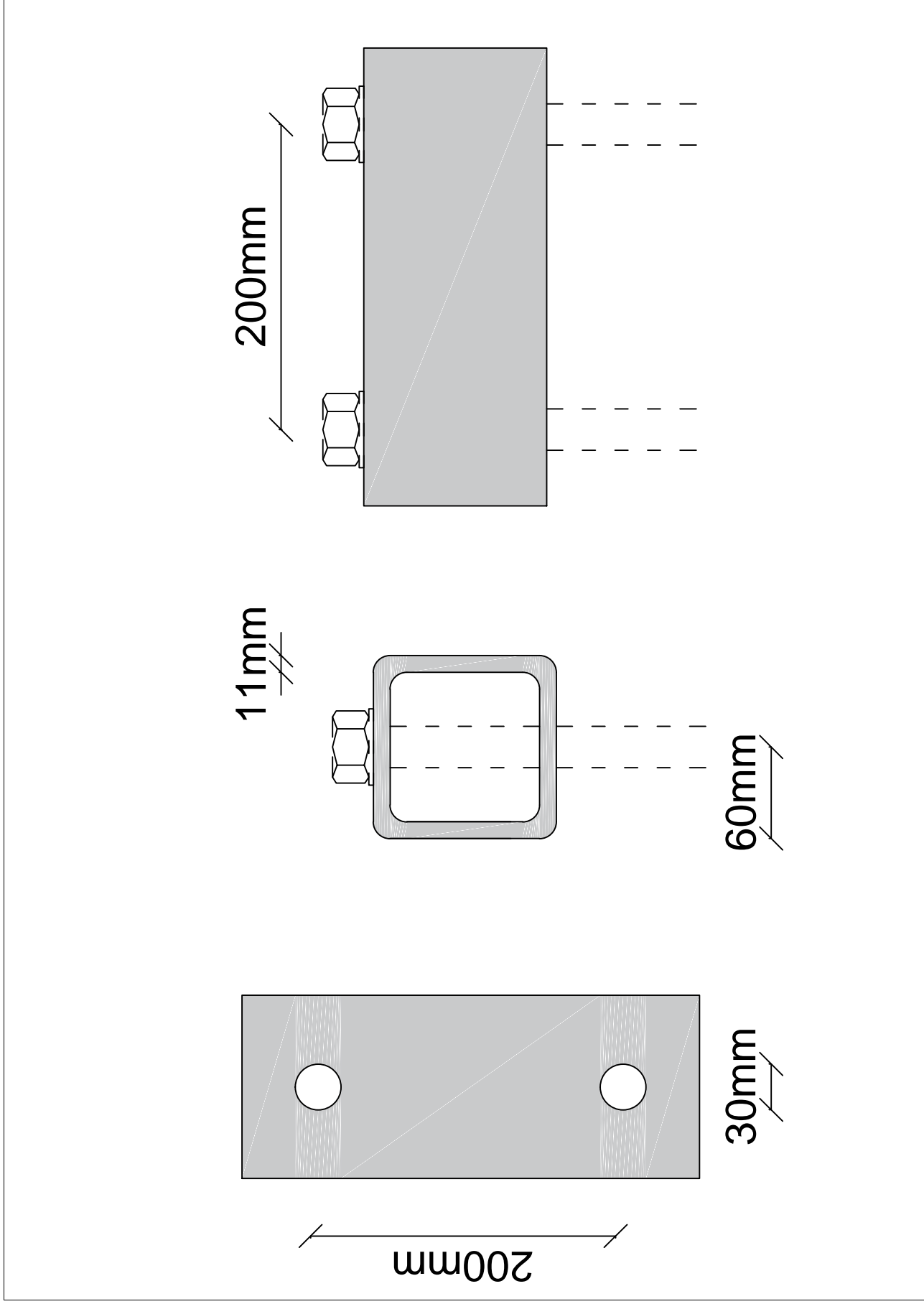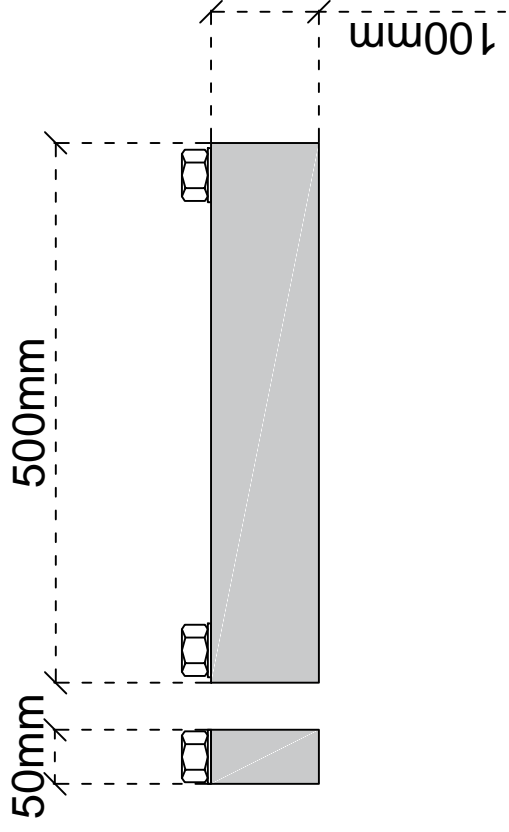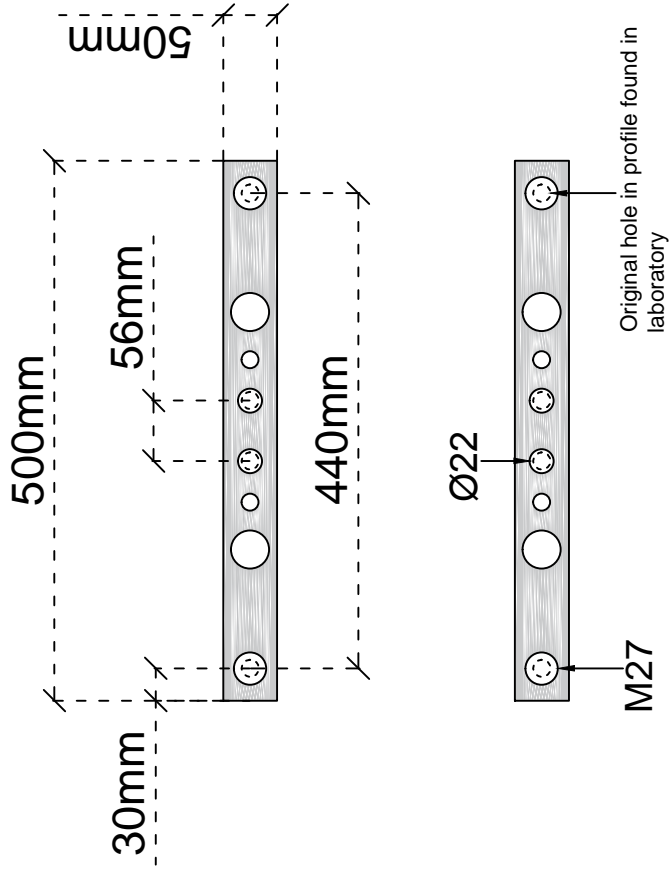timber. Predrill 16.5 mm

M20

440mm

600mm

472,5mm

Area of stronger
lamellas

M22

140mm

63,64mm
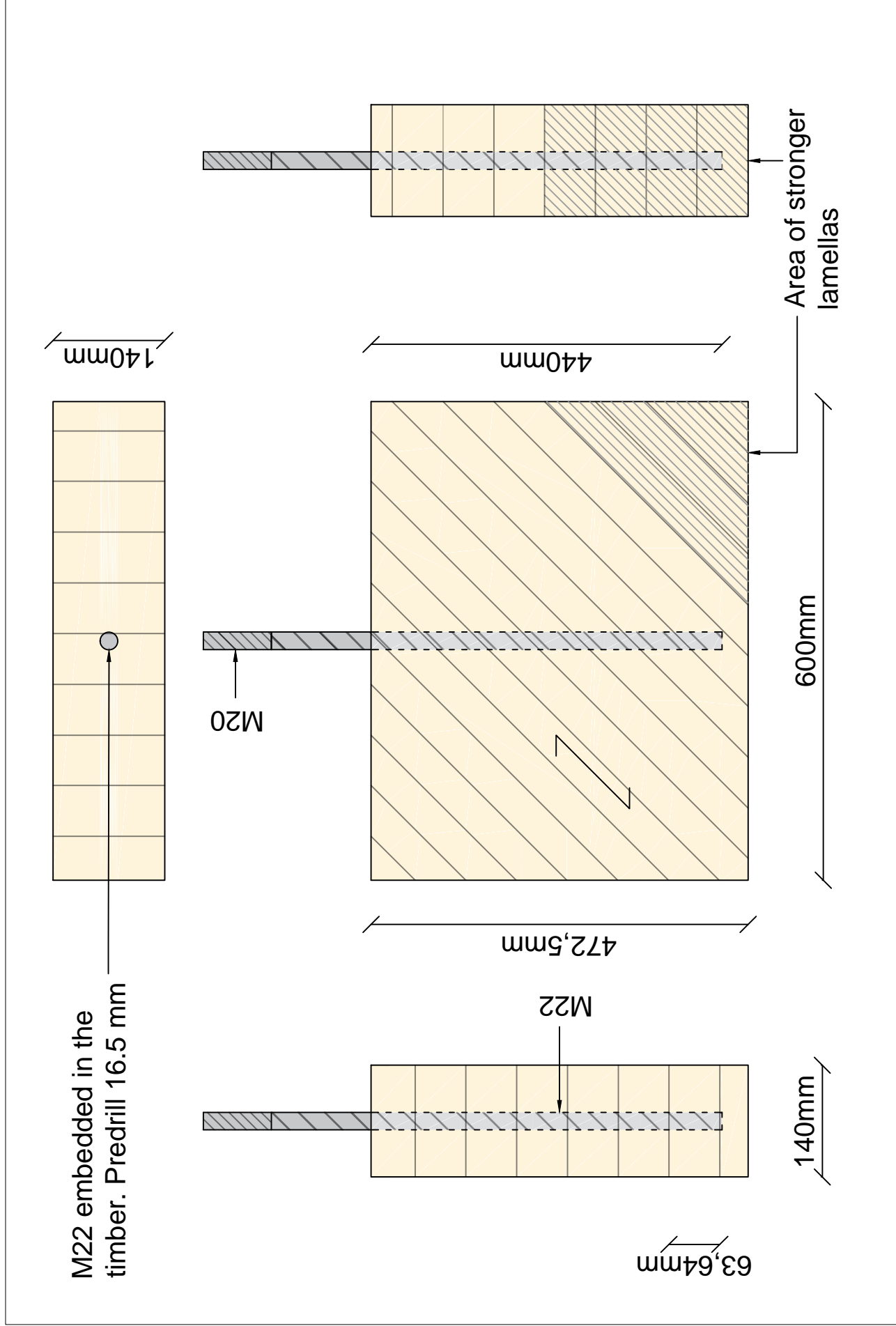
Annex F

AutoCad: Setup

All dimensions in [mm].

Rectangular hollow profile(120x120x11)

200mm

11mm

200mm

60mm

30mm

Steel profile in the setup

500mm

50mm

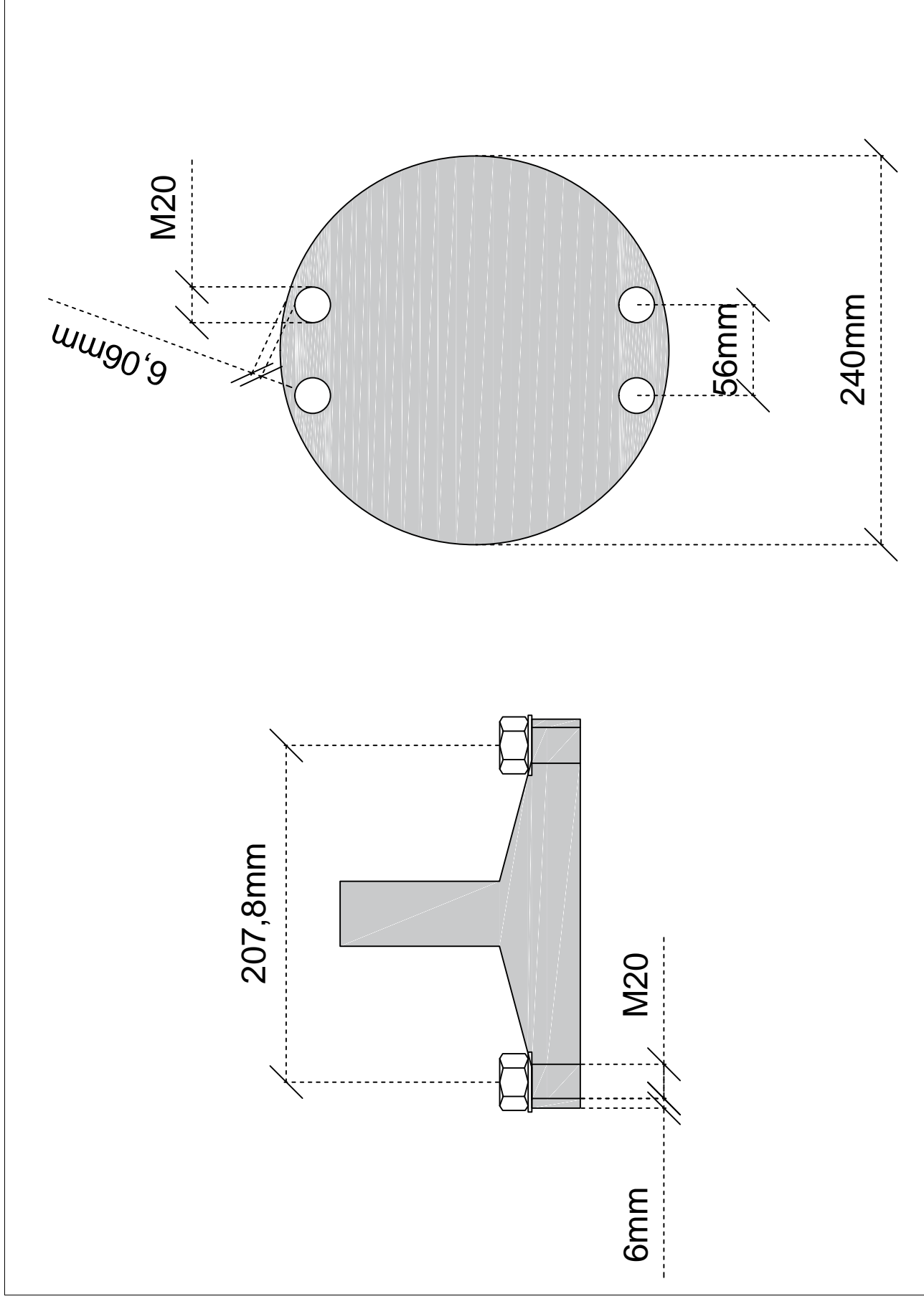100mm

50mm

500mm

56mm

440mm

30mm

Original hole in profile found in laboratory

Ø22

M27

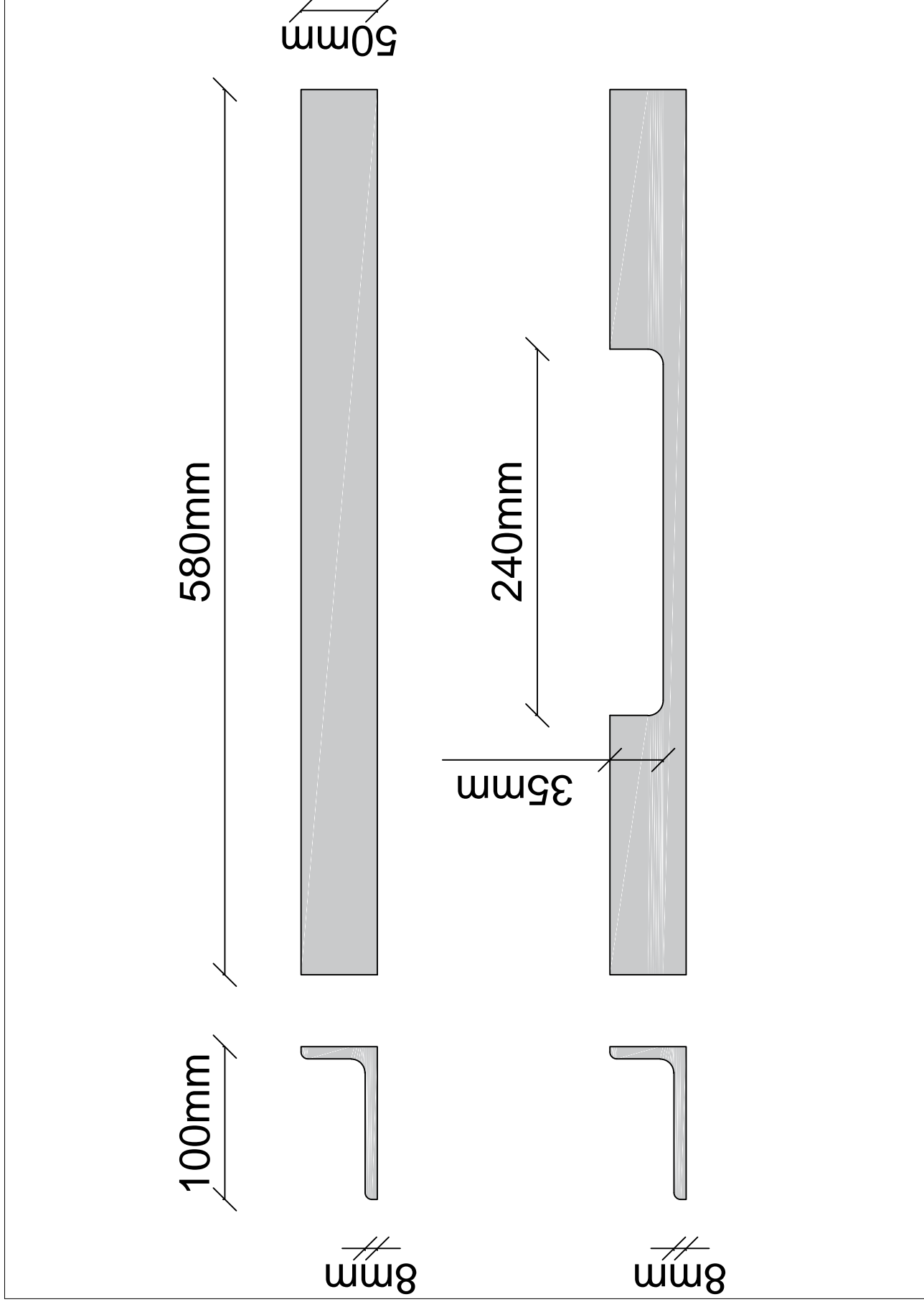The original profile nedded to be altered to M27 (d=30mm), while the inner holes had to be altered to fit M20 bolts.

Support held by the machine
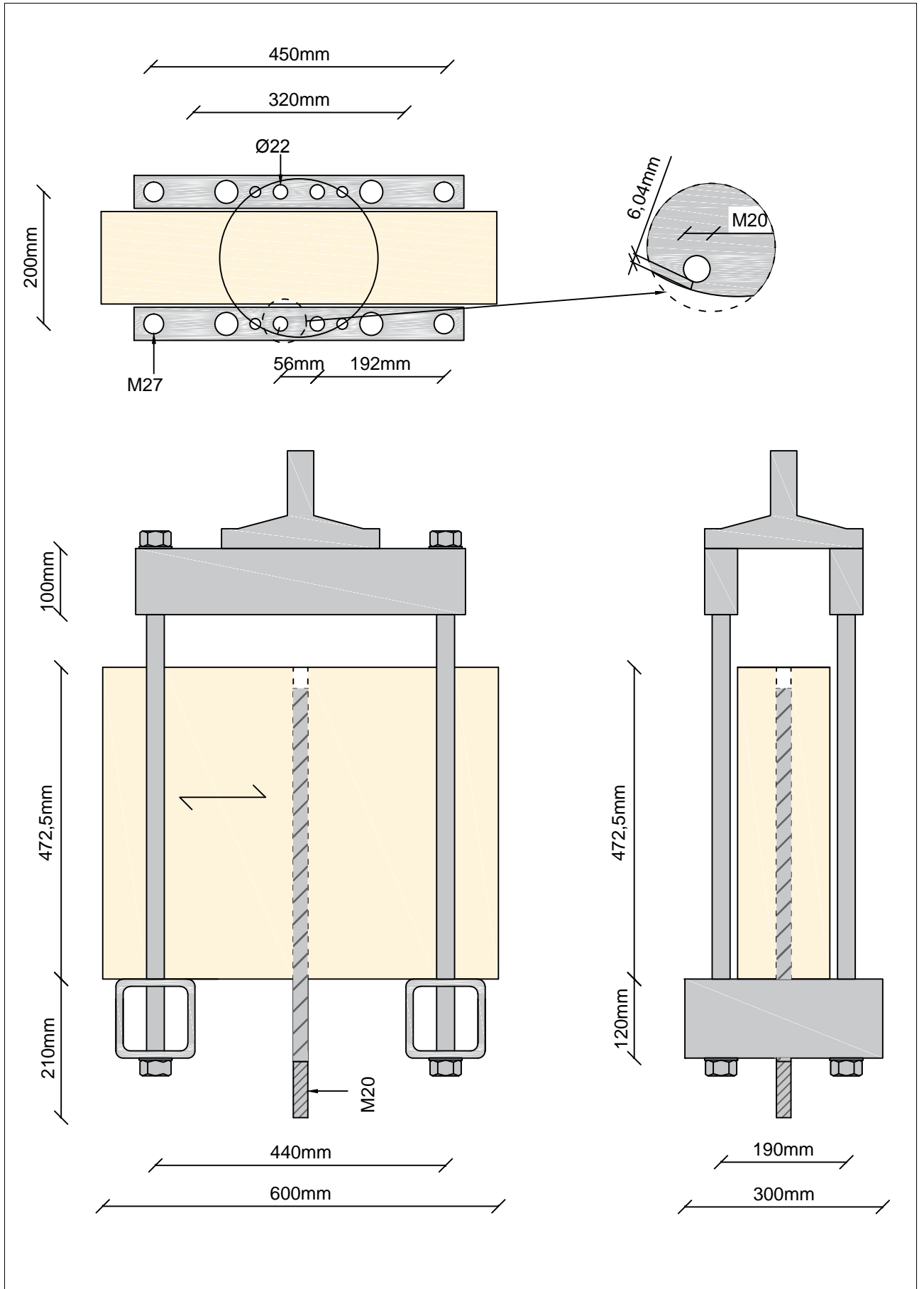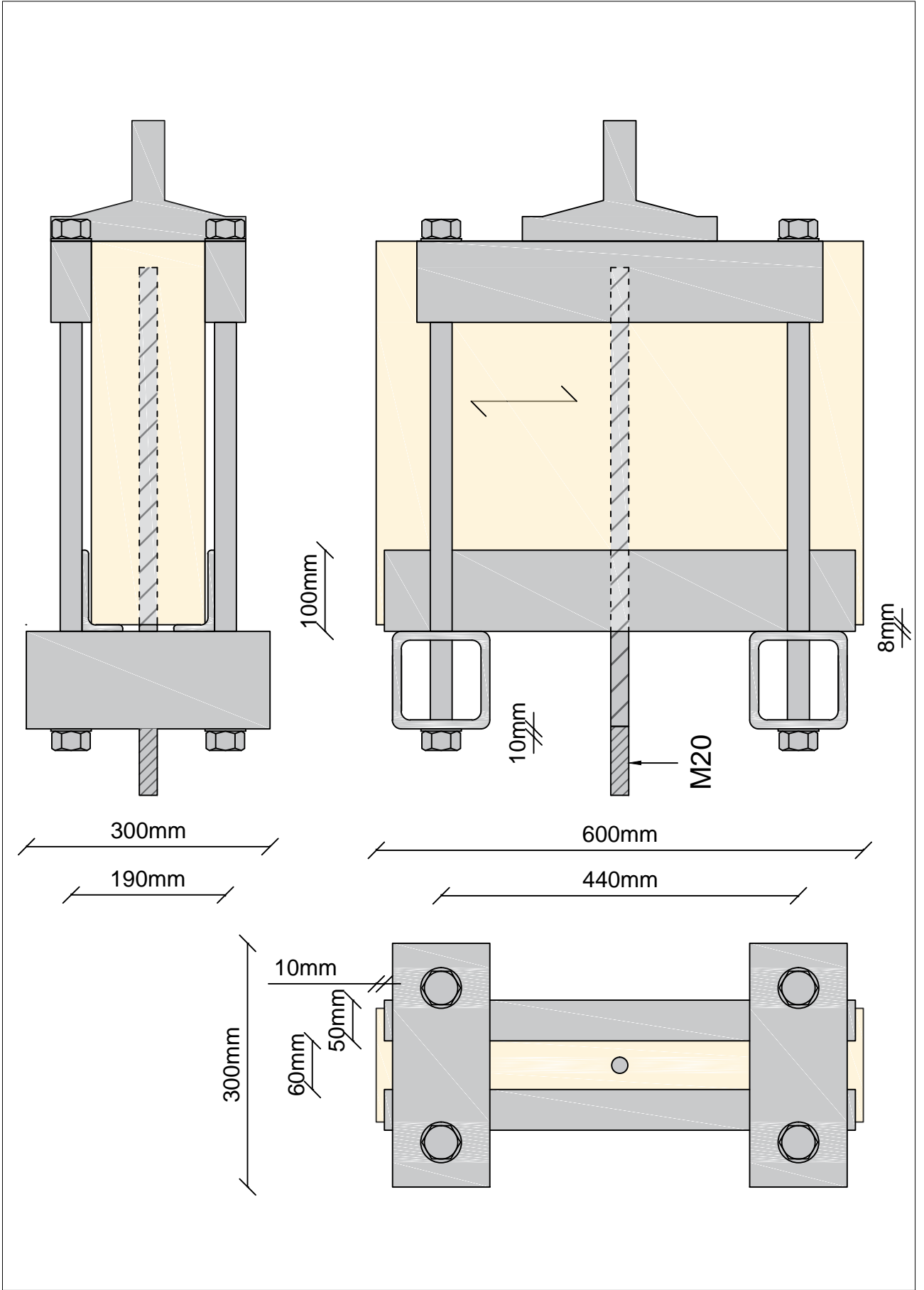
M20

6,06mm

56mm

240mm

207,8mm

M20

6mm

L-Profile (100x50x8)

50mm

580mm

240mm

35mm

100mm

8mm

8mm

Setup 1

450mm

320mm

Ø22

200mm

M27

56mm   192mm

6,04mm

M20

100mm

472,5mm

210mm

M20

440mm

600mm

472,5mm

120mm

190mm

300mm

Setup 2

300mm

190mm

100mm

600mm

440mm

8mm

10mm

M20

300mm

10mm

50mm

60mm

Setup 3

440mm

Top of threaded rod, M20

M27

Glulam
specimen

(120x120x11)

300mm
200mm
50mm

20mm 120mm 160mm

M20

M20

Glulam specimen

Rod for suspension

1365mm

945mm

120mm

65mm

440mm

210mm

85mm

M20

200mm

300mm

600mm

Threaded rod
embedded in glulam,
dt=22mm

Setup 4

300mm
190mm

100mm

600mm
440mm

10mm

8mm

M20

10mm
50mm
60mm

300mm

Setup 5

300mm

190mm

300mm

140mm

10mm

5mm

10mm

M20

600mm

440mm

140mm

Annex G

Fatigue failure modes

S90-9-d1 & S90-10-d2
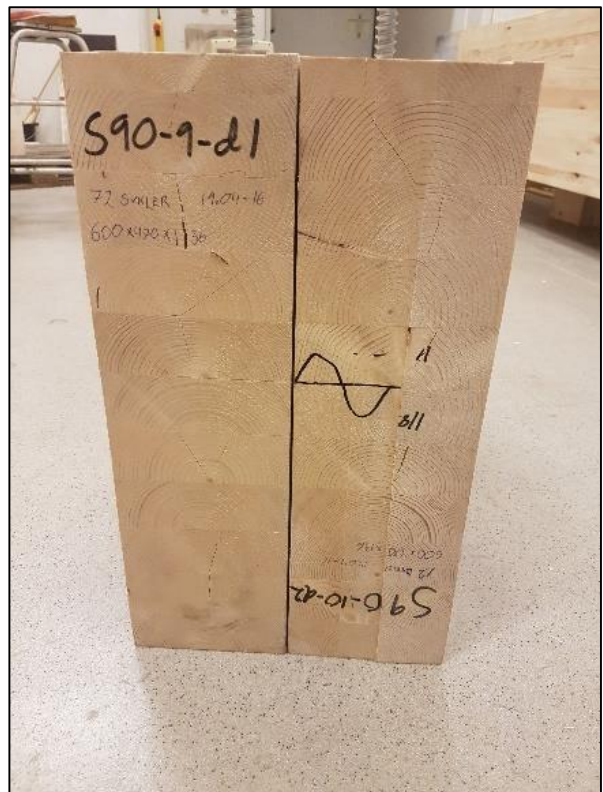
S90-11-d3
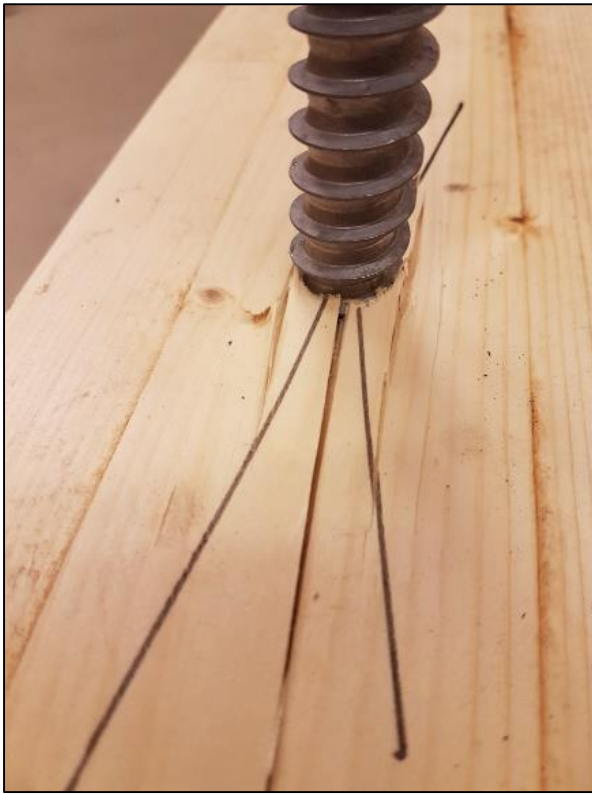
S90-12-d4

S90-8-d5

S90-14-d6
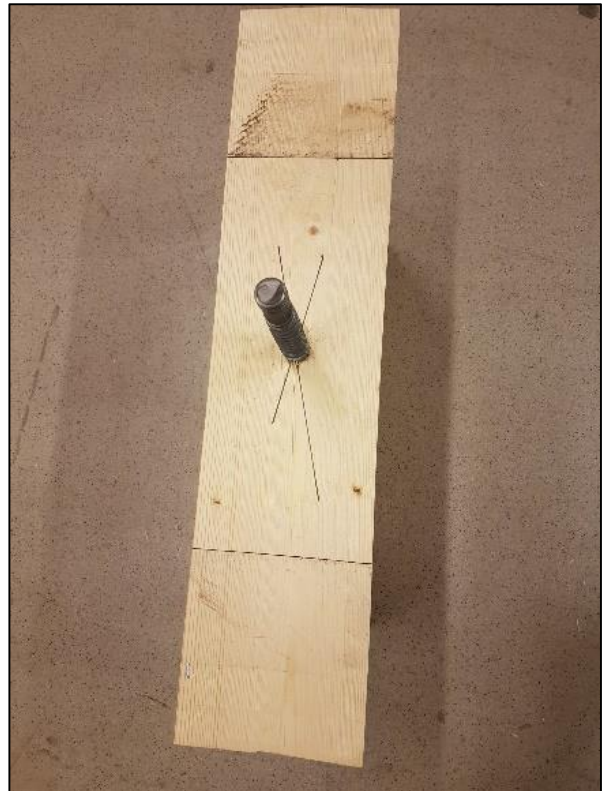
S45-27-d1
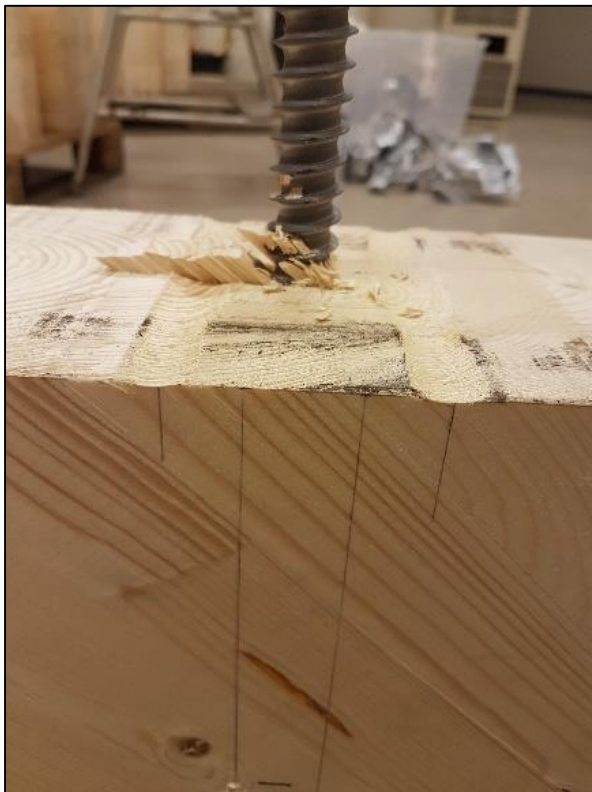
S45-6-d2

S45-4-d3

S45-26-d4
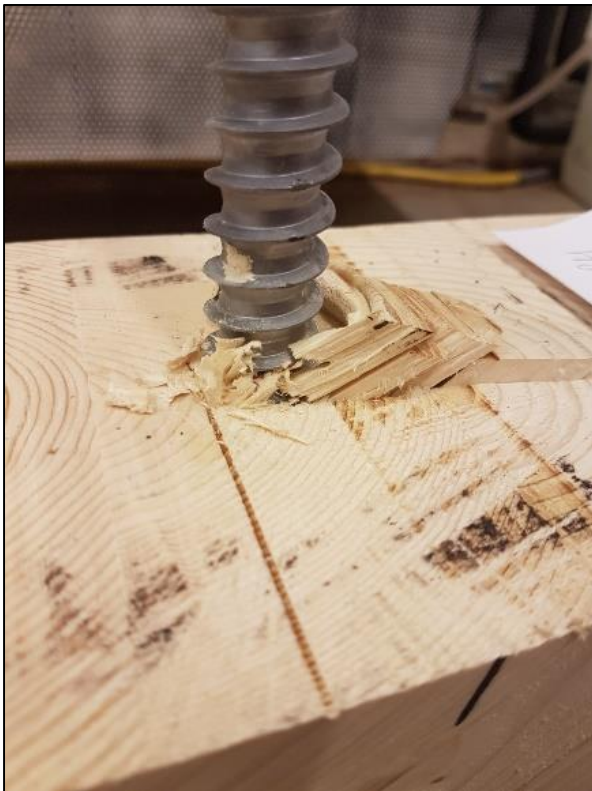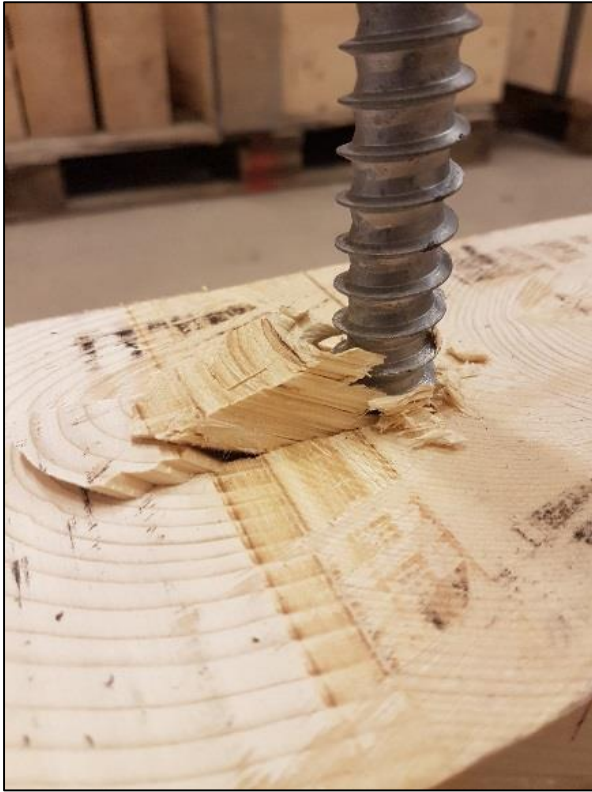
S45-25-d5
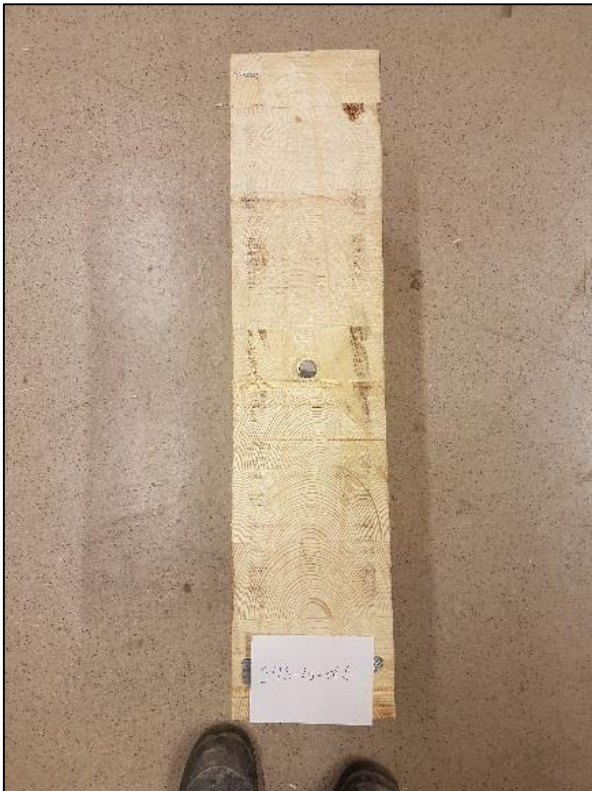
S45-30-d6

Annex H

Static testing: Results, graphs and calculations

Specimen I.D. [name]	Date [-]	Time [-]	Moisture [%]	Width b [mm]	Height h [mm]	Length L [mm]	Weight W [kg]	Density ρ [kg/m³]	Supp. above glulam surface l_1 [mm]	Max. force F_{max} [kN]	Disp. at F_{max} Δ_{max} [mm]	Setup [nr.]
S90-2-s1	18.03.2016		9.8	137	470	603	16.845	433.84	0	159.22	3.37	1
S90-11-s2	05.04.2016	08.30-11.00	10.8	138	471	600	16.83	431.55	0	155.18	3.62	1
S45-2-s1	05.04.2016	12.00-15.15	11.3	140	467	600	18.27	465.74	0	118.93	0.82	1
S45-7-s2	06.04.2016	09.30-10.30	12.8	140	470	600	19.67	498.23	9.5	188.03	3.16	2
S45-5-s3	06.04.201	14.00-15.1	12.	14	47	602	19.55	491.45	12.5	182.15	2.85	2

S45-x-sx

Force [kN] vs Time [s]
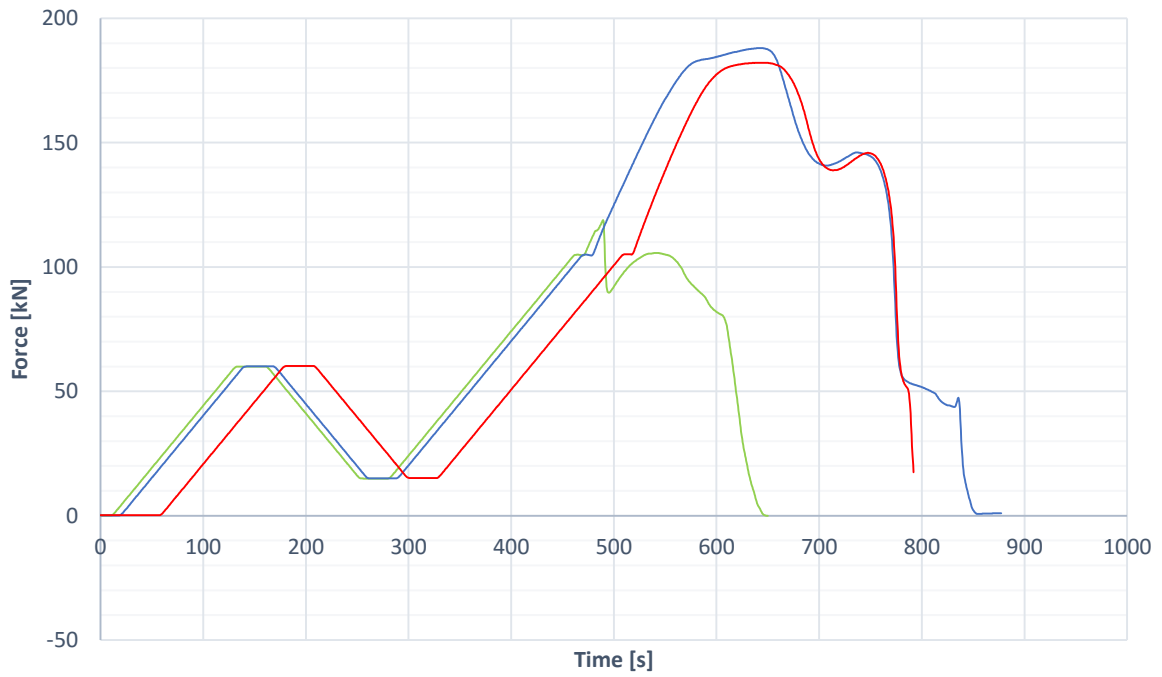
S45-2-s1 — S45-7-s2 — S45-5-s3

S45-x-sx

Force [kN] vs Mean displacement [mm]
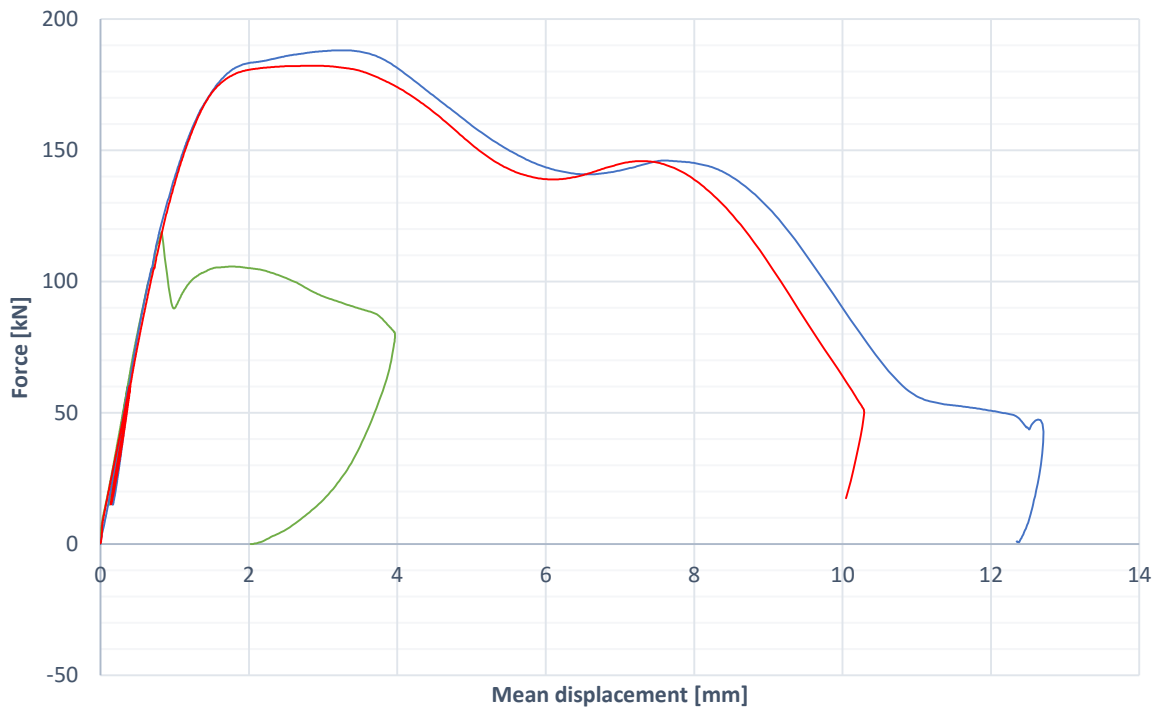
S45-2-s1 — S45-7-s2 — S45-5-s3
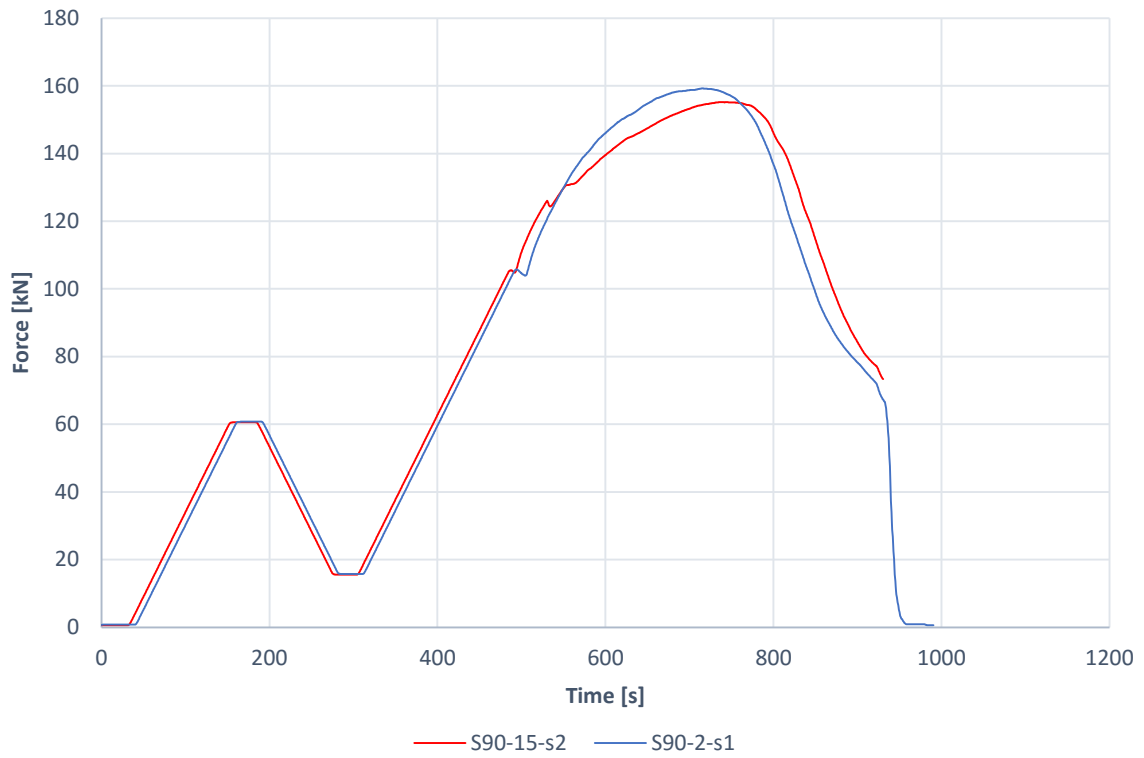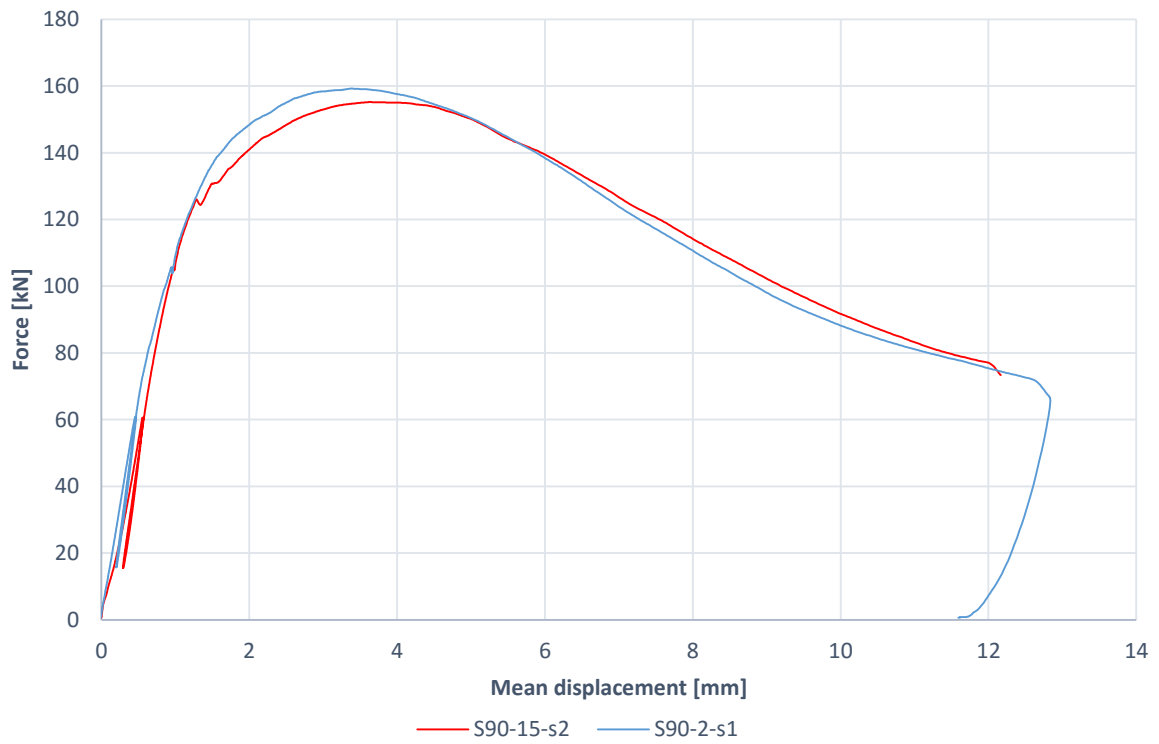
Calculation: withdrawal capacity

Classification: GL 30c

$l_{ef} := 440 \ mm$ Embedment depth.

$d_t := 22 \ mm$ Outer diameter of threaded rods embedded in wood.
NS-EN 14080:2013

$\rho_k := 390 \ \dfrac{N}{mm^2}$

$\rho_{m.90} := 433 \ \dfrac{N}{mm^2}$ Mean density, experimental S90

$\rho_{m.45} := 495 \ \dfrac{N}{mm^2}$ Mean density, experimental S45

Calculated according to DIN 1052

Withdrawal capacity with characteristic density:

$\rho_{k.DIN} := 390 \left(\dfrac{N}{mm^2} \right)^{\frac{1}{2}}$ --> changed to fit the empirical formula

$f_{1.k} := 70 \cdot 10^{-6} \ \rho_{k.DIN}^2 = 10.647 \ \dfrac{N}{mm^2}$

$F_{ax.k} := f_{1.k} \cdot l_{ef} \cdot d_t = 103.063 \ kN$

Withdrawal capacity with mean density from S90 tests:

$\rho_{m.90.DIN} := 433 \left(\dfrac{N}{mm^2} \right)^{\frac{1}{2}}$ --> changed to fit the empirical formula

$f_{1.m.90} := 70 \cdot 10^{-6} \ \rho_{m.90.DIN}^2 = 13.124 \ \dfrac{N}{mm^2}$

$F_{ax.m} := f_{1.m.90} \cdot l_{ef} \cdot d_t = 127.043 \ kN$

Withdrawal capacity with mean density from S45 tests:

$$\rho_{m.45.DIN} := 495 \left(\frac{N}{mm^2}\right)^{\frac{1}{2}}$$ --> changed to fit the empirical formula

$$f_{1.m.45} := 70 \cdot 10^{-6} \; \rho_{m.45.DIN}^{\,2} = 17.152 \; \frac{N}{mm^2}$$

$$F_{ax.m} := f_{1.m.45} \cdot l_{ef} \cdot d_t = 166.029 \; kN$$

Calculated according to NS-EN 1995-1-1

$$n_{ef} := 1$$ *NS-EN 1995-1-1, 8.7.3(1)*

$$\rho_a := \rho_k = 390 \; \frac{N}{mm^2}$$ $$\frac{\rho_k}{\rho_a} = 1$$ Simplification

Withdrawal capacity based on mean density for 90-degree specimens:

$$f_{ax.m} := f_{1.m.90} = 13.124 \; \frac{N}{mm^2}$$ NS-EN 1995-1-1 do not define a value for d>12mm. Using DIN 1052.

$$\alpha := 90 \; deg$$

$$F_{ax.m} := \frac{f_{ax.m} \cdot l_{ef} \cdot d_t}{1.2 \; \cos(\alpha)^2 + \sin(\alpha)^2} \left(\frac{\rho_k}{\rho_a}\right)^{0.8} = 127.043 \; kN$$

Withdrawal capacity based on mean density for 45-degree specimens:

$$f_{ax.m} := f_{1.m.45} = 17.152 \; \frac{N}{mm^2}$$ DIN 1052

$$\alpha := 45 \; deg$$

$$F_{ax.m} := \frac{f_{ax.m} \cdot l_{ef} \cdot d_t}{1.2 \; \cos(\alpha)^2 + \sin(\alpha)^2} \left(\frac{\rho_k}{\rho_a}\right)^{0.8} = 150.935 \; kN$$

Calculated according to Stamatopoulos and Malo (2015)

Withdrawal capacity 90-degree specimens:

$$\alpha := 90 \; deg \qquad d_1 := 16.18 \; mm$$

$$A_s := \pi \left(\frac{d_1}{2}\right)^2 = 205.611 \; mm^2$$

$$E_s := 210000 \; \frac{N}{mm^2}$$

$$E_{w.0} := 13000 \; \frac{N}{mm^2}$$

$$E_{w.90} := 300 \; \frac{N}{mm^2}$$

$$E_{w.\alpha} := \frac{E_{w.0} \cdot E_{w.90}}{E_{w.0} \cdot \sin(\alpha)^2 + E_{w.90} \cdot \cos(\alpha)^2} \qquad \text{Hankinson formula}$$

Push-pull setup 1:

$$A_{w.ef.1} := 2 \cdot 140 \; mm \; (120 \; mm + 20 \cdot mm + 73.3 \; mm) = 59724 \; mm^2$$

$$\beta := \frac{1}{A_s \cdot E_s} + \frac{1}{A_{w.ef.1} \cdot E_{w.\alpha}} = \left(7.897 \cdot 10^{-8}\right) \frac{s^2}{kg \cdot m}$$

$$\beta := \beta \cdot kg \cdot \frac{m}{s^2} = 7.897 \cdot 10^{-8} \qquad \text{Dimensionless parameter}$$

$$f_{w.\alpha} := \frac{4.35 \; MPa}{0.91 \cdot \sin(\alpha)^2 + \cos(\alpha)^2} = 4.78 \; MPa$$

$$m_\alpha := \frac{0.332}{1.73 \; \sin(\alpha) + \cos(\alpha)} = 0.192$$

$$\Gamma_{e.\alpha} := \frac{9.35}{1.5 \; \sin(\alpha)^{2.2} + \cos(\alpha)^{2.2}} = 6.233$$

$$\omega := \sqrt{\pi \cdot d_t \cdot \Gamma_{e.\alpha} \cdot \beta \cdot l_{ef}{}^2} = \left(8.116 \cdot 10^{-5}\right) m^{\frac{3}{2}}$$

$$\omega := \omega \cdot \frac{1}{m^{\frac{3}{2}}} = 8.116 \cdot 10^{-5} \qquad\qquad \text{Dimensionless parameter}$$

$$F_{ax.m} := \frac{\sin\left(m_\alpha \cdot \omega\right)}{m_\alpha \cdot \omega} \cdot \pi \cdot d_t \cdot f_{w.\alpha} \cdot l_{ef} = 145.369 \ kN$$

Withdrawal capacity 45-degree specimens:

$$\alpha := 45 \ deg$$

Push-pull setup 2:

$$A_{w.ef.2} := 2 \cdot 600 \ mm \ (40 \ mm + 0 \cdot mm + 30 \ mm) = 84000 \ mm^2$$

$$\beta := \frac{1}{A_s \cdot E_s} + \frac{1}{A_{w.ef.2} \cdot E_{w.\alpha}} = \left(6.284 \cdot 10^{-8}\right) \frac{s^2}{kg \cdot m}$$

$$\beta := \beta \cdot kg \cdot \frac{m}{s^2} = 6.284 \cdot 10^{-8} \qquad\qquad \text{Dimensionless parameter}$$

$$f_{w.\alpha} := \frac{4.35 \ MPa}{0.91 \cdot \sin(\alpha)^2 + \cos(\alpha)^2} = 4.555 \ MPa$$

$$m_\alpha := \frac{0.332}{1.73 \ \sin(\alpha) + \cos(\alpha)} = 0.172$$

$$\Gamma_{e.\alpha} := \frac{9.35}{1.5 \ \sin(\alpha)^{2.2} + \cos(\alpha)^{2.2}} = 8.017$$

$$\omega := \sqrt{\pi \cdot d_t \cdot \Gamma_{e.\alpha} \cdot \beta \cdot l_{ef}{}^2} = \left(8.21 \cdot 10^{-5}\right) m^{\frac{3}{2}}$$

$$\omega := \omega \cdot \frac{1}{m^{\frac{3}{2}}} = 8.21 \cdot 10^{-5} \qquad\qquad \text{Dimensionless parameter}$$
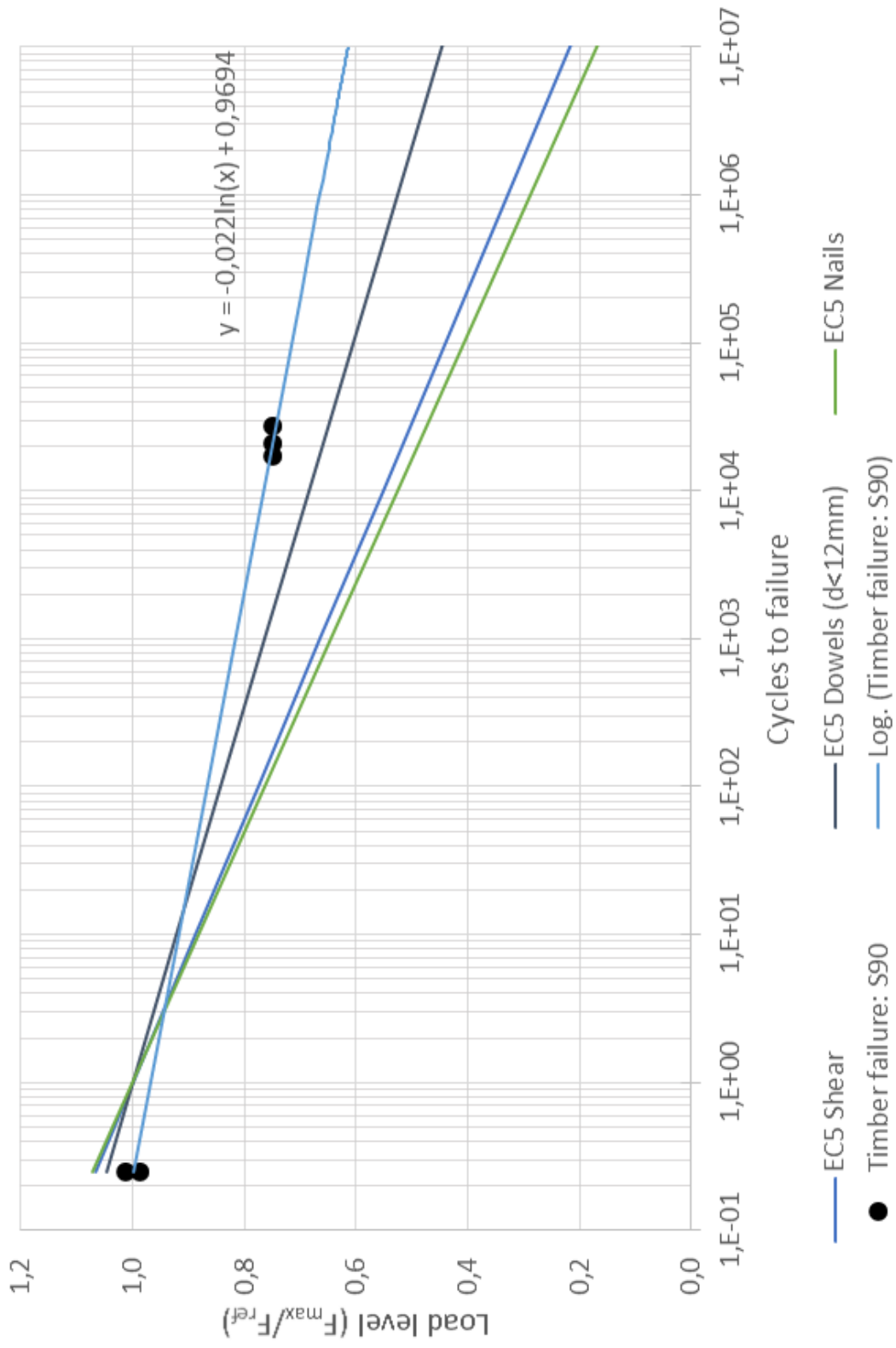
$$F_{ax.m} := \frac{\sin\left(m_\alpha \cdot \omega\right)}{m_\alpha \cdot \omega} \cdot \pi \cdot d_t \cdot f_{w.\alpha} \cdot l_{ef} = 138.52 \ kN$$
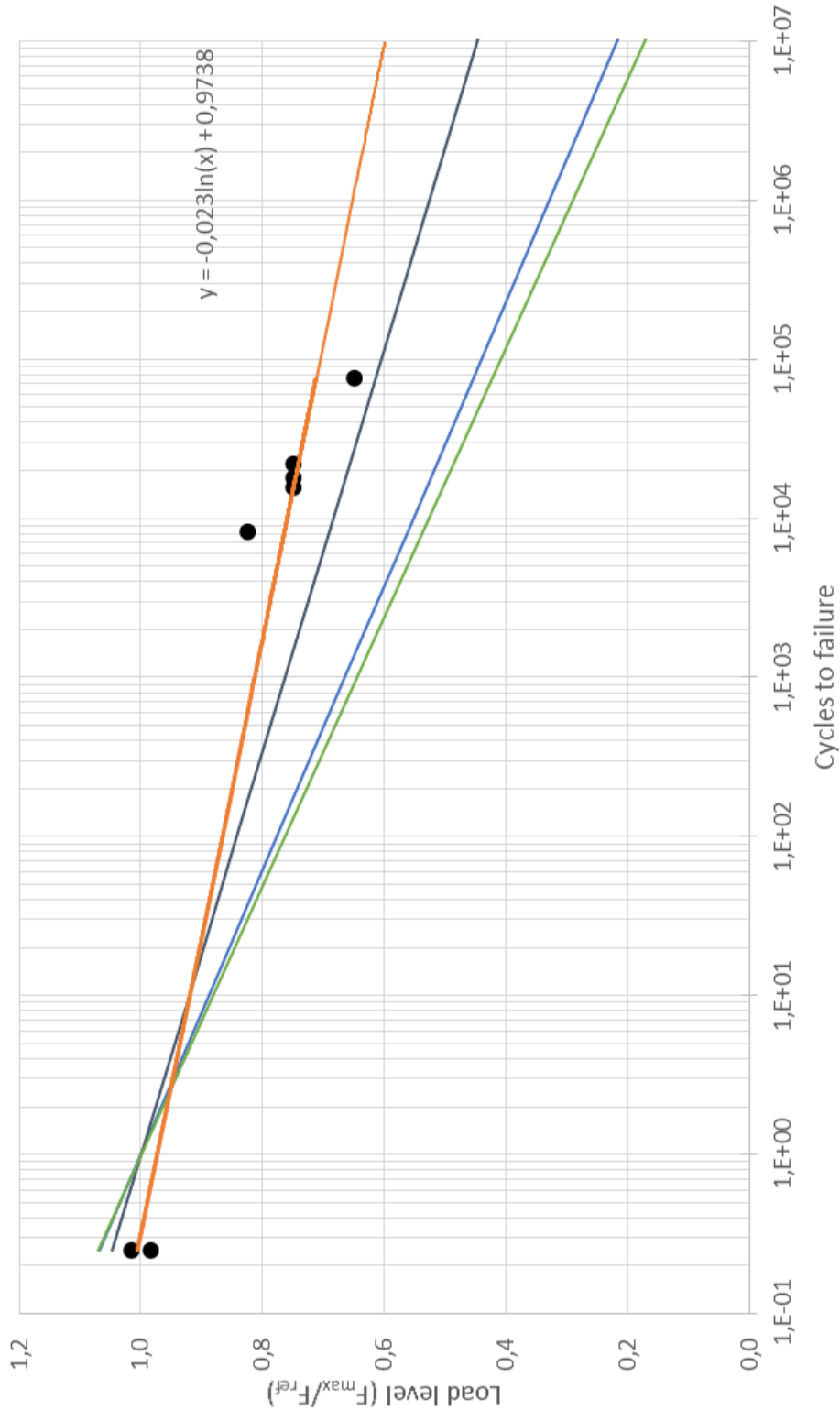
Annex I

Cyclic testing: Results and S-N curves

Specimen	Embedment depth l_eff [mm]	Load level f_max	Load range Δf	Max load F_max [kN]	Frequency	Length L [mm]	Height h [mm]	Width b [mm]	Moisture [%]	Weight W [kg]	Density P [kg/m³]	Supp.-glulam surface l_1 [mm]	Cycles, wood failure N	Cycles, first steel failure
S90-2-s1	440	1,013	Static	159,2		603	470	137	9,82	16,845	433,85	0	0,25	
S90-15-s2	440	0,987	Static	155,2		600	471	138	10,83	16,83	431,55	0	0,25	
S45-7-s2	440	1,016	Static	188,0		600	470	140	12,75	19,67	465,74	9,5	0,25	
S45-5-s3	440	0,984	Static	182,1		602	472	140	12,47	19,55	498,23	12,5	0,25	
S90-9-d1	440	0,75	0,675	118,0	0,1	600	470	136	9,87	17,76	463,08	0	0	
S90-10-d2	440	0,75	0,675	118,0	0,1	600	470	136	9,40	17,87	465,95	0	0	
S90-11-d3	440	0,75	0,675	118,0	2,5	600	473	138	10,50	17,34	442,75	8	27026	
S90-12-d4	440	0,75	0,675	118,0	2,5	600	470	138	10,70	17,38	446,60	8	20550	16919
S90-8-d5	440	0,75	0,675	118,0	2,5	600	470	138	10,10	17,196	441,87	8	16960	16725
S90-14-d6	440	0,6	0,54	94,0	2,5	603	473	138	10,64	16,91	429,62	8	79033	46982
S90-1-d7	330	0,6	0,54	71,0	2,5	600	472	140	10,77	16,852	425,04	8	464845	98414
S45-27-d1	300	0,824	0,742	104,0	2,5	600	472	140	12,00	19	479,22	9	8178	
S45-6-d2	330	0,75	0,675	104,0	2,5	600	472	140	12,04	19,58	493,85	9	15619	
S45-4-d3	330	0,75	0,675	104,0	2,5	600	472	140	11,80	19,16	483,25	9	21994	
S45-26-d4	330	0,75	0,675	104,0	2,5	600	472	140	11,60	19,2	484,26	9	17979	
S45-25-d5	330	0,6	0,54	83,3	2,5	600	472	140	12,13	19,3	486,78	9	91289	91289
S45-30-d6	330	0,65	0,585	90,2	2,5	600	472	140	11,68	18,5	466,61	9	75517	45721

S-N Curve - S90

$y = -0,022\ln(x) + 0,9694$

Load level (F_{max}/F_{ref})

Cycles to failure

EC5 Shear
EC5 Dowels (d<12mm)
EC5 Nails
Log. (Timber failure: S90)
Timber failure: S90

S-N Curve - S45

$y = -0,023\ln(x) + 0,9738$

Load level (F_{max}/F_{ref})

Cycles to failure
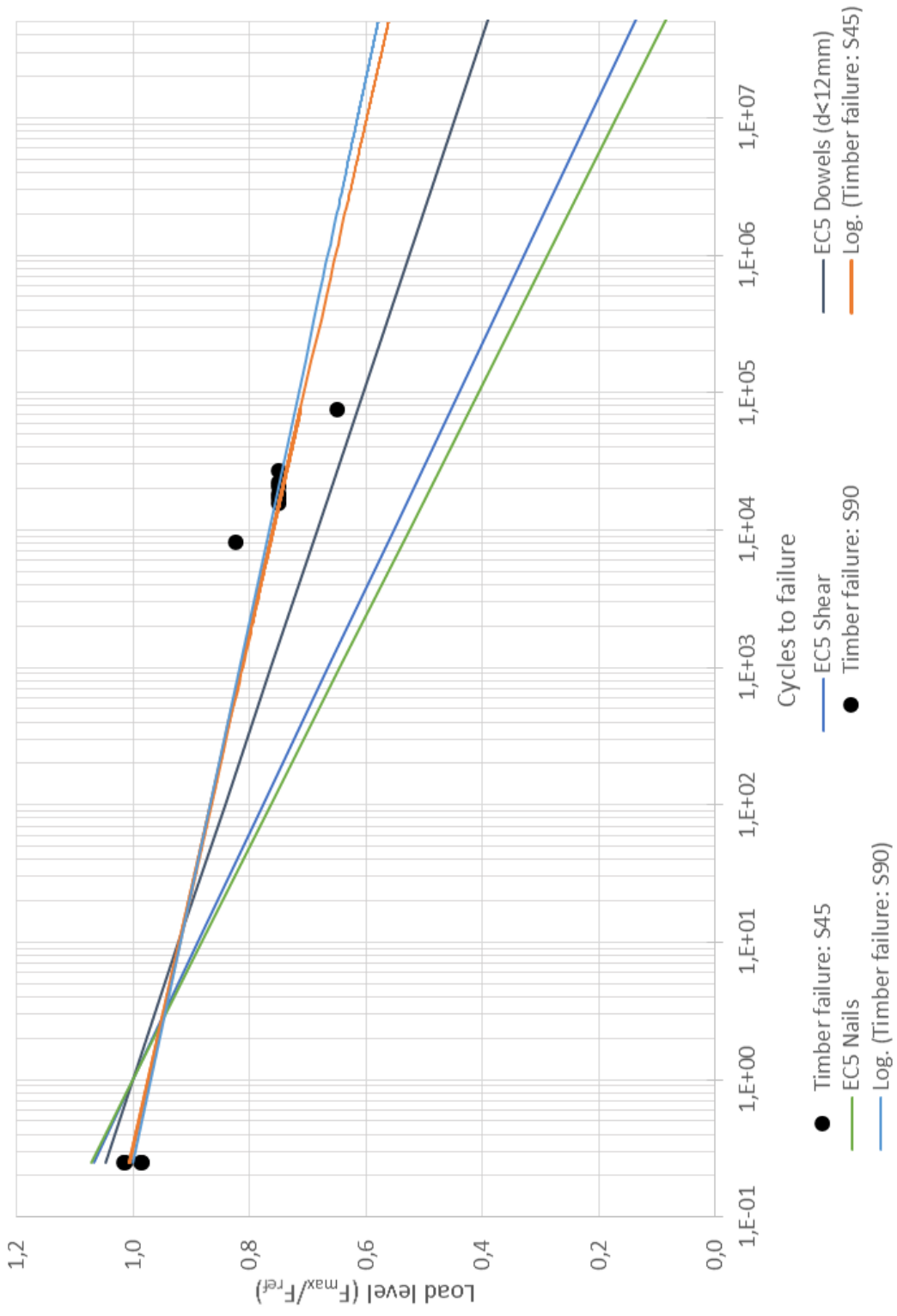
● Timber failure: S45   —— EC5 Shear   —— EC5 Dowels (d<12mm)

—— EC5 Nails   —— Log. (Timber failure: S45)

S-N Curve - Fatigue failure timber

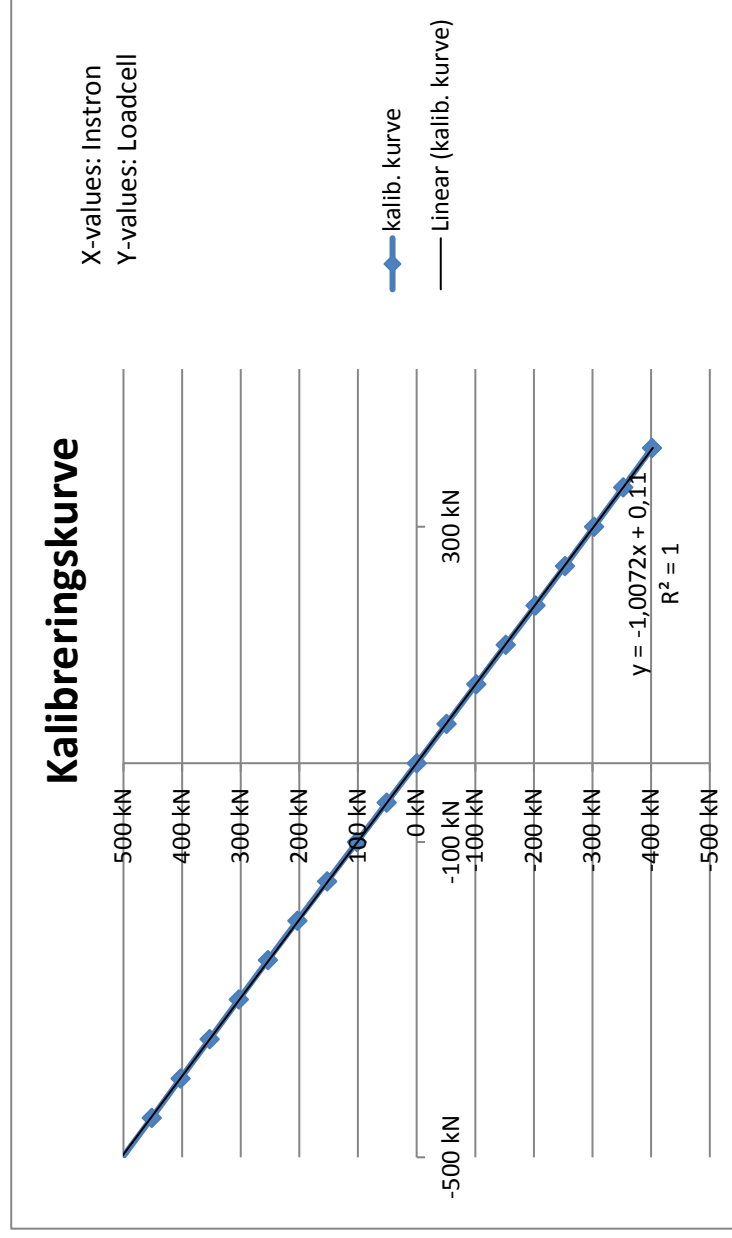Load level (F_{max}/F_{ref})

Cycles to failure

- Timber failure: S45
- EC5 Nails
- Log. (Timber failure: S90)
- EC5 Shear
- Timber failure: S90
- EC5 Dowels (d<12mm)
- Log. (Timber failure: S45)

Annex J

Calibration forms

Kalibreringsskjema, Instron 500 kN

NKT nr.	
Modell	Instron
F. nr.	
Type	500 kN
Følsomhet(mV/V)	2 mV/V
Kalibrator	Kalibreringslastcelle

Sporbarhet	Lille prøvesal
Akkreditert	Zwick Roell
Kalibreringsdato	12.06.2014
Neste kalibrering	12.06.2016

Kal. Celle	Instron	Instron	Gj.snitt	Linear
-500	502	500,9	501,45	503,6
-450	452,6	451,4	452	453,24
-400	403	401,8	402,4	402,88
-350	353,4	352,3	352,85	352,52
-300	303,5	303	303,25	302,16
-250	253,5	253,3	253,4	251,8
-200	203	203,4	203,2	201,44
-150	152,3	153	152,65	151,08
-100	101,6	102,3	101,95	100,72
-50	50,8	51,3	51,05	50,36
0	0	0	0	0
50	-50,6	-51,3	-50,95	-50,36
100	-101,2	-102,1	-101,65	-100,72
150	-151,8	-152,7	-152,25	-151,08
200	-202,3	-203	-202,65	-201,44
250	-252,6	-253	-252,8	-251,8
300	-302,8	-302,7	-302,75	-302,16
350	-352,5	-352	-352,25	-352,52
400	-402,1	-401,2	-401,65	-402,88
450	-451	-450,2	-450,6	-453,24
500	-499,7	-499,1	-499,4	-503,6

Kalibreringskurve

X-values: Instron
Y-values: Loadcell

— kalib. kurve
— Linear (kalib. kurve)

$y = -1,0072x + 0,11$
$R^2 = 1$

Underskrift: Dato:

Kalibreringsskjema, Schenk 1000 kN

NKT nr.	
Modell	Schenk
F. nr.	
Type	1000 kN
Følsomhet(mV/V)	2 mV/V
Kalibrator	NKT-102

Sporbarhet	MarinTek
Akkreditert	
Kalibreringsdato	16.09.2013
Neste kalibrering	16.09.2015

Kalibreringskurve

X-values: Instron
Y-values: Loadcell

kalib. kurve
Linear (kalib. kurve)

y = -0,9935x + 0,25
R² = 1

Underskrift:

Dato:

Instron	Kal. Cel	Kal. Cel	Gj.snitt	Linear
1000	-989,9	-990,1	-990	-993,5
900	-892,7	-891,1	-891,9	-894,15
800	-793,7	-791,7	-792,7	-794,8
700	-695,8	-693	-694,4	-695,45
600	-597,8	-594,8	-596,3	-596,1
500	-499,7	-496,7	-498,2	-496,75
400	-401,1	-398,4	-399,75	-397,4
300	-301,6	-299,7	-300,65	-298,05
200	-201,6	-200,3	-200,95	-198,7
100	-101,2	-100,1	-100,65	-99,35
0	0	0	0	0
-100	101	100,3	100,65	99,35
-200	201,5	200,9	201,2	198,7
-300	300,6	299,8	300,2	298,05
-400	399,2	397,6	398,4	397,4
-500	497,9	496,7	497,3	496,75
-600	597,2	596,3	596,75	596,1
-700	696,5	695,8	696,15	695,45
-800	795,8	795,3	795,55	794,8
-900	895	894,8	894,9	894,15
-1000	994,3	994,3	994,3	993,5